ELECTROMAGNETIC INTERFERENCE BEHAVIOR OF MULTIWALL

CARBON NANOTUBES AND CARBON NANOFIBERS COMPOSITES UNDER

FATIGUE

THESIS

Peter A. Hunt, Captain, USAF

AFIT/GMS/ENY/12-M01

DEPARTMENT OF THE AIR FORCE
AIR UNIVERSITY

AIR FORCE INSTITUTE OF TECHNOLOGY

Wright-Patterson Air Force Base, Ohio

AFIT/GMS/ENY/12-M01

ELECTROMAGNETIC INTERFERENCE BEHAVIOR OF MULTIWALL CARBON NANOTUBES AND CARBON NANOFIBERS COMPOSITES UNDER FATIGUE

THESIS

Presented to the Faculty

Department of Aeronautics and Astronautics

Graduate School of Engineering and Management

Air Force Institute of Technology

Air University

Air Education and Training Command

In Partial Fulfillment of the Requirements for the

Degree of Master of Science in Materials Science Engineering

Peter A. Hunt, BS

Captain, USAF

March 2012

ELECTROMAGNETIC INTERFERENCE BEHAVIOR OF MULTIWALL

CARBON NANOTUBES AND CARBON NANOFIBERS COMPOSITES UNDER

FATIGUE

Peter A. Hunt, BS

Captain, USAF

Approved:

//signed//_____   __2 Mar 12__
Dr. Shankar Mall (Chairman)   Date

//signed//_____   __2 Mar 12__
Dr. Som Soni (Member)   Date

//signed//_____   __2 Mar 12__
Dr. Vinod Jain (Member)   Date

Abstract

The United States (U.S.) military is researching the use of nanocomposite materials for structural applications on space vehicle systems. To reduce the weight and mitigate electromagnetic interference (EMI), brought on by the harsh space environment, composites coated with expensive conductive materials are used in today's space vehicles. Research on composites with carbon nanotubes (CNT) and carbon nanofibers (CNF) have shown better EMI shielding and offer the potential to replace the current composites coated with expensive conductive materials as a high specific strength material.

This study evaluated the effects of EMI behavior on one control composite (i.e. without nanocomposite) and five different configured nanocomposites under fatigue. The control specimen, 8G, consisted of eight plies S-glass (Astroquartz II) fiber in CYCOM 5575-2 cyanate ester matrix. The first nanocomposite, 8G/CNT, consisted of eight plies of 6781 S-2 glass fiber in CYCOM 5250-4 Bismaleimide (BMI) matrix with a externally deposited layer of CNTs. The second nanocomposite, 8G/CNF, consisted of eight plies of 6781 S-2 glass fiber in CYCOM 5250-4 BMI matrix with a externally deposited layer of CNFs. The last three nanocomposites, $(G/CNT)_4$, 2CNT/4G/2CNT, and 4G/4CNT, consisted of different stacking sequences of multi-wall CNTs (MWNT) with S-glass (Astroquartz II) fiber in CYCOM 5575-2 cyanate ester matrix. The $(G/CNT)_4$ configuration was an alternating configuration of glass fiber ply and CNT ply. The 2CNT/4G/2CNT configuration had two plies of CNTs, four plies of glass fiber in the

middle section, and finally two plies of CNTs. The 4G/4CNT configuration had four plies of glass fiber followed by four plies of CNTs. All nanocomposites in this study were fatigue at the applied stress ranging from 18% to 75% of ultimate tensile strength (UTS) and showed no change in EMI shielding effectiveness (SE) until their failure. The nanocomposite that showed the best EMI SE performance had the exterior CNT configuration, 2CNT/4G/2CNT, with an initial EMI of 67.65 decibels (dB). The EMI SE performance was dependent upon the concentration of CNTs. The 2CNT/4G/2CNT, 4G/4CNT, and $(G/CNT)_4$ nanocomposites had 3.6 times more grams of CNTs compared to 8G/CNT and 8G/CNF. All the nanocomposites EMI SE performance was independent of the applied stress level during fatigue testing. Five of the test specimens survived 600,000 cycles of fatigue testing without failure. The two nanocomposites that showed the most resistance to fatigue failure at the higher stress levels were 8G/CNT and 8G/CNF. Fatigue failure resistance was dependent upon the type of matrix material used in this study.

Failure mechanisms were the same irrespective of the stacking sequence. Transverse matrix cracks formed initially leading to delamination, which lead to more matrix cracks and additional delamination that eventually caused ultimate failure. Microscopic analysis of the CNT and CNF plies showed minimal to no damage away from the fracture region. Therefore, EMI SE performance was not affected under mechanical fatigue. In summary, CNT based composites are promising material to be used as shield against EMI in space structures.

To my parents, children, and loving wife

Acknowledgments

I would like to thank the following individuals that provided support and helped me complete my research. Without the individuals mentioned below I wouldn't have had the necessary support to complete this research. First, my thesis advisor, Dr. Shankar Mall, who expertly guided me through my research by directing and answering questions throughout the entire research process. Second, the AFIT instructors that paved the way for me to grasp the concepts and theory that I applied towards this research. Third, Dr. Fred Meisenkothen from the Materials and Manufacturing Directorate, Air Force Research Laboratory (AFRL), who sacrificed several hours of his time helping me collect microscopic images for my thesis. Fourth, Dr. Max Alexander and Benjamin Wilson from the Materials and Manufacturing Directorate, AFRL, who helped me with my EMI tests. Fifth, Dr. Volodymyr Sabelkin, from AFIT, who showed me how to setup my test specimens and run fatigue tests. Lastly, my classmates that spent the numerous hours with me in the classroom and outside of the classroom studying the concepts and tools that I used in this research.

Peter A. Hunt, Captain, USAF

Table of Contents

List of Figures

xi

xiii

List of Tables

List of Abbreviations and Symbols

AFIT	Air Force Institute of Technology
AFB	Air Force Base
AFRL	Air Force Research Laboratory
ASI	Applied Sciences Inc.
BMI	Bismaleimide
CNF	Carbon Nanofiber
CNT	Carbon Nanotube
cm	centimeter
dB	decibels
DoD	Department of Defense
EMI	Electromagnetic Interference
FL	Florida
g/m^2	grams per square meter
GPS	Global Positioning System
in	inches
MA	Massachusetts
MI	Michigan
mm	millimeter
MWNT	Multi-wall Carbon Nanotubes
HRTEM	High Resolution Tunneling Electron Microscope
NASA	National Aeronautics and Space Administration
NS	Nickel Nanostrands

NTI	Nanocomp Technologies Inc.
nm	nanometer
OH	Ohio
OM	Optical Microscope
SE	Shielding Effectiveness
SEM	Scanning Electron Microscope
SWNT	Single-wall Carbon Nanotubes
U.S.	United States
USAF	United States Air Force
UTS	Ultimate Tensile Strength
μm	micrometer
σ	Stress
8G	Eight plies of S-glass (Astroquartz II) fiber in CYCOM 5575-2 cyanate ester matrix
8G/CNT	Eight plies of 6781 S-2 glass fiber in CYCOM 5250-4 BMI matrix with externally deposited layer of CNTs
8G/CNF	Eight plies of 6781 S-2 glass fiber in CYCOM 5250-4 BMI matrix with externally deposited layer of CNFs
$(G/CNT)_4$	Alternating eight ply laminate of S-glass (Astroquartz II) fiber in CYCOM 5575-2 cyanate ester matrix stacked with a CNT ply
2CNT/4G/2CNT	Two plies of CNTs stacked with 4 plies of S-glass (Astroquartz II) fiber in CYCOM 5575-2 cyanate ester matrix followed by two more plies of CNTs
4G/4CNT	Four plies of S-glass (Astroquartz II) fiber in CYCOM 5575-2 cyanate ester matrix stacked with four plies of CNTs

List of Equations

ELECTROMAGNETIC INTERFERENCE BEHAVIOR OF MULTIWALL CARBON NANOTUBES AND CARBON NANOFIBERS COMPOSITES UNDER FATIGUE

I. Introduction

The idea of reaching space was first proposed by Konstantin Tsiolkovsky, an Imperial Russian and Soviet rocket scientist, in 1903. It would be almost 41 years later when the first space launched V-2 Rocket from Germany reached an altitude of 100 km. The most common structural material for space vehicles was aluminum. Aluminum's material properties, and low cost, was a suitable design choice for early space vehicle designs. As space vehicle capabilities increased over the last two decades the space industry was forced to research structural material alternatives with improved material properties. Weight reduction was a major influence in the material selection process. This led to the use of composite structures made of Kevlar/epoxy and graphite/epoxy. The U.S. military today are researching and testing nanotechnology, specifically nanocomposites, that possess low weight, high specific strength, high specific modulus, and high electrical and thermal conductivity.

One of the many challenges that space design engineers are faced with when designing a space vehicle is the harsh operating environment. Radiation, space debris, electrostatic charging, meteoroids, etc. are common hazards in this harsh operating space environment. Fortunately, research has shown that nanocomposites have the potential to withstand this harsh space environment, provide the desired weight reduction, and

required structural material properties. As the demand for lighter, stronger, and space environmental resistance increases the demand for more research on nanocomposites to fit the structural design requirement will also increase.

Nanocomposites consists of a solid composite material where at least one phase of the material's dimension is less than 100 nanometer (nm). Structurally, the nanoscale reinforcement has a tremendous impact on the macroscale properties of the composite. For all the great strides in the recent years in nanocomposites technology that led to improved mechanical and electrical properties, the challenge compared to traditional composites is production control at the nanoscale level. If the nanocomposite industry can control production at the nanoscale level then the materials' mechanical and electrical properties can be manipulated at the macroscale level. Ongoing research in production control has the potential to revolutionize nanocomposites for endless space applications. One area of research that has Department of Defense (DoD) agencies' interests is the effects of EMI on nanocomposites that are used in space vehicle structural applications.

This chapter will discuss current space vehicle systems requirements and the space structural materials used. A section on historical perspective on nanocomposites will also be provided in this chapter. Next section will cover the thesis objective, which is effect of EMI on the nanocomposites under fatigue. The last section in chapter I will summarize all five chapters that makeup the framework for this thesis.

1.1 Space Vehicle Systems

In Sun Tzu's *Art of War*, all armies prefer high ground to low [1]. This old military strategy forced the U.S. military to occupy space and use it as the ultimate high ground on the battlefield. The Global Positioning System (GPS), shown in Figure 1, is just one example of how the U.S. military today uses space vehicle systems to provide the capability to support the mission at the highest point on the battlefield.
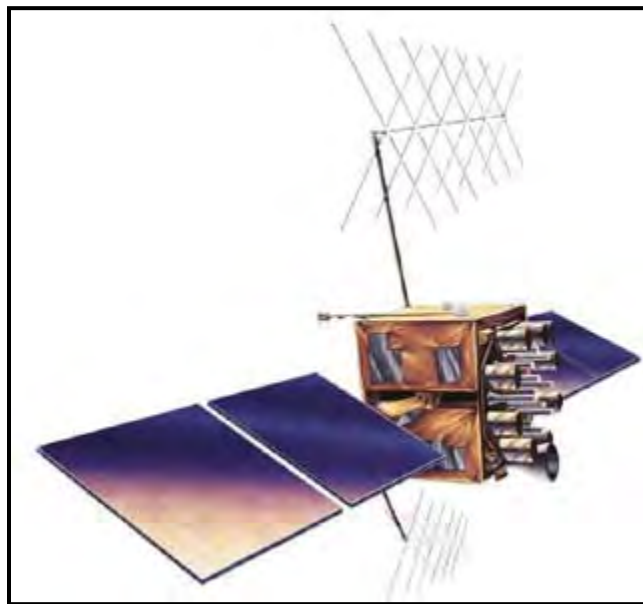
Figure 1. GPS space vehicle [2]

The most recent Joint National Security Space Strategy Unclassified Summary stated:

> *Space is vital to U.S. national security and our ability to understand emerging threats, project power globally, conduct operations, support diplomatic efforts, and enable global economic viability* [3].

As National Security defines the strategic objectives through policy and doctrine for space, the U.S. military will continue to rely on space vehicle systems for military

operations, and intelligence gathering to meet these strategic objectives. Ultimately, space vehicle systems evolving requirements will force the space industry to remain energized in finding new ways to sustain the dynamic space mission.

One way for space industry to fulfill the mission is outlined by the National Aeronautics and Space Administration's (NASA's) 2005 report on Exploration Systems Architecture Study, where one of the major areas for architecture research and technology needs are in structures and materials [4]. Specifically, outlined in a 1996 NASA fact sheet space vehicle systems, must be light weight, environmentally stable and durable, possess strength/stiffness, manufacturability, and cost effectiveness [5].

Space vehicle systems have had past success in meeting these requirements through research and testing, but the constant advances in material science technology have given way to new materials that can provide more capabilities to the customer. As the shift in use of structural materials has been from aluminum to ceramics, polymers, and composites the new material of choice is nanocomposites. Nanocomposites have proven their value from research and testing in search for a lighter, stronger, conductive, and reliable structural material for space vehicle systems.

1.2 Space Vehicle Materials

Some common space vehicle structural materials currently used are aluminum alloys, polymer matrix composites, and ceramics. Aluminum alloys were one of the first chosen structural materials for space vehicles for their light weight, and electrically conductive properties. As new materials with stronger and lighter properties were

4

developed and researched by scientists and engineers the use of composite materials became a ideal alternative to aluminum alloys. A polymer matrix composite showed promise in reducing the weight and increasing the strength compared to aluminum alloys. The only negative to this direct material replacement from aluminum to a polymer composite is the lack of protection against the harsh space environment. The buildup of electrical charges on space vehicle surfaces from the large amounts of ionizing radiation lead to undesired electrostatic discharge (ESD) and EMI, which leads to structural failure and electronic failure for the expensive electronics stored within the space vehicle system. Ultimately, the material selection for polymer composites over aluminum alloys leads to a decrease in electrical property capability because they can't protect against ESD and EMI.

One technique to still use polymer composites over aluminum alloys is by introducing conductive metallic materials onto or into the polymer composite. The earlier process steps included metallic paint coating, insertion of metal foil, meshes, and metal foil tapes adhered directly on the exterior surface of the polymer composite. Later process steps introduced metallic strands infused directly into the composite matrix. The early processing steps of coating and inserting metal foil, meshes didn't show promising conductive results when subject to mechanical fatigue and harsh space environments. At nearly the same time metallic strands were being infused directly into the polymer composites, research and testing of CNTs and CNFs composites for space structural applications was initiated. Nanocomposites bear the desired increased strength to weight

ratio, and if manufactured correctly can also display highly desired conductive electrical properties.

1.3 Nanocomposites

A composite is a material made of two or more specific phases. In one phase the, fibrous material, act as the reinforcement to the second phase, which is called the matrix [6]. Fibrous composite materials were used as early at 4,000 B.C. when Egyptians made laminated writing materials from the papyrus plant [6]. The history of advanced composite materials started when synthetic materials matured back around the 1970s. Carbon fiber composites were developed around the 1970s. The carbon fiber industry has perfected their manufacturing, quality, and operating costs in the last 40 years. Multiple industries have taken advantage of the improved mechanical properties that carbon fiber composites have by replacing heavy and expensive metal materials with lighter and cheaper carbon fiber composites.

Today the composite producing industry, universities, and other material science driven organizations are on the cutting edge of technology by researching how to grow carbon based tubes or fibers at the nano scale to take advantage of the very low fiber volume fraction, mechanical, optical, electrical, thermal, and electrochemical properties. Nanocomposites are defined by having any component of length less than 100 nm. The first individual to mention "nano-technology" was a Japanese scientist, Taniguchi, from the Tokyo University of Science in a 1974 conference. It wasn't until the 1980s when nanotechnology could be experimentally analyzed in the laboratory after the invention of

the scanning tunneling microscope by Binning and Rohrer at the IBM Zurich Research

Laboratory. The first discovery of a carbon nano scaled molecule was in 1985 with

fullerenes by Kroto, Smalley, and Curl at Rice University. A fullerene is a molecule

composed of entirely carbon in several forms: hollow sphere, ellipsoid, or tube. The

hollow spherical shape is commonly known as buckyballs and the cylindrical tube are

commonly called single-wall CNT (SWNT). Shown in Figure 2 is buckyball

(buckminsterfullerene) and SWNT.
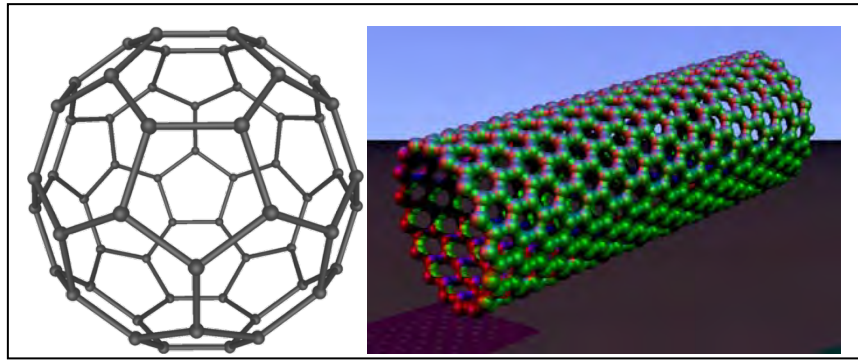
Figure 2. Buckminsterfullerene C_{60} (left) and CNT (right) [7], [8]

1.4 Thesis Objective

The objective of this thesis was to characterize the EMI SE of CNT and Carbon

Nanofiber (CNF) composites under cyclic fatigue loading condition. The

nanocomposites tested consisted of the following: (1) SWNTs and MWNTs deposited on

one side of eight ply glass fiber/epoxy composite laminate (6781 S-2 glass fiber in

CYCOM 5250-4 BMI matrix), (2) vapor grown CNF (about 100 nm diameter and 100

micrometer (μm) long) deposited on one side of eight ply glass fiber/epoxy composite

laminate (6781 S-2 glass fiber in CYCOM 5250-4 BMI matrix), and (3) MWNT and

fiberglass composite plies arranged in four different stacking sequence configurations.

The CNTs and CNFs layers in the first two nanocomposites listed above are about 0.1 millimeter (mm) thick, and contains 20 grams per square meter (g/m^2) [9]. The reinforcement plies in the four different configurations of the MWNT and fiberglass composite plies consisted of S-glass fiber (Astroquartz II) in CYCOM 5572-2 cyannate ester matrix. The cyanate ester matrix syntactic core for the CYCOM 5575-2 is derived from FM 6555-1. The MWNTs plies were approximately 84.89 μm thick in the four different configurations of the MWNT and fiberglass composite. The MWNTs were approximately 700 μm in length and 8-15 nm in diameter, 90% weight percentage, and had a concentration of 18.3 g/m^2 of CNTs in each CNT ply. Refer to Appendix A, Appendix B, Appendix C, Appendix D, and Appendix E for specific material properties on 6781 S-2 glass fiber, CYCOM 5240-4 BMI matrix, S-glass fiber (Astroquartz II), and FM 6555-1 cyanate ester syntactic core and CNTs respectively. Figure 3 illustrates the individual CNFs. Figure 4 shows a molecular schematic of MWNT.
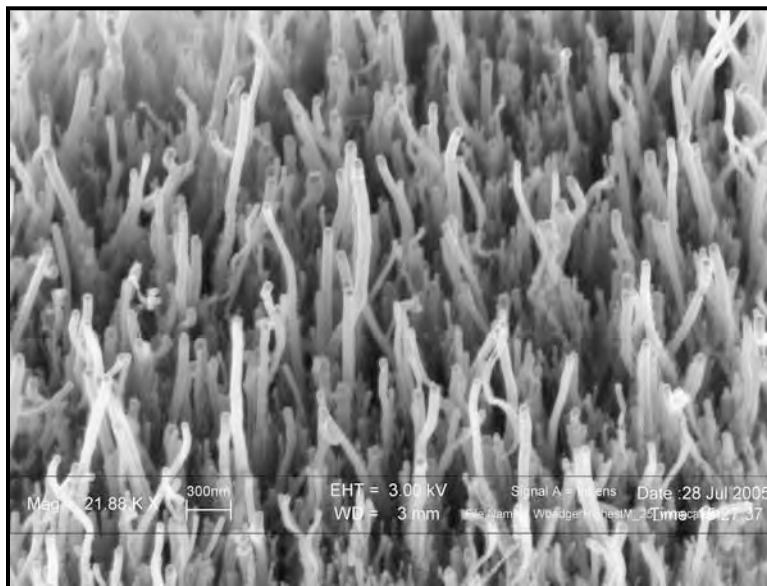
Figure 3. CNFs under magnification [10]
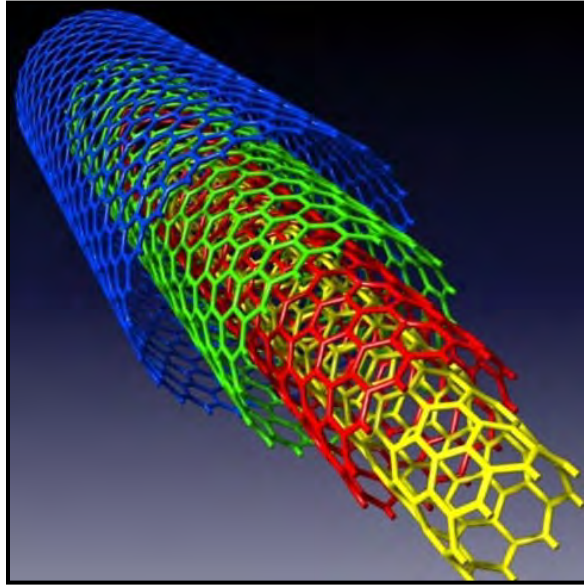
Figure 4. MWNT [8]

The testing process began by specimen preparation, initial EMI testing, followed by fatigue testing at different percentages of UTS with a constant stress ratio. Each specimen was subjected to a prescribed number of fatigue cycles followed by EMI testing to characterize the effects of EMI at intermediate fatigue cycles. Fatigue tests and EMI tests were run to failure or to a maximum number of cycles (i.e. 600,000 cycles were reached.

1.5 Summary

This thesis is divided into five chapters. Chapter I covers the introduction of space vehicle systems and the space vehicle materials used. The historical background of composites and nanocomposites with the requirement to find a nanocomposite that has EMI shielding properties. Chapter II discusses the literature review of the space environment, EMI, CNTs and CNFs composites, other relevant research topics, and

focused beam tunnel testing results. Chapter III will mention specimen preparation, EMI and fatigue test procedures and test equipment. Chapter IV will cover the analysis and results from testing the nanocomposites EMI effects under fatigue. Finally, chapter V will summarize the conclusions of this study.

II. Literature Review

2.1 Space Environment

Space exploration presents many challenges when designing space vehicles. Specifically, the space environment is hostile with particle charged solar winds, extreme temperatures, radiation, and space debris [11]. Today's space vehicles contain electromechanical systems and increasingly more microelectronics onboard that are sensitive to the harsh space environment.

The Earth's space environment is defined as a plasma. Understanding Earth's space plasma environment is critical to space vehicle design. A plasma is defined as a gas of charged particles, which consists of equal numbers of free positive and negative charge carriers [12]. Space vehicles will interact with this space plasma and become charged [13].

The Earth's space weather is controlled by the Sun in the form of solar winds. Solar winds are constantly emitted by the Sun known as a highly conductive plasma at supersonic speeds of about 500 kilo-meters per second into the interplanetary space as a result of supersonic expansion of the solar corona [12]. The highly conductive emitted plasmas from the Sun disturb the Earth's space plasma and cause geomagnetic storms and substorms. The disturbed space plasmas can adversely react with space vehicles and affect electromagnetic wave communications and even lead to power failures on the space vehicles.

Historically, sudden failures of geosynchronous communication satellites, such as ANIK-1, AT&T Telstar, and Motorola Galaxy-4 were caused from solar maxima and solar coronal mass ejection cloud passages that led to the loss of communication services to millions of customers [14]. Shown in Figure 5 is the Sun-Earth relationship and how the Sun's solar winds impact Earth's space plasma.
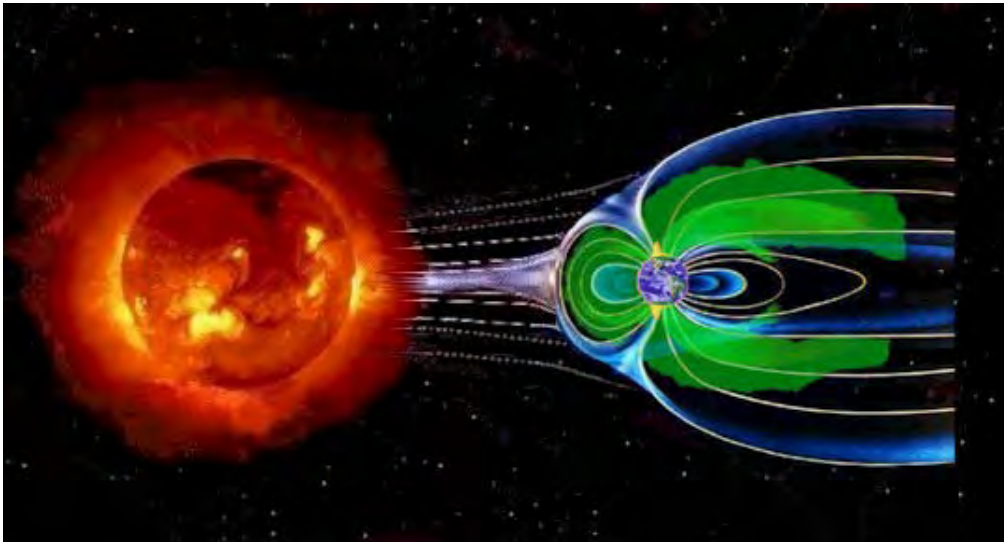
Figure 5. Sun-Earth connection [15]

Space vehicle's electronics must be designed to operate in space's extreme temperatures. In cold temperature applications electronic circuits must be designed with the aiding of heating systems onboard to operate down to -190 °C (83 K). In hot temperature applications electronics must be designed with the aiding of cooling systems onboard to operate up to 200 °C (473 K) [16].

The radiation in space near Earth can be broken down into two environments. The first one can be classified as trapped radiation environment and the second one can be classified as the transient radiation environment. The trapped environment is due to the Earth's magnetic field confining charged particles to certain regions in space called

"Van Allen Belts." These "Van Allen Belts" will generally be one proton and two electron belts and can temporarily change with large solar events [17]. The effects of radiation on electronics are described by the total ionizing dose. Radiation deposits energy thus moving the electrons to a higher energy state. This higher energy state makes the space vehicle's available for conduction and mobile inside of nonconductive materials [17]. The effects of radiation can change the material's mechanical and electrical properties and lead to mechanical failure and increased EMI during the lifetime of a space vehicle system [9]. To mitigate this total ionizing dose effects engineers use EMI shielding materials.

Space debris is a ever growing problem that current and future space vehicle systems must combat. Space debris, better known as space junk, consists of broken satellite components and discarded rocket boosters. It is reported that more than 13,000 objects occupy the Earth's orbit larger than 10.16 centimeter (cm) (4 inches (in)) in diameter, and millions of paint chip-like pieces that are smaller than 1 cm (0.39 in) [18]. A critical part to U.S. Strategic Command's mission consists of detecting, tracking, cataloging, and identifying space debris.

As the call for increased space vehicle capabilities drives future requirements for stronger and lighter materials, designers still have to mitigate the risks and design issues stemming from space's harsh operating environment. Nanocomposites have the potential to offer relief in this area of research.

2.2 Electromagnetic Interference

EMI is an undesired disturbance that affects the electrical circuits used onboard in space vehicle systems. This transfer in energy can come from radiation, conduction, or induction. In the case of electromagnetic radiation, this is emitted from the ionizing radiation that is abundant in space's harsh environment. This undesired disturbance can have a costly effect on space vehicle systems by degrading the performance of the electrical systems found onboard from critical data loss to permanent damage. The ionized radiation strips electrons from atoms in the space plasma, creating charged particles. When the conductive space vehicle materials are exposed to the charged particles in the space plasma the positively and negatively charge surfaces attract ions opposite in charge [19]. The surfaces build up these charges until electrical discharge occurs on the surface. This electrical discharge leads to EMI on the space vehicle if the surface materials don't have effective EMI shielding. Equation 1 is the Poisson equation that explains this charge relationship.

$$\nabla^2 \phi = -4\pi\rho \qquad (1)$$

where

ϕ is the potential

ρ is the charge density

Several ways to prevent EMI is through source elimination, grounding, filters, and shielding [20]. In the case of shielding EMI, carbon nanocomposite materials offer electrical properties that aid in EMI shielding due to their highly conductive nature. The

14

current requirement of EMI SE for space vehicle structures is greater than 60 dB. It is important to consider the effects of reflection and absorption when analyzing the effects of EMI. The reflected radiation can be characterized by the impedances of the incident medium and the material through the following equation.

$$R = \left(\frac{Z_a - Z_m}{Z_a + Z_m}\right)^2 \qquad (2)$$

where

R is reflected radiation

Z_a is the impedance of air

Z_m is the material impedance

The absorption is related through the skin depth in which the radiation penetrates the material by the following relationship.

$$\delta = \sqrt{\frac{1}{\pi f \mu \sigma}} \qquad (3)$$

where

δ is absorption

μ is the magnetic permeability

f is the frequency

σ is electrical conductivity

The higher the electrical conductivity (σ) and the lower the material's impedance (Z_m) leads to higher EMI SE. CNTs and CNFs are promising materials in this respect.

Research conducted by Park *et al*. showed that as the volume fraction of CNTs increased the conductivity increased by a power law relationship of percolation type behavior [21]. Figure 6 shows the results from this electrical conductivity tests.
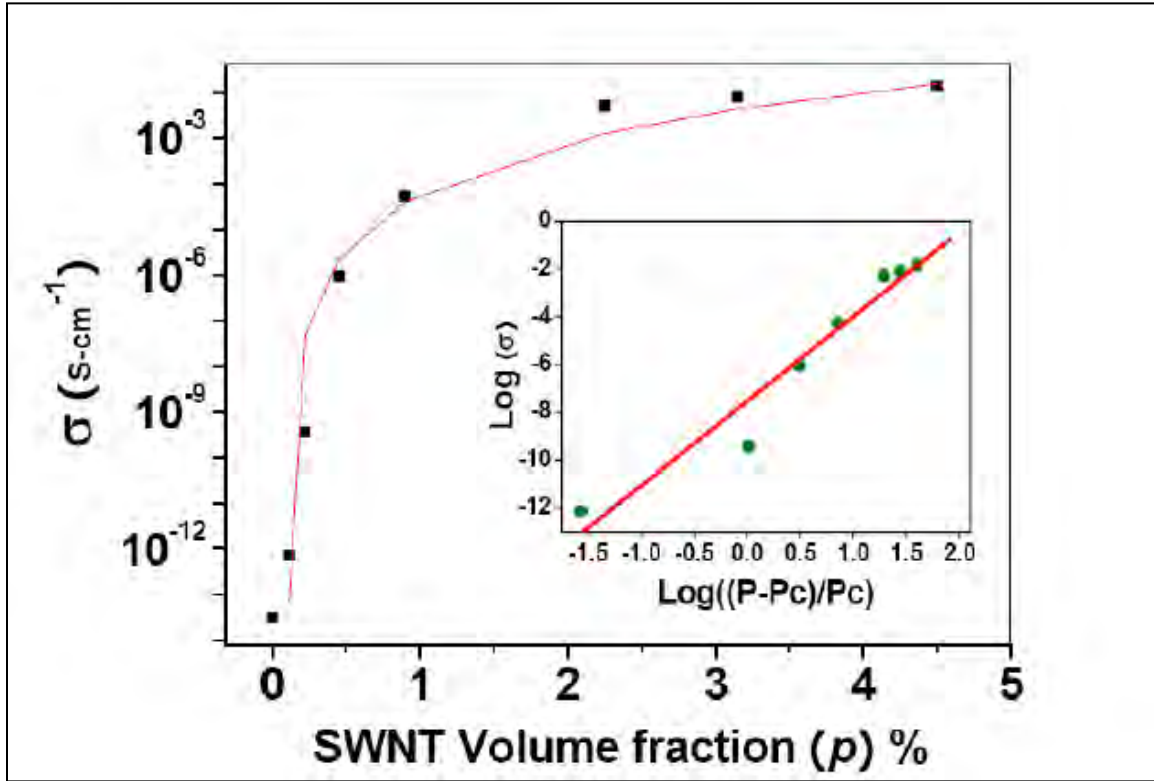
Figure 6. Electrical conductivity of SWNT composite [21]

Park *et al*. also showed the relationship of increased volume fraction of CNTs and SE when measured in the microwave (X-band) frequency range of 8.2 GHz to 12.4 GHz. The results showed an increase in SE with an increased volume fraction of CNTs. Shown in Figure 7 are the results from Park *et al*. study.
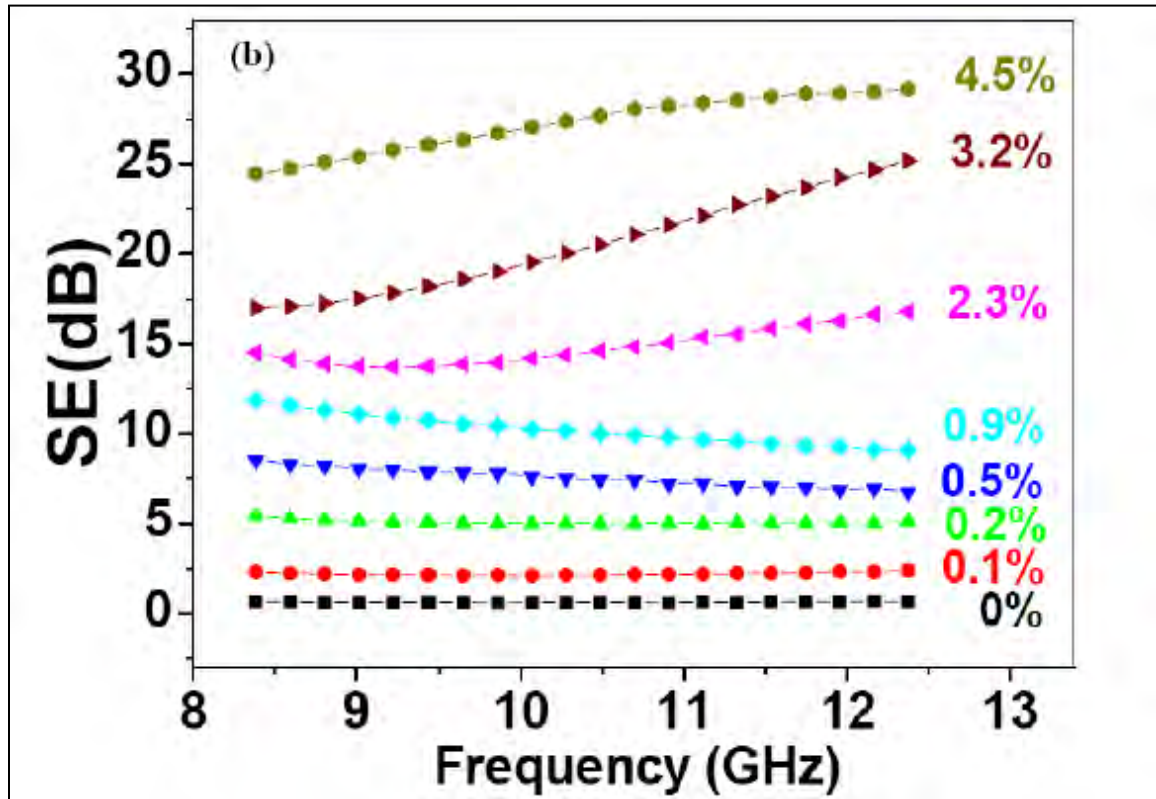
Figure 7. EMI compared to CNT volume fraction [21]

2.3 Carbon Nanotubes and Carbon Nanofibers Composites

SWNT is the simplest case of carbon nanotubes configuration in nature. It is made up a single strip of graphene that is rolled into a hollow tube [22]. Shown in Figure 8 is a schiematic of how the graphene sheet wraps around and forms a carbon lattice hollow tube configuration known as SWNT. This configuration depicted in Figure 8 is called a zigzag configuration. The SWNT structurally has been classified with armchair (n,n), zigzag (n,0), and chiral (n,m), where a graphene sheet is wrapped by a pair of indices. The diameter of a SWNT can be determined from its (n,m) indices by using Equation 4.

17

$$d = \frac{a}{\pi}\sqrt{n^2 + nm + m^2} \qquad (4)$$

where

        d is the diameter (nm)

        a is equal to 0.246 nm

        n is an index

        m is an index
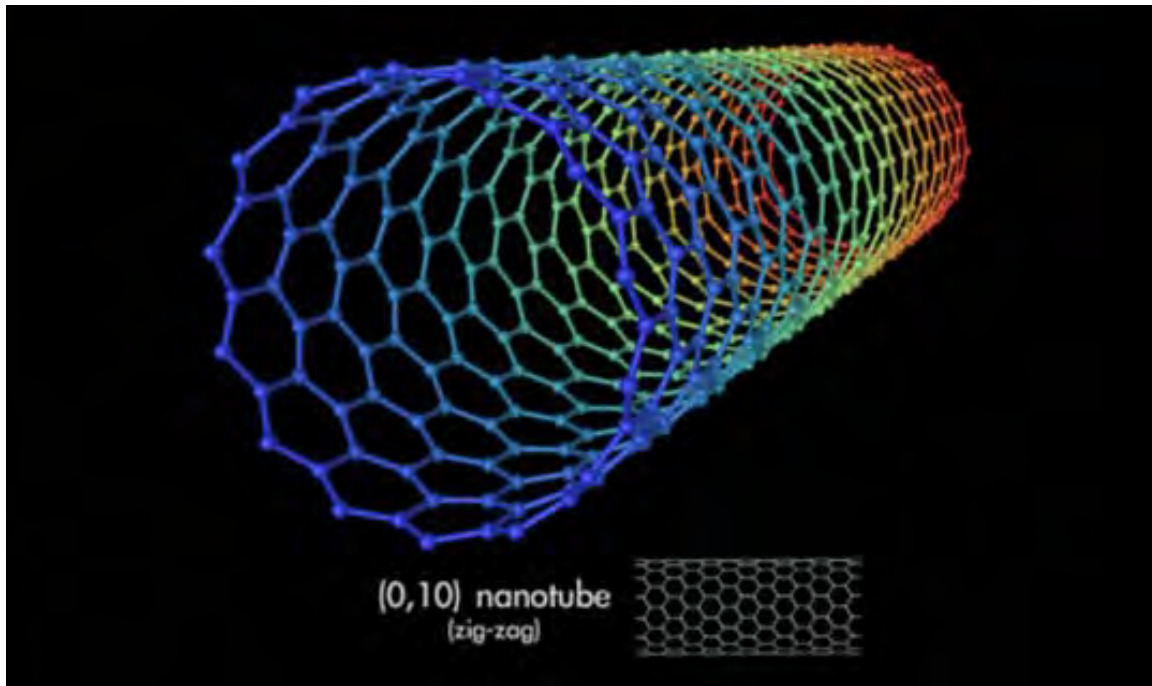
Figure 8. SWNT [23]

The advancement of CNTs has come a long way since 1991. First reported in 1991, MWNTs came in different lengths and diameters [24]. In the last two decades scientists have researched the synthesis process and made leaps and bounds on how to produce SWNT, MWNTs, and CNFs at various diameters, lengths, and the weight concentrations to meet the desired mechanical, electrical, optical, chemical, and thermal

properties required for the various applications. The common synthesis methods for

producing CNTs involve high temperatures, including the carbon arc discharge, pulsed-

laser vaporization of graphite, thermal or plasma-assisted chemical vapor deposition,

high-pressure carbon monoxide decomposition [25]. Due to the fact that CNTs are

practically synthesized at the atomic level this opens the door for a wide range of

applications. CNFs are in the same class of MWNTs but produced by a floating catalyst

method. The graphene sheets are synthesized to stack onto each other forming a hollow

tube fiber configuration. Like CNTs, CNFs show improved mechanical, electrical,

thermal, and optical properties when compared to traditional carbon fibers. Due to the

fact that CNFs are discontinuous and highly graphitic this warrants them to be highly

compatible with a majority of polymer processing techniques [26]. Figure 9 depicts high

resolution tunneling electron microscope (HRTEM) image of PR-25 CNF.
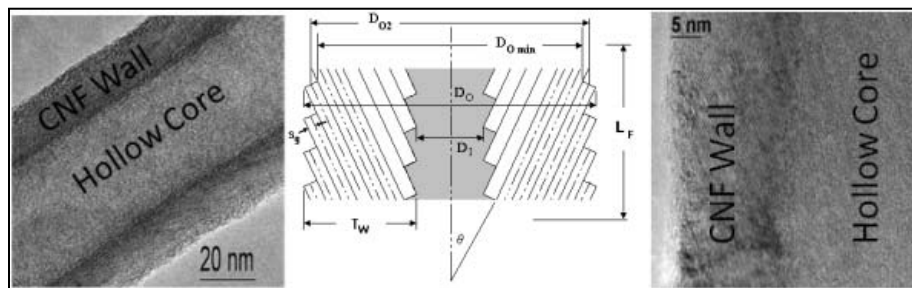
Figure 9. HRTEM images of PR-25 CNFs [26]

2.4 Relevant Previous Research

Air Force Institute of Technology (AFIT) and the Materials and Manufacturing

Directorate of the AFRL are the first to research the effects of different mechanical

loadings, thermo-mechanical, EMI shielding, radiation, and electrical conductive performance on different configurations of nanocomposites for satellites.

Two AFIT students, Harder and Rodriguez, conducted research on nickel nanostrands (NS) based nanocomposites. The NS nanocomposites consisted of M55J graphite fibers and NS reinforced in RS-3 polycyanate resin. The control specimen was configured as a symmetric 8 ply layup of carbon fibers (M55J) and toughened polycyanate (RS-3) resin with its fibers oriented at 0/90/45/-45 degrees. The other three nanocomposites had NS layers on the (1) exterior, (2) midplane (between -45° plies), (3) interlaminar (between 0° and 90° laminates and between the 45° and -45° laminates) [27].

Harder researched the effects of EMI SE and resistivity before, during, and after monotonic tension tests [28]. Harder also researched the effects of ultimate tensile strength and EMI SE before and after exposure to the space environment [28]. Rodriquez researched the effects of the resistivity and EMI SE while under fatigue.

Chong investigated the effects of EMI SE under monotonic tension tests and thermal fatigue on three nanocomposites and a composite control specimen. The three nanocomposites configurations consisted of MWNT plies and S-glass (Astroquartz II) fiber in CYCOM 5575-2 cyannate ester matrix plies. The MWNTs were about 8-15 nm in diameter, 700 μm long, 90% weight percentage, and a concentration of 18.3 g/m^2 of CNTs. The control specimen composite was S-glass (Astroquartz II) fiber in CYCOM 5575-2 cyannate ester matrix will be referred to as 8G. Depicted in Figure 10 is the configuration and shorthand nomenclature for these four different composites.

20

a	b	c	d
Glass (0°/90°)	Glass (0°/90°)	CNT	Glass (0°/90°)
Glass (0°/90°)	CNT	CNT	Glass (0°/90°)
Glass (0°/90°)	Glass (0°/90°)	Glass (0°/90°)	Glass (0°/90°)
Glass (0°/90°)	CNT	Glass (0°/90°)	Glass (0°/90°)
Glass (0°/90°)	Glass (0°/90°)	Glass (0°/90°)	CNT
Glass (0°/90°)	CNT	Glass (0°/90°)	CNT
Glass (0°/90°)	Glass (0°/90°)	CNT	CNT
Glass (0°/90°)	CNT	CNT	CNT
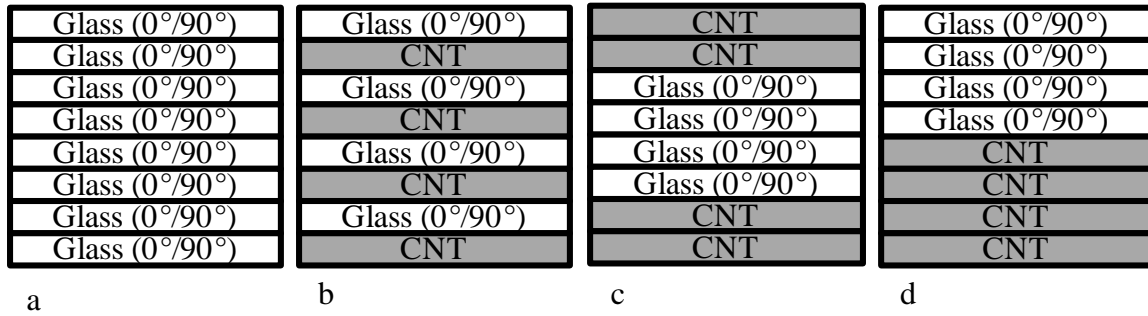
Figure 10. Composites: (a) 8G, (b) (G/CNT)$_4$, (c) 2CNT/4G/2CNT, (d) 4G/4CNT

Results have shown that CNTs possess improved mechanical, electrical, thermal, and optical material properties when compared to traditional carbon filaments not synthesized at the nano-scale level.

2.4.1 Monotonic Tension Testing of M55J/RS-3 with Nickel Nanostrands

Harder machined the four different configured composites into 15.25 cm x 2.7 cm (6 in x 1 in) test specimens with an average thickness of 0.1016 cm (0.04 in). EMI measurements were conducted before and after each monotonic tension test. Shown in Figure 11 are the EMI SE results when tested under monotonic tension tests. The test results show that the exterior configuration showed the best EMI SE performance compared to the other test specimens in the study.
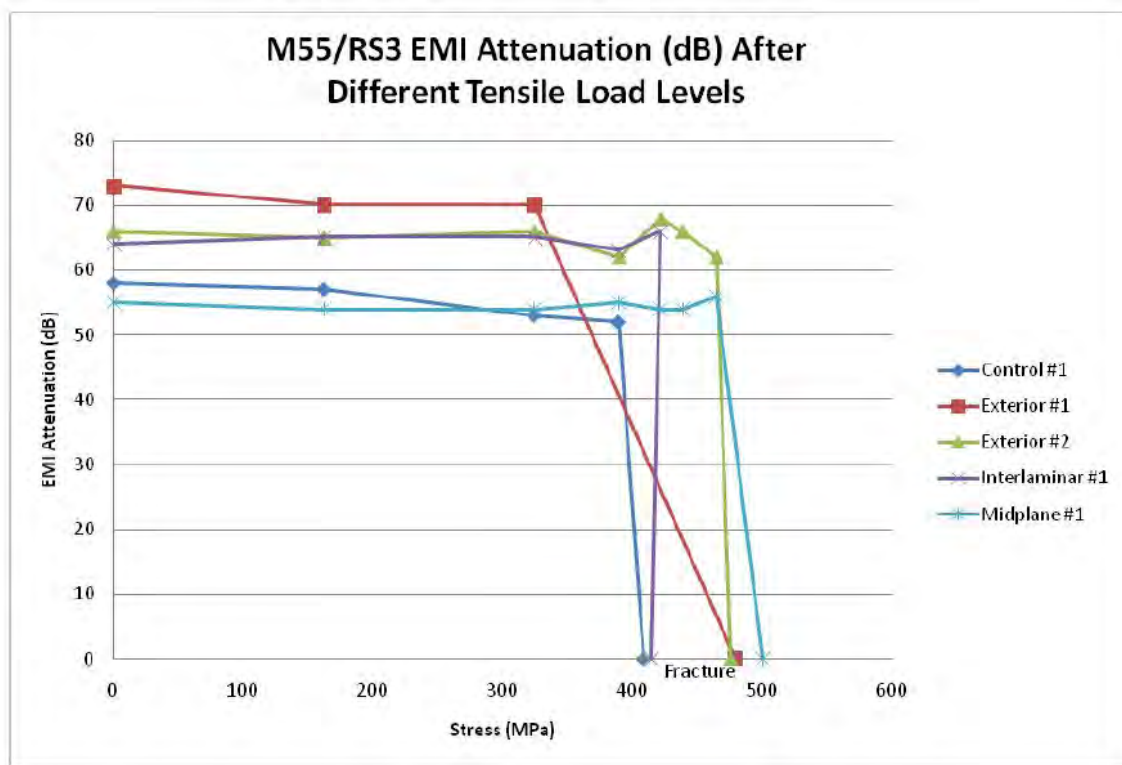
Figure 11. Harder's EMI SE under monotonic tension test results [28]

2.4.2 Fatigue Testing of M55J/RS-3 with Nickel Nanostrands

Rodriguez machined the four different configured composites into 15.25 cm x 2.7 cm (6 in x 1 in) test specimens with an average thickness of 0.1016 cm (0.04 in). EMI measurements were conducted before and after fatigued tests at 60%, 75%, and 90% UTS with a 0.1 stress ratio on the four configured composites. Shown in Figures 12, 13, and14 are the EMI results from Rodriguez's research versus total number of fatigue cycles for 60%, 75%, and 90% UTS respectively. The test results showed that the exterior configuration had the highest initial and final EMI SE results for all the selected stress levels. All three NS layered configurations responded well to the effects of EMI SE under fatigue.

22
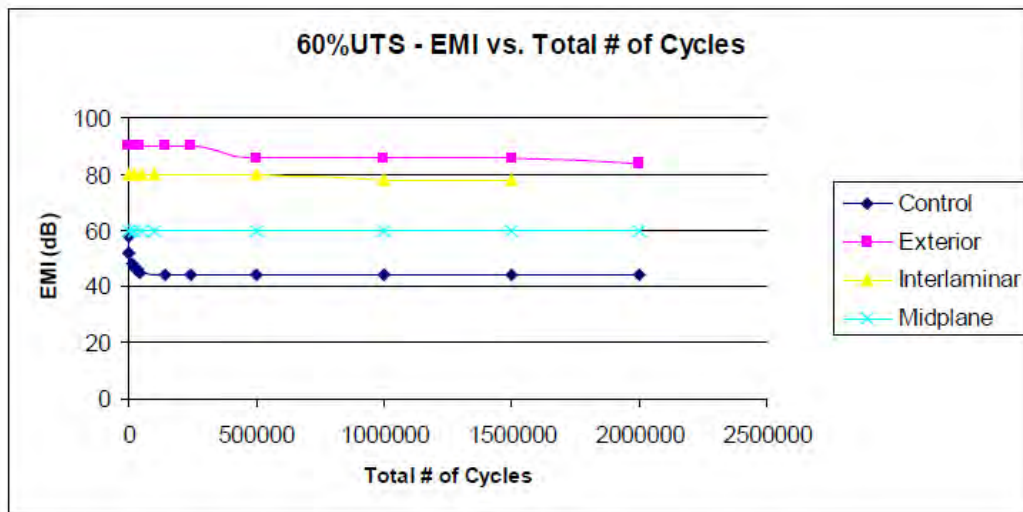
Figure 12. Rodriguez's 60% UTS EMI versus total cycles results [27]
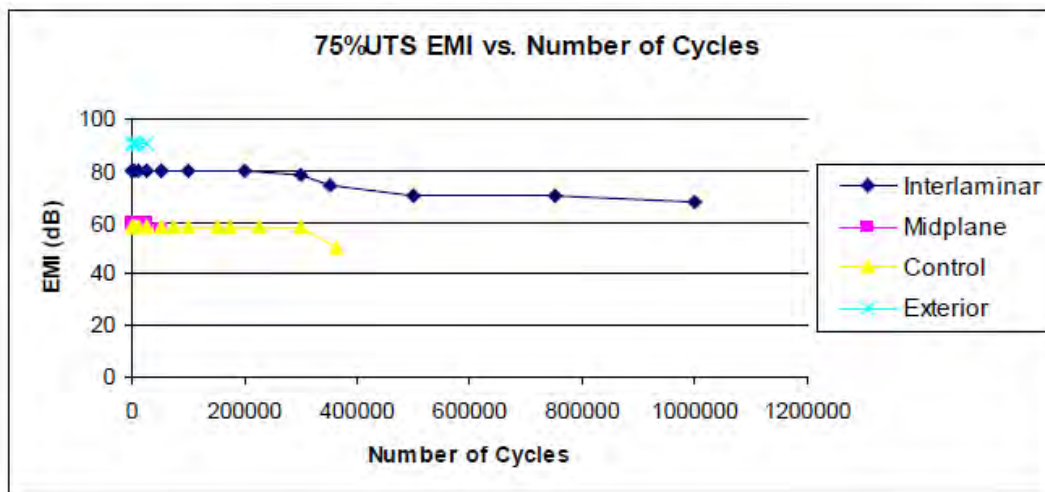
Figure 13. Rodriguez's 75% UTS EMI versus total cycles results [27]
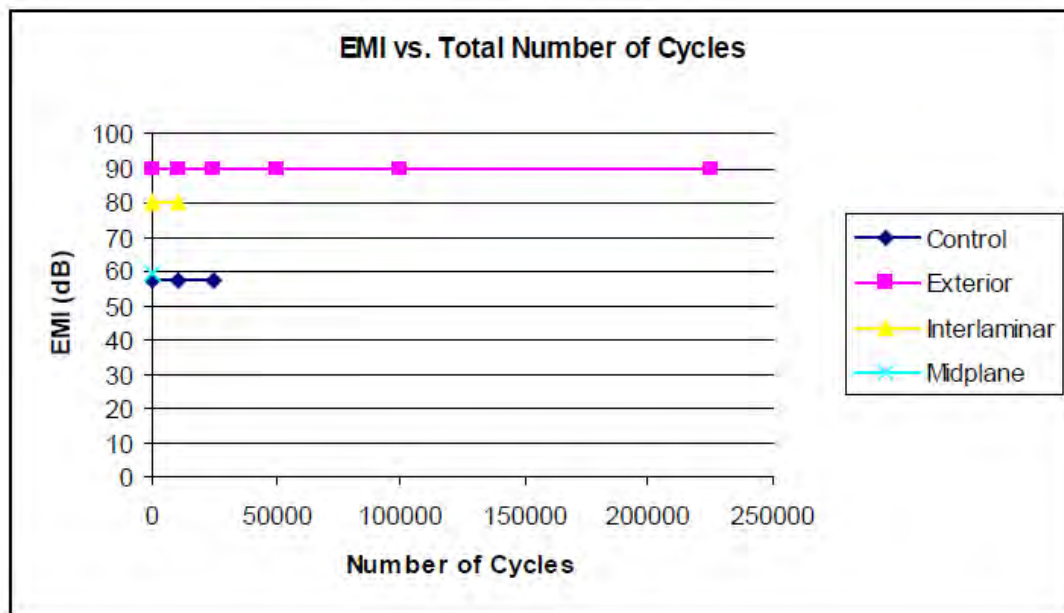
Figure 14. Rodriguez's 90% UTS EMI versus total cycles results [27]

2.4.3 Monotonic Tension Testing of Carbon Nanotubes

Chong machined the four different composites into 15.24 cm x 2.54 cm (6 in x 1 in) test specimens with an average thickness of 0.1215 cm (0.0478 in). Chong characterized the effects of EMI shielding under monotonic tension load, thermal cycling, and a combination of thermal cycling followed by monotonic tension load [29]. A baseline EMI measurement was taken prior to conducting monotonic tension load, thermal cycling, and the combination of thermal cycling followed by tension load. All the EMI measurements were conducted using a PNA wave guide analyzer in the X-band frequency range of 8.2 GHz to 12.4 GHz. The monotonic tension tests consisted of incrementally increasing the load until complete failure using a MTS 810 servo-hydraulic test machine rated for a load capacity of 22 kips (98 kN) [29]. The thermal cycling tests were conducted with a total soak time of 20 seconds with the first 10 seconds at +60 °C

24

and the last 10 seconds at -60 °C on a ThermoJet ES Precision Temperature Cycling

System. 17,500 thermal cycles were run on each composite. The initial EMI

measurements in dB for the four different composites are shown in Table 1 along with

the average results for the thermal cycling and/or monotonic tension tests until failure

[29]. Chong's results showed that the MWNT nanocomposite configured with

2CNT/4G/2CNT showed the best results for EMI shielding.

Table 1. Chong's EMI results

Composite	Initial EMI (dB)	Post EMI (dB)
8G	0.33	1.01
(G/CNT)$_4$	71.76	68.45
2CNT/4G/2CNT	87.5	83.49
4G/4CNT	87.5	60.98

2.4.4 Focused Beam Tunnel Testing

Focused beam tunnel testing is relevant to get a baseline measurement of the EMI

for all the different nanocomposites. The focused beam tunnel test equipment was

custom made by Georgia Tech Research Institute. Shown in Figure 15 is the focused

beam tunnel testing equipment.
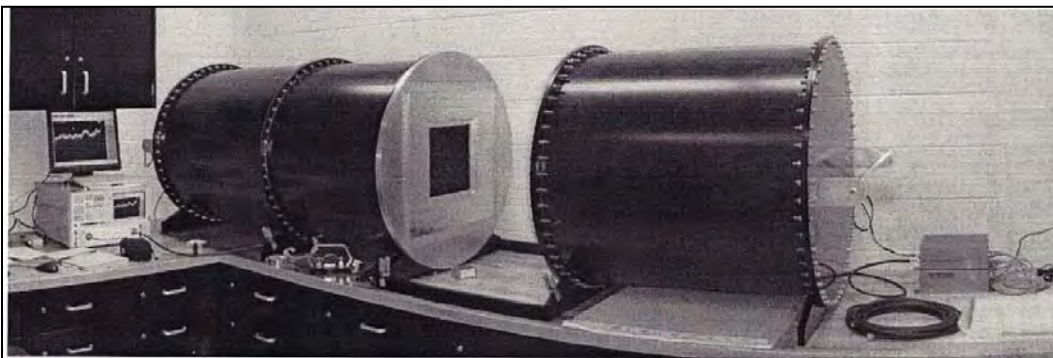
Figure 15. Focused beam tunnel test equipment

The focused beam tunnel test is located at AFRL's Materials Directorate, Wright-Patterson Air Force Base (AFB), Ohio (OH). Each of six nanocomposite specimens were cut into 12 in by 12 in panels and tested by an AFRL/RX laboratory technician. The technician performed calibration on the focused beam tunnel tester first, followed by the actual tests on the six nanocomposites. The tests were performed in the frequency range of 2 GHz to 18 GHz in increments of 10 MHz. Figure 16 are the test results from the focused beam tunnel tests.
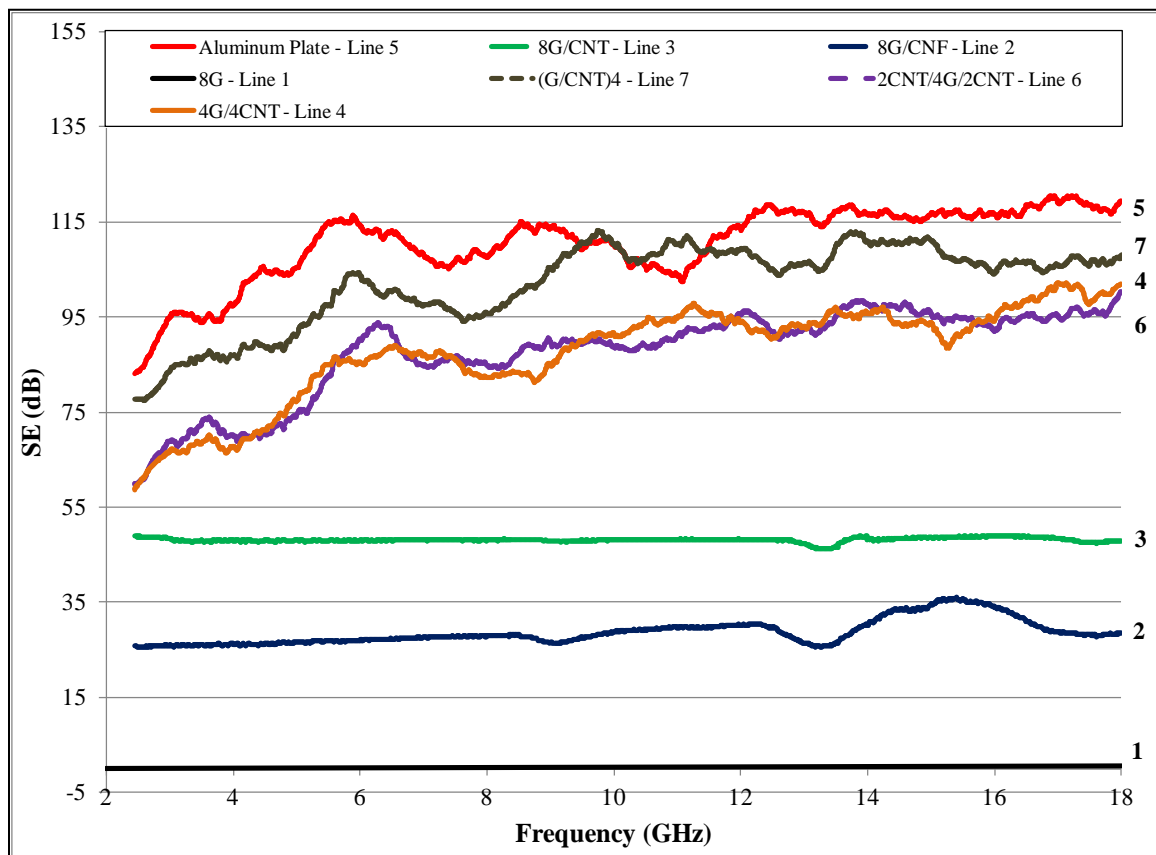
Figure 16. Focused beam tunnel test results

The focused beam tunnel tests show EMI SE of the six nanocomposites tested in this research compared against aluminum which is used as a conductive material in space vehicle systems to mitigate EMI. The short hand notations in Figure 16 for 8G,

(G/CNT)$_4$, 2CNT/4G/2CNT, and 4G/4CNT are the same stacking sequence shown in Figure 10. Refer to Appendix F for focused beam tunneling test procedures.

2.5 Summary

The space environment is a challenging place for electronic systems to operate effectively without any EMI disturbances. Space vehicle systems are subject to charged solar winds, extreme temperatures, radiation, and space debris. With all the onboard electronics it is critical to find material solutions that provide EMI shielding protection from the present ionizing radiation found in the space plasma.

EMI mitigation requires researching materials that are highly conductive in nature, and display high strength to weight ratios to reduce the weight of the overall space vehicle. Composites configured with CNTs and CNFs have shown promise by offering a high conductive material that leads to EMI shielding attributes and a high strength to weight ratio compared to traditional composites that don't offer conductive nanomaterials.

Current and past research support the proposal to use composites configured with NS, CNTs, or CNFs in space vehicle systems to mitigate EMI and reduce the weight of the overall system. Past test results have shown that EMI shielding is barely affected by monotonic tension up to failure, thermal cycling, and cyclic fatigue at a large number of cycles for the different configured nanocomposites.

This thesis will cover the research on the EMI effects of CNTs and CNFs composites under fatigue. Thus this research will complement the past and current

research conducted to identify which nanomaterial and configuration offers the best

material option for future space vehicle applications.

III. Methodology

3.1 Introduction

The intent of this chapter is to provide the reader the details of test specimen preparation and testing procedures. This chapter will cover the specimen preparation, EMI test equipment and procedures, fatigue test equipment and procedures. Specimen preparation and fatigue testing occurred at AFIT, located at Wright-Patterson AFB, OH. EMI testing were conducted at the AFRL's Materials and Manufacturing Directorate, located at Wright-Patterson AFB, OH.

3.2 Specimen Preparation

The first type of test specimens consisted of a nanocomposite manufactured from Nanocomp Technologies, Inc. (NTI) based at Concord, New Hampshire. The nanocomposite consisted of a external ply of MWNTs and SWNTs deposited on eight plies of 6781 S-2 glass fiber in CYCOM 5250-4 BMI matrix. The CNTs were about 25 nm in diameter and 1 mm long. The CNTs were about 0.1 mm thick and contained 20 g/m^2 concentration of CNTs. The shorthand notation, 8G/CNT, will be used to identify this nanocomposite.

The second type of test specimens consisted of a nanocomposite manufactured from Applied Sciences Inc. (ASI) based out of Cedarville, OH. The nanocomposite consisted of a external ply of CNFs deposited on eight plies of 6781 S-2 glass fiber in CYCOM 5250-4 BMI matrix. The CNFs were about 100 nm in diameter and 100 μm

long. The CNFs were about 0.1 mm thick and contained 20 g/m^2 concentration of CNFs.
The shorthand notation, 8G/CNF, will be used to identify this nanocomposite.

The last four composites consisted of a composite manufactured by NTI. The
first of the four composites was the control specimen, i.e. baseline, with all the eight plies
being S-glass (Astroquartz II) fiber in CYCOM 5575-2 cyanate ester matrix, and will
have a shorthand notation 8G. The last three composites were different stacking
sequences of MWNT plies with S-glass (Astroquartz II) fiber in CYCOM 5575-2 cyanate
ester matrix. The first nanocomposite out of the three was an alternating ply of S-glass
(Astroquartz II) fiber in CYCOM 5575-2 cyanate ester matrix and a ply of CNTs, and
will have a shorthand notation (G/CNT)$_4$. The second nanocomposite out of the three
was a symmetrical laminate of two external plies of CNTs with two plies of S-glass
(Astroquartz II) fiber in CYCOM 5575-2 cyanate ester matrix, and will have shorthand
notation 2CNT/4G/2CNT. The last nanocomposite out of the three was four plies of S-
glass (Astroquartz II) fiber in CYCOM 5575-2 cyanate ester matrix stacked on four plies
of CNTs, and will have a shorthand notation 4G/4CNT. The S-glass (Astroquartz II)
fiber was made from 99.95% SiO_2 quartz crystals which was fabricated into a 3-harness
satin weave. The CNTs in the three other nanocomposites had an estimated length of 700
μm and a diameter of 8-15 nm, 90% weight percentage, and a concentration of 18.3 g/m^2.
The average thickness of the CNT ply was 84.49 μm. The average thickness of the
glass/epoxy ply containing warp strands was 212.53 μm, while the average thickness of
the glass/epoxy ply containing fill strands was 271.25 μm. The total average thickness
for the entire eight ply composite was 1.215 mm (0.048 in).

Figure 17 shows schematically the configuration of all six types of composites as described and which were used in this study. Refer to Appendices A-E for material properties on the glass fibers, matrix, and CNTs described above for the six different composites manufactured for this research.
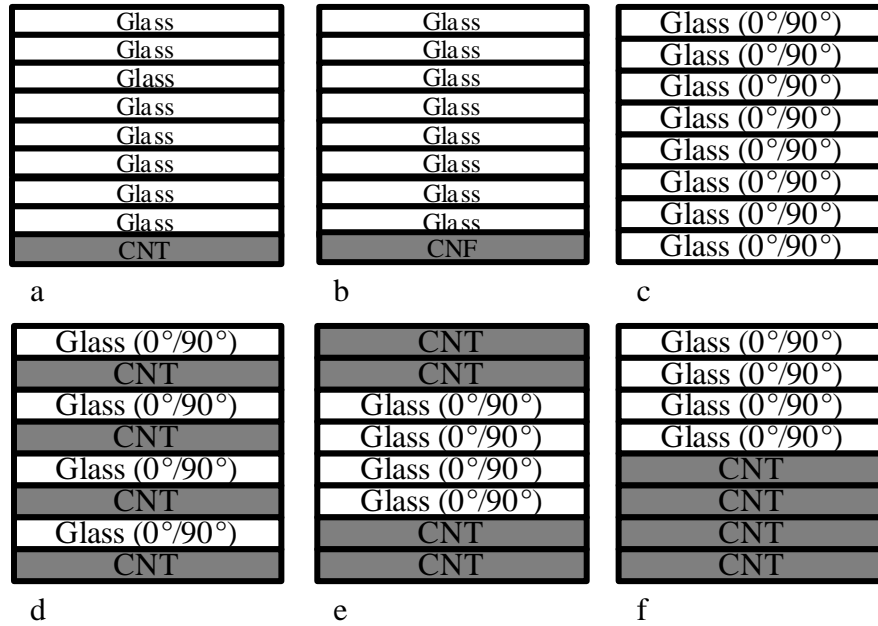
Figure 17. Composite configurations: (a) 8G/CNT, (b) 8G/CNF, (c) 8G, (d) (G/CNT)$_4$, (e) 2CNT/4G/2CNT, (f) 4G/4CNT

All six different composites were manufactured as 30.48 cm (12 in) by 30.48 cm (12 in) panels by NTI and ASI. The test specimens were machined into 2.54 cm (1 in) by 15.24 cm (6 in) strips by a water jet cutter or diamond circular blade cutter by a technician at the AFIT machine shop. Four 8G/CNF test specimens, and three test specimens each of 8G/CNF, 8G, (4G/CNT)$_4$, 2CNT/4G/2CNT, and 4G/4CNT were cut for a total of 20 test specimens. To prevent damage from potential surface cracks and premature failure from gripping the test specimens during fatigue testing, 2.54 cm (1 in) by 2.54 cm (1 in) glass/epoxy composite tabs were adhered to the ends of the test

specimens on both sides with M-bond 200 catalyst and M-bond 200 adhesive. AFIT

provided the M-bond 200 catalyst, M-bond 200 adhesive, and the glass/epoxy composite

tabs. Figure 18 illustrates a test specimen with the glass/epoxy composite tabs.
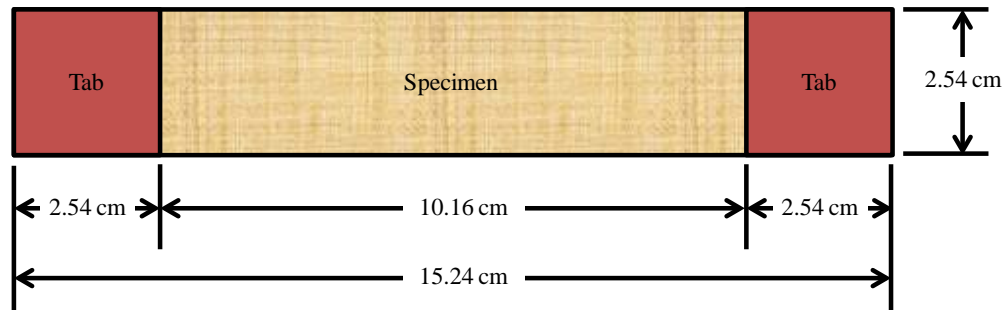
Figure 18. Composite test specimen

3.3 EMI Test Equipment and Procedures

EMI tests were conducted at the AFRL Materials and Manufacturing Directorate's

Characterization Lab in building 654, room 324. The test specimens were analyzed by

using a Agilent PNA Microwave Network Analyzer that handles the frequency range

from 10 MHz to 20 GHz at room temperature. Each specimen was analyzed with the

PNA Microwave Network Analyzer before and after a desired number of fatigue cycles

were applied. The PNA Microwave Network Analyzer was calibrated with a X11644A

WR-90 calibration kit which is listed in Table 2, including all the other test equipment

used to analyze EMI. The general definitions, mechanical and electrical characteristics of

the X11644A WR-90 calibration kit can be accessed by clicking this link:

http://cp.literature.agilent.com/litweb/pdf/11644-90371.pdf. The data sheet for the

Agilent PNA Microwave Network Analyzer can be accessed by clicking this link:

http://cp.literature.agilent.com/litweb/pdf/5988-7988EN.pdf. For a complete version of

the PNA Help User's and Programming Guide follow this link:

http://na.tm.agilent.com/pna/help/PNAHelp9_33.pdf.

Table 2. EMI calibration and test equipment

Description	Qty	Agilent Part Number
EMI Calibration Equipment (X11644A WR-90)		
Short	1	11644-20018
1/4 Wavelength shim	1	11644-20021
EMI Test Equipment (PNA Network Analyzer)		
PNA Network Analyzer (10 MHz to 20 GHz) (see Figure 19)	1	E8362B
3.5mm (F) to 7 mm test port return cables (see Figure 20)	2	85132E
7 mm coax-to-waveguide adapter (see Figure 21)	2	X281C Option 006
8-32 Philips head drive screw (1.0 in length)	4	NA
8-32 hex nut	4	2580-0002
Philips head screw driver	1	NA
1/4 wrench	1	8720-0014
Computer Monitor (Optional)	1	NA
Keyboard (Optional)	1	NA
Mouse (Optional)	1	NA

Figure 19. PNA Microwave Network Analyzer

Figure 20. PNA Microwave Network Analyzer cable

Figure 21. PNA Microwave Network Analyzer adaptor

Before starting calibration ensure that the frequency range is set from 8.2 GHz to 12.4 GHz and proper trace, S_{12} is selected. Refer to Appendix G for the detailed steps on how to set the frequency range, calibrate the PNA Microwave Network Analyzer and run the EMI tests.

The two port measurement is a transmission measurement. In this case the setting is a S_{12} where the first subscript represents the PNA port number where the device signal output is measured. The second subscript represents the PNA port number where the device signal input is applied (incident) to the device (source). The output measurement is provided in negative dB values for each step in the frequency range. Equation 5 represents this EMI SE relationship in dB:

$$SE(dB) = 10Log_{10}\frac{P_{in}}{P_{out}} = 10Log_{10}\frac{P_{Port\,2}}{P_{Port\,1}} \qquad (5)$$

Where

34

SE is the EMI SE (dB)

P_{in} is the measured output frequency power into port 2

P_{out} is the measured frequency power transmitted from port 1

All 20 of the 2.54 cm (1 in) by 15.24 cm (6 in) test specimens were labeled into three equal sections identified as a top, middle, and bottom section. Each section of the specimen was measured between 3 to 5 times, for a total of 9 to 15 .prn files, and the average EMI was calculated for the different sections as well as the overall EMI average for the test specimen. The .prn files recorded the measurements as negative dB values and converted to the reciprocal (positive) value, which is more commonly used to represent EMI SE. Figure 22 shows the schematic of the PNA Network Analyzer setup.
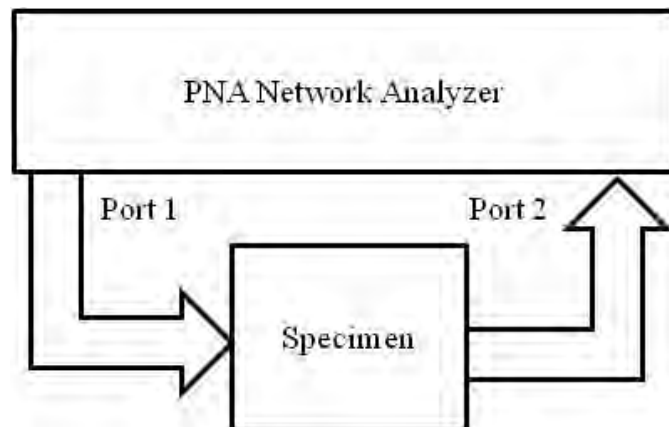
Figure 22. PNA Network Analyzer schematic setup

Shown in Figure 23 is the complete setup of the PNA Network Analyzer.

Figure 23. PNA Network Analyzer test setup

The saved .prn EMI files are text files that can be transferred to Excel files to conduct further data analysis. A single EMI specimen test conducted on the PNA Microwave Network Analyzer would generate between 9 and 15 .prn text files. To minimize the importing time, MATLAB code was written to take the .prn files and load them directly into Excel files. The MATLAB code was written into two .m files. The first .m file pulled the data off the .prn text files and imported directly into MATLAB. The second .m file calculated the average from all the .prn text files and then exported the EMI data into an Excel file. Please refer to Appendix H for the detailed MATLAB code.

3.4 Fatigue Test Equipment and Procedures

Fatigue testing was conducted using a Material Test System (MTS) 810 in the AFIT building 640, room 271. Two servo hydraulic MTS machines were used in this research. One had a capacity of 22 kips (98 kN), while the second one had a capacity of 5 kips (22 kN). A configuration file was created with the Station Builder program for

both MTS machines. In accordance with the manufacturer's instructions both MTS

machines were warmed up for 30 minutes in displacement mode at a target amplitude of

6.35 mm (0.250 in), 2 Hz frequency, and square wave input using the MTS 793 software

program. A screen shot of the Station Manager's main screen is shown in Figure 24.
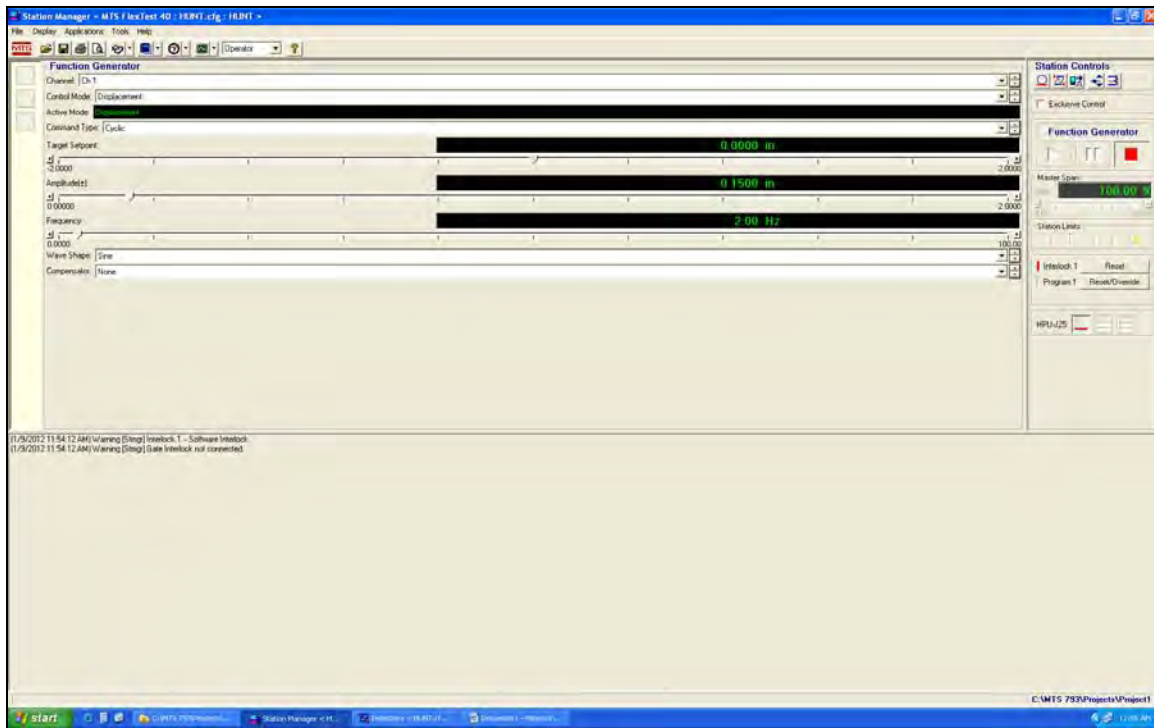
Figure 24. Station Manager screen shot

After warm-up of the MTS machine was completed the next important step is to

tune the MTS machine for the specimen either by auto-tuning or by manually tuning.

Manual tuning is generally not required to tune the MTS machine for testing the

specimens identified in this research. If manual tuning is required, refer to the MTS help

files, conveniently located by clicking the MTS software's help button. Tuning is only

required if the MTS was not tuned previously for the same type of test specimen or the

fatigue loads varied greatly between the same type of test specimens.

After tuning is completed, test procedures were created using the MultiPurpose TestWare (MPT) function located under the application menu on the Station Manager program. A screen shot of the MPT is shown in Figure 25.
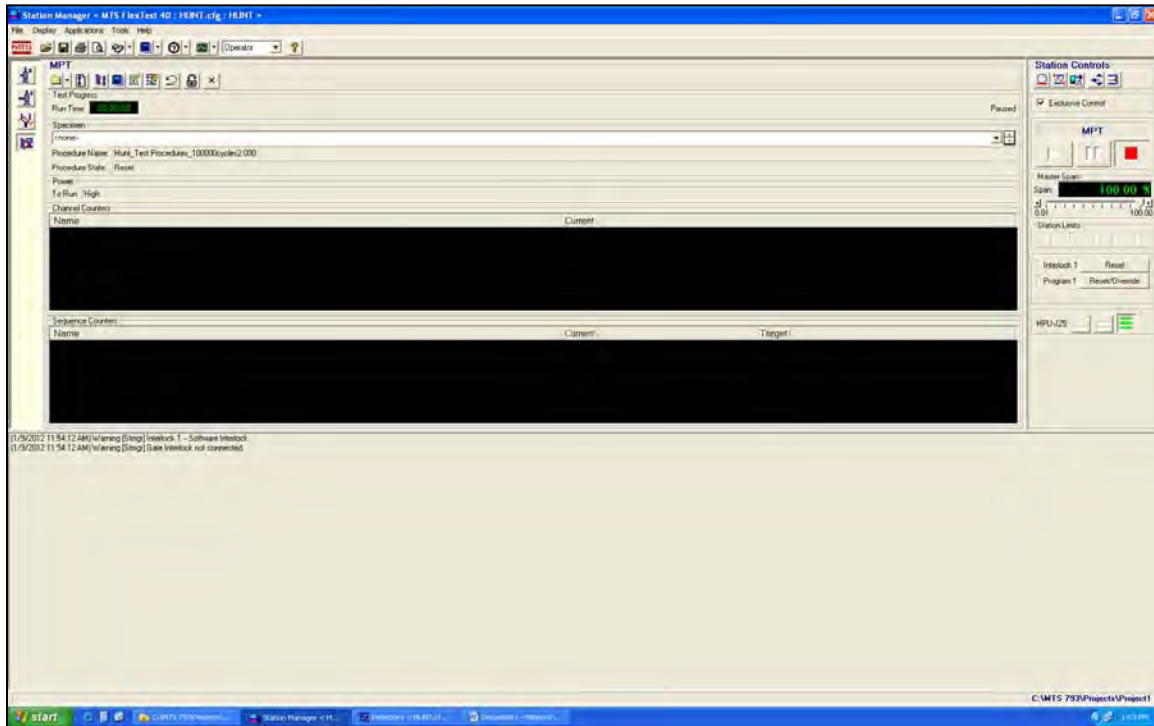
Figure 25. MPT screen shot

The MPT procedure editor should look like Figure 26 after the test procedures have been created. Refer to Appendix I for the detailed MTS steps on how to run MTS warm-up, MTS auto-tuning, and MPT.
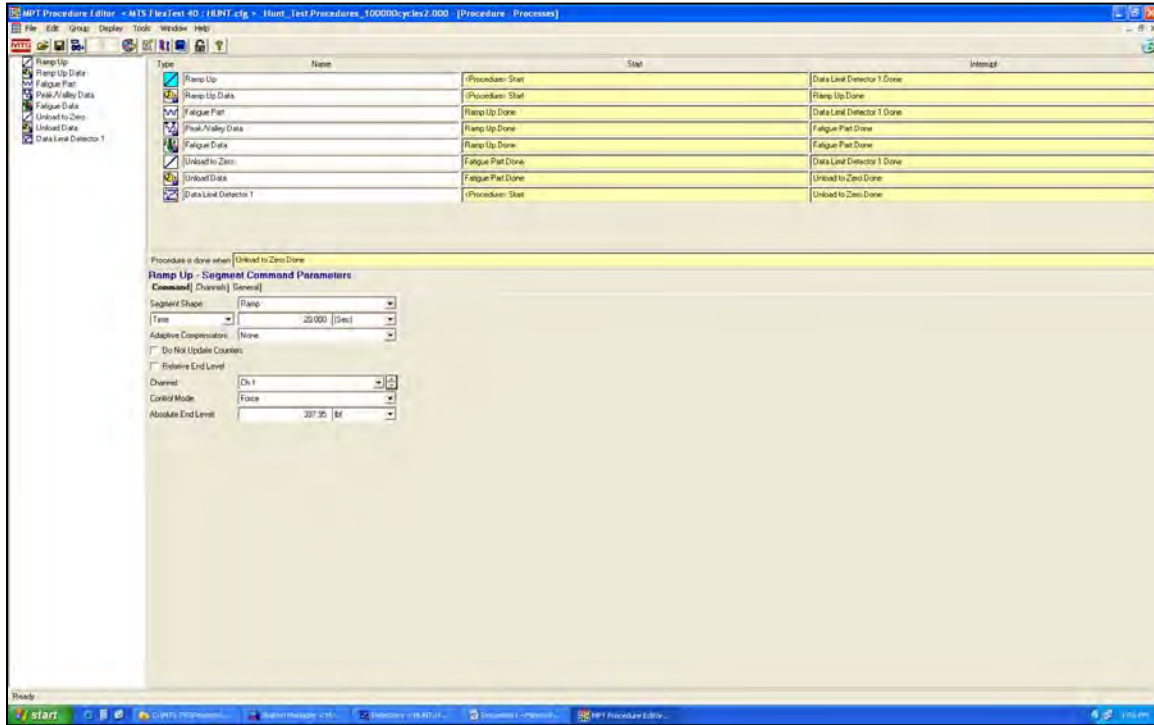
Figure 26. MPT Procedure Editor screen shot

Certain calculations must be done prior to running the fatigue test. The first calculation is to determine the average area of the test specimen. The average area calculation is done by taking the length of the test specimen and calculating three measurement points equally spaced with respect to the specimen's length. A width and depth measurement was recorded using a caliper at the three measurement point locations. Equation 6 shows how the average area calculation was carried out.

$$A_{avg} = \frac{\sum_{n=1}^{3} W_n * D_n}{3} \tag{6}$$

Where

A is the average (mm^2)

$$\Sigma \text{ is the summation}$$

$$W \text{ is the width measurement (mm)}$$

$$D \text{ is the depth measurement (mm)}$$

The maximum force required is calculated based on the selected percentage of UTS. The UTS for the different test specimen types was determined from running monotonic tension tests. Using the selected percentage of UTS and the UTS from monotonic tension tests the required maximum force was calculated with Equation 7.

$$F_{max}(lb_f) = \%UTS * UTS\left(\frac{N}{mm^2}\right) * A_{avg}(mm^2) * \frac{1lb_f}{4.448\ N} \tag{7}$$

where

F_{max} is force (lb_f)

%UTS is the percentage of UTS selected

UTS is UTS $\left(\frac{N}{mm^2}\right)$

A_{avg} is the average area (mm^2)

The stress ratio used in this research was 0.1. Since the stress ratio is a ratio of the minimum stress compared to the maximum stress in the fatigue cycle, Equation 8 can be reduced to the following:

$$R = \frac{\sigma_{min}}{\sigma_{max}} = \frac{F_{min}}{F_{max}} \tag{8}$$

where

R is the stress ratio

σ_{min} is the minimum stress

σ_{max} is the maximum stress

F_{min} is the minimum force

F_{max} is the maximum force

The minimum force is calculated from Equation 8 with the given stress ratio 0.1 and the calculated maximum force. The last calculation required for the test input into the MPT Procedure Editor is the stress amplitude or in the case of the MPT software the force amplitude, which can be calculated using Equation 9.

$$F_{amp} = \frac{(F_{max} - F_{min})}{2} \tag{9}$$

The grip pressure of 600 psi (4.14 MPa) or 800 psi (5.52 MPa) was used. In most cases if the maximum stress was greater than 50% UTS of the test specimen then the higher grip pressure was selected to prevent the specimen from slipping in the grips. The average specimen length between the two grips was approximately 105 mm (4.13 in). To run the fatigue tests in the MPT, select new specimen button and type the desired specimen name and click the run button. Shown in Figure 27 is the 5 kips (22 kN) MTS machine.

Figure 27. 5 kips MTS machine

3.5 Test Plan Summary

The EMI and fatigue testing procedures indentified in this chapter were designed

and implemented to meet the objective of characterizing the effects of EMI SE on CNTs

and CNFs composites under fatigue. 20 tests specimens were cut into 2.54 cm (1 in) by

15.24 cm (6 in) test strips. 2.54 cm (1 in) by 2.54 cm (1 in) glass/epoxy tabs were

adhered to both sides with M-Bond 200 catalyst and M-Bond 200 adhesive to prevent

damage from the MTS grips. All 20 of the 6 different composite types were tested

initially for baseline EMI values in the X-band frequency range 8.2 GHz to 12.4 GHz

using the PNA Microwave Network Analyzer and subjected to various fatigue cycle

intervals using a MTS machine followed by additional EMI testing to determine the

effects of EMI SE when subjected to tension-tension fatigue cycling.

The fatigue tests were conducted on two different MTS 810 servo-hydraulic

testing machines. One MTS machine was 22 kips (98 kN) and the second was 5 kips

(22 kN). Using the MTS 793 software program and Station Manager a test program was

written using the MPT Procedure Editor. The tension-tension fatigue tests were done at

0.1 stress ratio at selected percentage of UTS, 1 Hz, and a grip pressure of 600 psi

(4.14 MPa) or 800 psi (5.52 MPa). In most test events the initial number of cycles was

100,000 cycles. In some test events the interval of fatigue tests was less 100,000 cycles.

In other test events the interval of fatigue was greater than 100,000 cycles. The fatigue

interval was greater than 100,000 cycles when the test specimen had previously reached

approximately 300,000 cycles and the test objective was to reach a minimum of 600,000

cycles before failure occurred. Shown in Table 3 is test matrix that shows the UTS,

percentage of UTS, the maximum applied stress, and the minimum applied stress used in

this study. Table 3 shows 21 test specimens because the 75% UTS 8G/CNT test

specimen was tested again at 50% UTS due to the fact the first test only achieved 453

cycles before failure.

Table 3. Test matrix

Specimen	UTS (MPa)	% UTS	Applied Stress	
			Max (MPa)	Min (MPa)
8G/CNT	685	75	514	51
8G/CNT	685	50	343	34
8G/CNT	685	36	247	25
8G/CNT	685	26	178	18
8G/CNF	551	55	303	30
8G/CNF	551	45	248	25
8G/CNF	551	32	176	18
8G/CNF	551	25	138	14
8G/CNF	551	18	99	10
8G	519	52	270	27
8G	519	51	265	26
8G	519	30	156	16
(G/CNT)$_4$	479	50	240	24
(G/CNT)$_4$	479	40	192	19
(G/CNT)$_4$	479	26	125	12
2CNT/4G/2CNT	372	50	186	19
2CNT/4G/2CNT	372	40	149	15
2CNT/4G/2CNT	372	30	112	11
4G/4CNT	399	50	200	20
4G/4CNT	399	40	160	16
4G/4CNT	399	25	100	10

IV. Analysis and Results

4.1 Introduction

This chapter will cover the results obtained during the course of this research. EMI SE was evaluated during fatigue on five different configured nanocomposites and a control specimen composite free of CNTs or CNFs. One of the five nanocomposites consisted of MWNTs and SWNTs configured into a ply that is externally deposited onto a reinforced composite laminate of 6781 S-2 glass fiber in CYCOM 5250-4 BMI resin laminate. The CNTs were about 25 nm in diameter and 1 mm long. The CNTs ply were about 0.1 mm thick and contained 20 g/m^2 concentration of CNTs. This nanocomposite is referred to as 8G/CNT. The second of the five nanocomposites consisted of CNFs configured into a ply that is externally deposited onto a reinforced composite laminate of 6781 S-2 glass fiber in CYCOM 5250-4 BMI resin laminate. The CNFs were about 100 nm in diameter and 100 μm long. The CNFs ply were about 0.1 mm thick and contained 20 g/m^2 concentration of CNFs. This nanocomposite is referred to as 8G/CNF.

The last three of the five nanocomposites consisted of a 3-harness satin weave, S-glass (Astroquartz II) fiber in a CYCOM 5575-2 cyanate ester matrix combined with different MWNT ply stacking sequence to make a 8 ply laminate. One was alternating ply of S-glass (Astroquartz II) fiber in CYCOM 5575-2 cyanate ester matrix and a single ply of CNTs, and referred to as (G/CNT)₄. The second nanocomposite out of the three was a symmetrical laminate of two external plies of CNTs with two plies of S-glass (Astroquartz II) fiber in CYCOM 5575-2 cyanate ester matrix, and referred to as

2CNT/4G/2CNT. The last nanocomposite out of the three was four plies of S-glass (Astroquartz II) fiber in CYCOM 5575-2 cyanate ester matrix stacked on four plies of CNTs, and referred to as 4G/4CNT. The control specimen composite was absent of CNTs and consisted of a 8 ply laminate of S-glass (Astroquartz II) fiber in CYCOM 5575-2 cyanate ester matrix and referred to as 8G. The S-glass (Astroquartz II) fiber was made from 99.95% SiO_2 quartz crystals and CYCOM 5575-2 cyanate ester matrix in a 3-harness satin weave. The CNTs plies in the three nanocomposites had an estimated length of 700 μm and a diameter of 8-15 nm, 90% weight, and a CNT concentration of 18.3 g/m^2. The average thickness of the CNT ply was 84.49 μm. The average thickness of the glass/epoxy ply containing warp strands was 212.53 μm, while the average thickness of the glass/epoxy ply containing the fill strands was 271.25 μm. The total average thickness for the entire eight ply composite was 1.215 mm (0.048 in).

EMI measurements were taken before and after each cyclic interval of fatigue testing for all the test specimens. The initial values recorded from the EMI SE were used as a baseline to see the effects of EMI SE under fatigue testing for the different test specimens.

4.2 EMI Under Fatigue - Carbon Nanotubes Composites

This set of CNT composites consisted of 8G/CNT, $(G/CNT)_4$, 2CNT/4G/2CNT, and 4G/4CNT. The control specimen, 8G, is also included in this test set for comparison. The composites were subjected to fatigue testing at different fatigue stress levels from a range of 25% UTS to 75% UTS. The stress ratio in all the fatigue tests was constant at

0.1. The configuration that seemed to show the greatest drop in EMI SE under fatigue cycling was 4G/4CNT at 40% UTS with a 15% loss after 100,000 cycles. The other configurations showed minimal loss in dB or remained constant after each addition of cyclic loading.

Of all the CNT nanocomposites the configuration that had the highest initial EMI SE, using the PNA network analyzer from the 8.2 GHz to 12.4 GHz X-band frequency, was 2CNT/4G/2CNT with an average of 67.65 dB. The CNT nanocomposite configuration with the second highest initial EMI SE was 4G/4CNT with an average of 60.59 dB. The initial average for the remaining CNT nanocomposites were the following: 1) 8G/CNT - 47.87 dB, 2) (G/CNT)$_4$ - 65.10 dB. The control specimen, 8G, initial EMI average was 1.49 dB, which is close to the expected 0 dB measurement. Figure 28 shows the EMI SE versus fatigue cycles for all the CNT nanocomposites and control specimen, 8G at the selected fatigue stress levels.

The 2CNT/4G/2CNT, 4G/4CNT, and (G/CNT)$_4$ nanocomposites had 3.6 times more grams of CNTs compared to 8G/CNT. The 2CNT/4G/2CNT, 4G/4CNT, and (G/CNT)$_4$ nanocomposites each had a total of 4 plies with a CNT ply concentration of 18.3 g/m^2. This equates to 73.2 g/m^2 or 0.28 g of CNTs for a 0.00387 m^2 (6 in^2) cut test specimen area. The 8G/CNT nanocomposite ply had a single ply with a CNT ply concentration of 20.0 g/m^2. This equates to 20.0 g/m^2 or 0.08 g of CNTs for a 0.00387 m^2 (6 in^2) cut test specimen area.
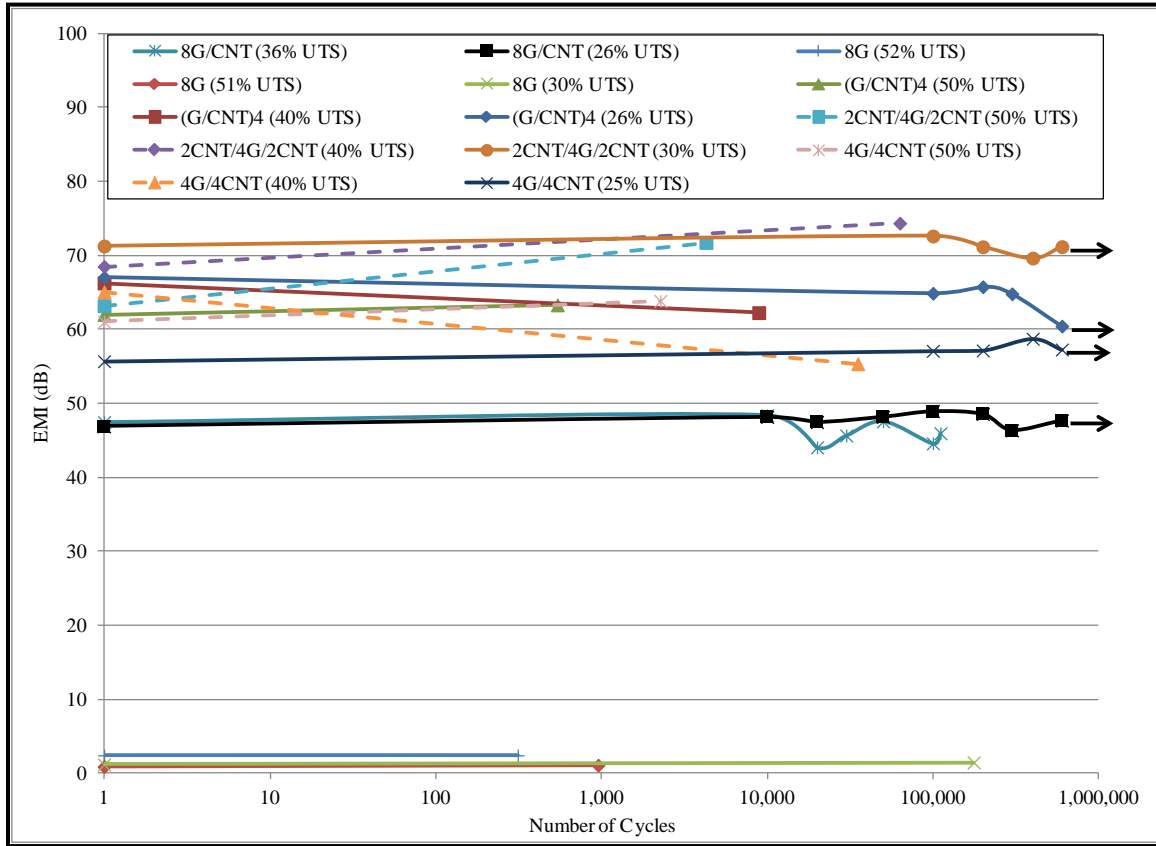
Figure 28. EMI versus fatigue cycles for CNT nanocomposites

4.2.1 EMI Under Fatigue - 8G

The 8G composite was identified as the control specimen during this research. The 8G composite's initial EMI average was 1.49 dB. The UTS was determined to be 519 MPa from monotonic tension tests in a previous study [29]. The UTS percentage selected for the three fatigue tests was 52%, 51%, and 30%. Table 4 shows the EMI and fatigue results for the 8G composite.

Table 4. 8G EMI and fatigue results

Specimen	UTS (MPa)	% UTS	Cycles	Fail (Y/N)	EMI Avg
8G	519	52	0	N	2.41
8G	519	52	313	Y	0
8G	519	51	0	N	0.89
8G	519	51	955	Y	1.08
8G	519	30	0	N	1.18
8G	519	30	176,234	Y	1.46

Figure 29 shows the 8G EMI SE versus fatigue cycles for the different stress levels. All three 8G test specimens initial and final EMI measurements were close to the expected 0 dB since the test configurations were free of conductive CNTs. The collected measurements above 0 dB can be attributed to noise.
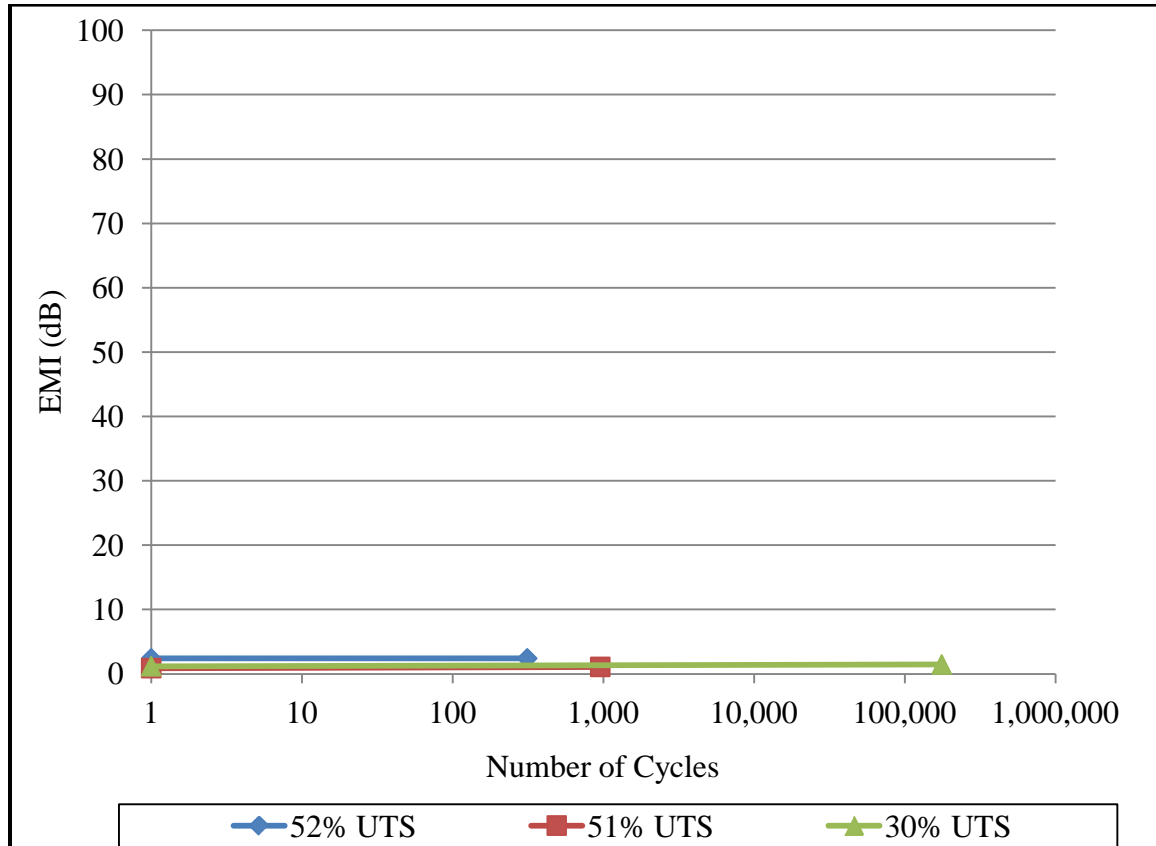
Figure 29. 8G EMI versus fatigue cycles at different stress levels

Shown in Figure 30, the normalized 8G EMI SE versus fatigue cycles for the different stress levels were not affected by the different stress levels. The EMI was normalized with respect to its initial value before fatigue. The change in EMI from the initial to the post failure measurement for all the different stress levels remained relatively unchanged and showed that the different stress levels don't affect EMI SE.
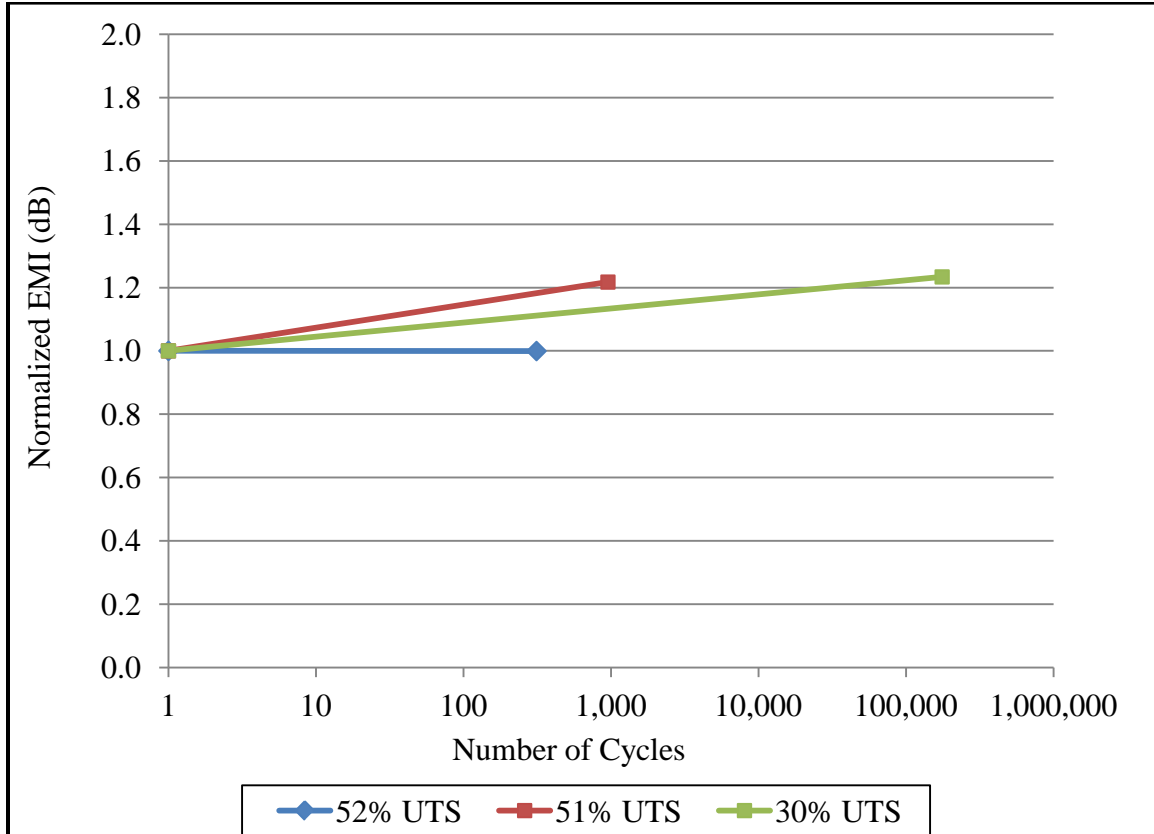
Figure 30. 8G normalized EMI versus fatigue cycles at different stress levels

Figure 31 shows a typical 8G at 30% UTS stress-strain curve from fatigue testing. The strain increased 886% from the initial cycle to the last cycle, which in this case was the 100,000th cycle before it failed at 176,234 cycles. The strain for the first 100 fatigue cycles remained relatively constant until the strain increased considerably in the 1,000th, 10,000th, and 100,000th fatigue cycles.
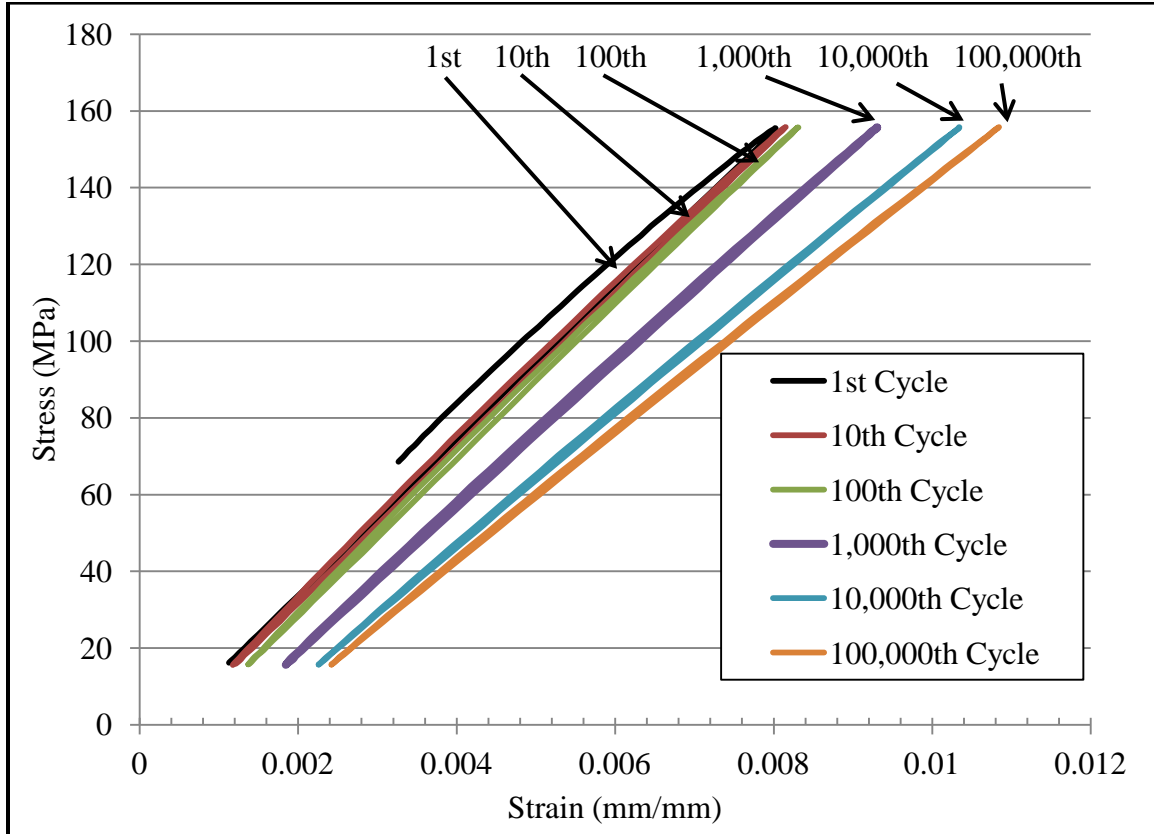
Figure 31. 8G (30% UTS) stress versus strain curve

4.2.2 EMI under Fatigue - 8G/CNT

The 8G/CNT nanocomposite's initial EMI average was 47.87 dB. The UTS was determined to be 685 MPa from monotonic tension tests in a previous study. The UTS percentage selected for the three fatigue tests was 75%, 50%, 36%, and 26%. Table 5 shows the EMI and fatigue results for the 8G/CNT nanocomposite. No EMI data for 50% UTS was collected because the specimen was not big enough to properly fit in the network analyzer after failure from the 75% UTS fatigue test.

Table 5. 8G/CNT EMI and fatigue results

Specimen	UTS (MPa)	% UTS	Cycles	Fail (Y/N)	EMI Avg
8G/CNT	685	75	0	N	49.25
8G/CNT	685	75	100,000	Y	ND
8G/CNT	685	36	0	N	47.45
8G/CNT	685	36	10,000	N	48.39
8G/CNT	685	36	20,000	N	44.05
8G/CNT	685	36	30,000	N	45.65
8G/CNT	685	36	50,000	N	47.56
8G/CNT	685	36	100,000	N	44.59
8G/CNT	685	36	111,064	Y	45.96
8G/CNT	685	26	0	N	46.90
8G/CNT	685	26	10,000	N	48.15
8G/CNT	685	26	20,000	N	47.45
8G/CNT	685	26	50,000	N	48.17
8G/CNT	685	26	100,000	N	48.94
8G/CNT	685	26	200,000	N	48.55
8G/CNT	685	26	300,000	N	46.34
8G/CNT	685	26	600,000	N	47.66

Figure 32 shows the 8G/CNT EMI SE versus fatigue cycles for the different stress levels. The two 8G/CNT test specimens EMI measurements from initial to final under fatigue testing showed minimal impact between the two different stress levels. 75% UTS EMI data is not available since the specimen was not big enough to properly fit in the network analyzer after fatigue failure.
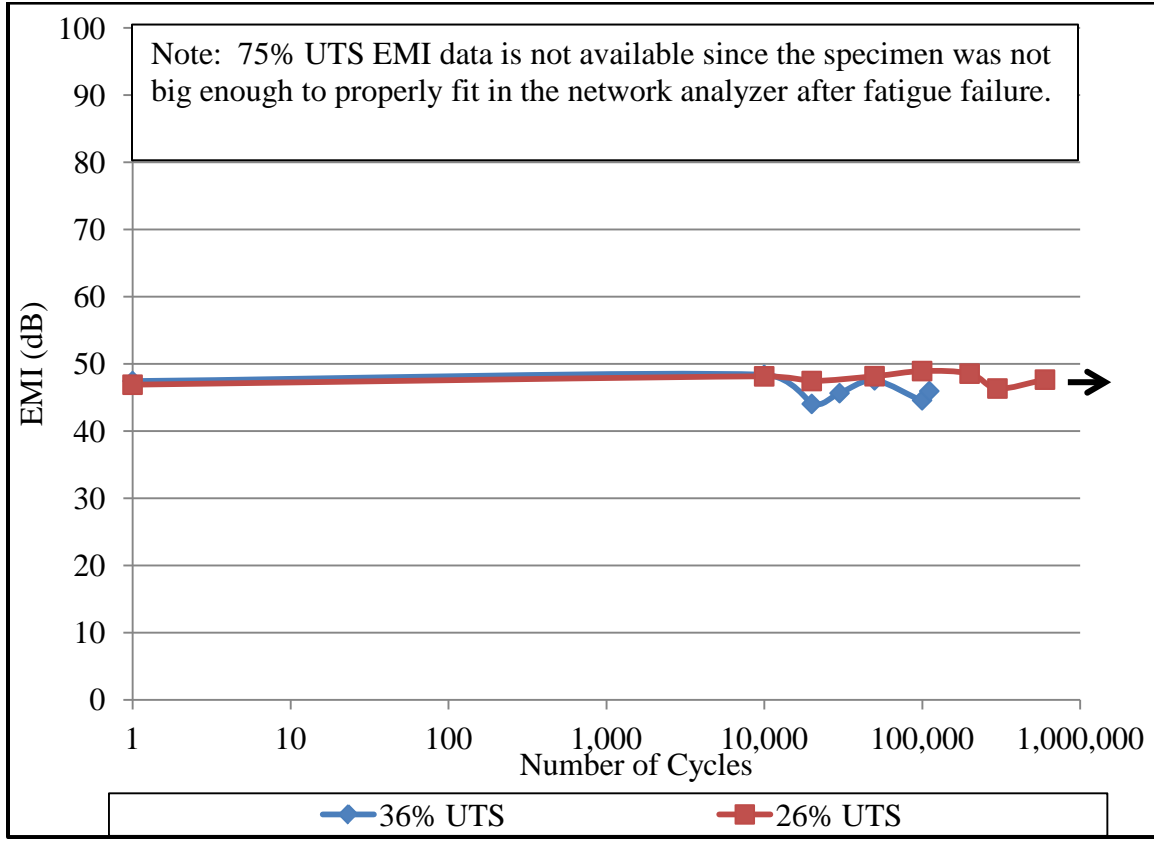
Figure 32. 8G/CNT EMI versus fatigue cycles at different stress levels

Shown in Figure 33, the normalized 8G/CNT EMI SE versus fatigue cycles for the different stress levels was not affected by the different stress levels. The EMI was normalized with respect to its initial value before fatigue. The change in EMI from the initial to the post failure measurement for all the different stress levels remained relatively unchanged and showed that the different stress levels don't affect EMI SE.
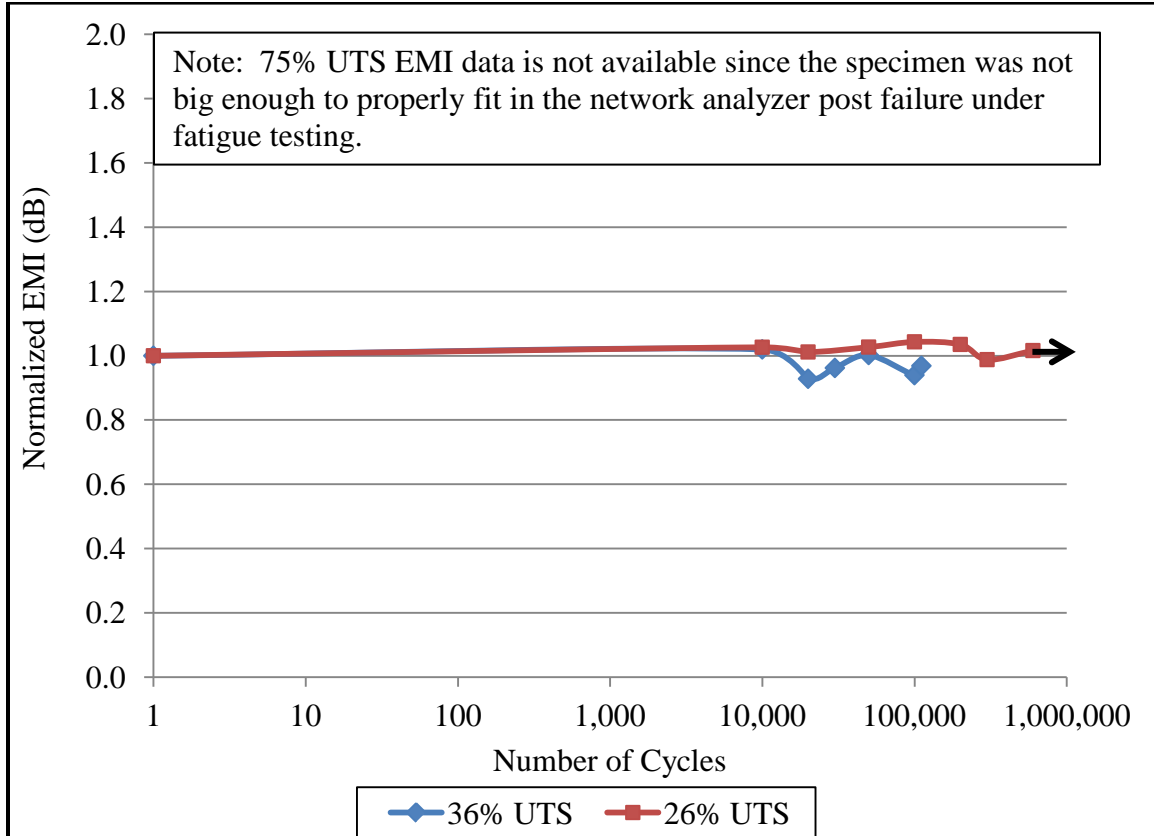
Figure 33. 8G/CNT normalized EMI versus fatigue cycles at different stress levels

4.2.3 EMI under Fatigue - (G/CNT)$_4$

The (G/CNT)$_4$ nanocomposite's initial EMI average was 65.10 dB. The UTS was determined to be 479 MPa from monotonic tension tests in a previous study [29]. The UTS percentage selected for the fatigue tests was 50%, 40%, 26%. Table 6 shows the EMI and fatigue data for (G/CNT)$_4$ nanocomposite.

Table 6. (G/CNT)$_4$ EMI and fatigue results

Specimen	UTS (MPa)	% UTS	Cycles	Fail (Y/N)	EMI Avg
(G/CNT)$_4$	479	50	0	N	62.01
(G/CNT)$_4$	479	50	543	Y	63.30
(G/CNT)$_4$	479	40	0	N	66.26
(G/CNT)$_4$	479	40	8,899	Y	62.25
(G/CNT)$_4$	479	26	0	N	67.03
(G/CNT)$_4$	479	26	100,000	N	64.87
(G/CNT)$_4$	479	26	200,000	N	65.75
(G/CNT)$_4$	479	26	300,000	N	64.79
(G/CNT)$_4$	479	26	600,000	N	60.43

Figure 34 shows the (G/CNT)$_4$ EMI SE versus fatigue cycles for the different stress levels. The three (G/CNT)$_4$ test specimens EMI measurements from initial to final under fatigue testing showed minimal change between the three different stress levels.
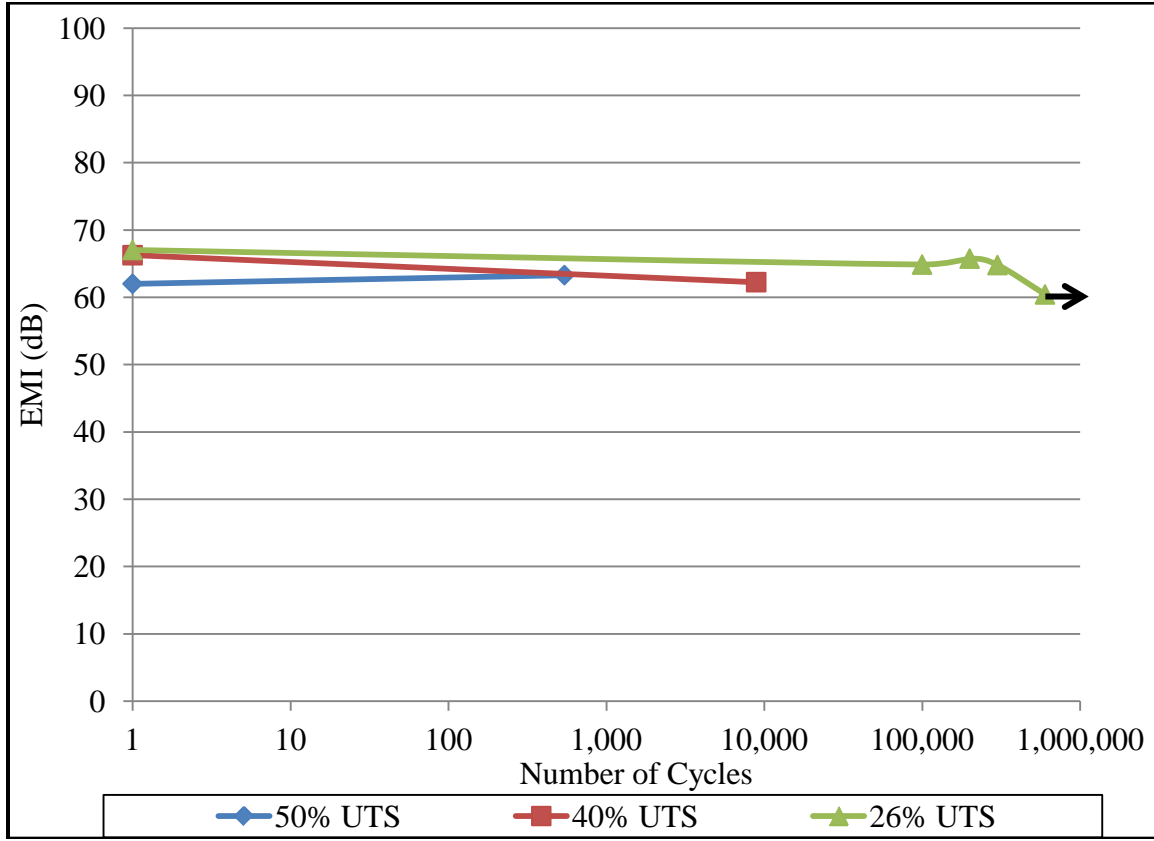
Figure 34. (G/CNT)$_4$ EMI versus fatigue cycles at different stress levels

Shown in Figure 35, the normalized (G/CNT)$_4$ EMI SE versus fatigue cycles for the different stress levels was not affected by the different stress levels. The EMI was normalized with respect to its initial value before fatigue. The change in EMI from the initial to the post failure measurement for all the different stress levels remained relatively unchanged and showed that the different stress levels don't affect EMI SE.
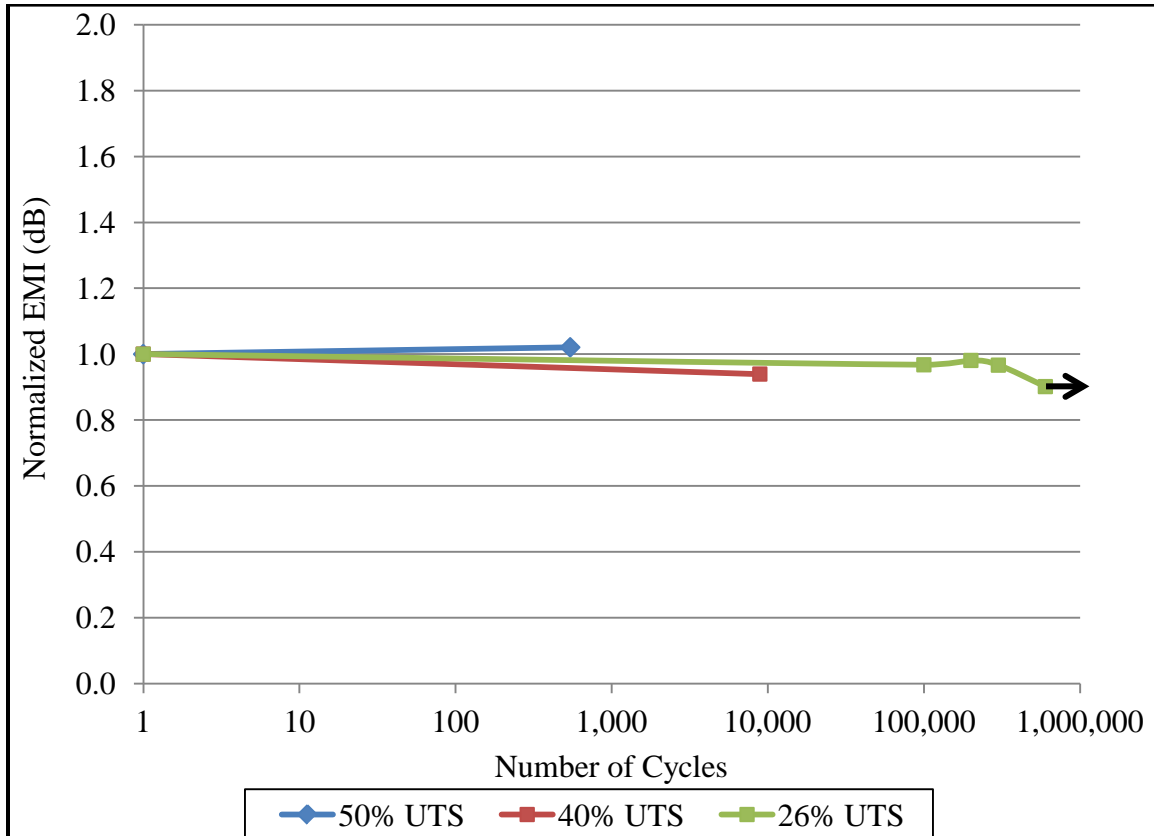
Figure 35. (G/CNT)$_4$ normalized EMI versus fatigue cycles at different stress levels

Figure 36 shows a typical (G/CNT)$_4$ at 26% UTS stress-strain curve from fatigue

testing. The strain increased 640% from the initial cycle to the last cycle, which in this

case was the 100,000th cycle.
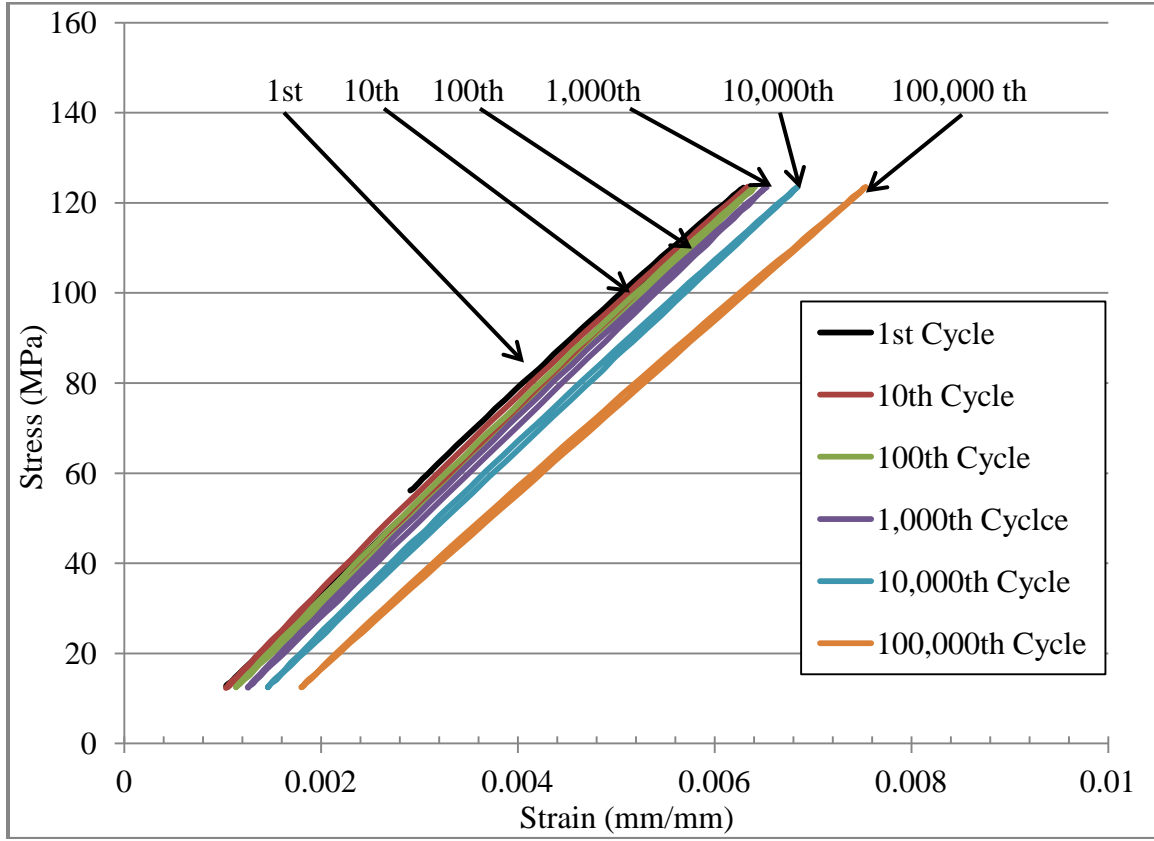
**Figure 36.** (G/CNT)$_4$ (26% UTS) stress versus strain curve

4.2.4 EMI under Fatigue - 2CNT/4G/2CNT

The 2CNT/4G/2CNT nanocomposite's initial EMI average was 67.65 dB. The UTS was determined to be 372 MPa from monotonic tension tests in a previous study [29]. The UTS percentage selected for the fatigue tests was 50%, 40%, and 30%. Table 7 shows the EMI and fatigue data for 2CNT/4G/2CNT nanocomposite.

Table 7. 2CNT/4G/2CNT EMI and fatigue results

Specimen	UTS (MPa)	% UTS	Cycles	Fail (Y/N)	EMI Avg
2CNT/4G/2CNT	372	50	0	N	63.19
2CNT/4G/2CNT	372	50	4,274	Y	71.74
2CNT/4G/2CNT	372	40	0	N	68.49
2CNT/4G/2CNT	372	40	63,103	Y	74.35
2CNT/4G/2CNT	372	30	0	N	71.26
2CNT/4G/2CNT	372	30	100,000	N	72.61
2CNT/4G/2CNT	372	30	200,000	N	71.16
2CNT/4G/2CNT	372	30	400,000	N	69.63
2CNT/4G/2CNT	372	30	600,000	N	71.17

Figure 37 shows the 2CNT/4G/2CNT EMI SE versus fatigue cycles for the different stress levels. The three 2CNT/4G/2CNT test specimens EMI measurements from initial to final under fatigue testing showed minimal change between the three different stress levels.
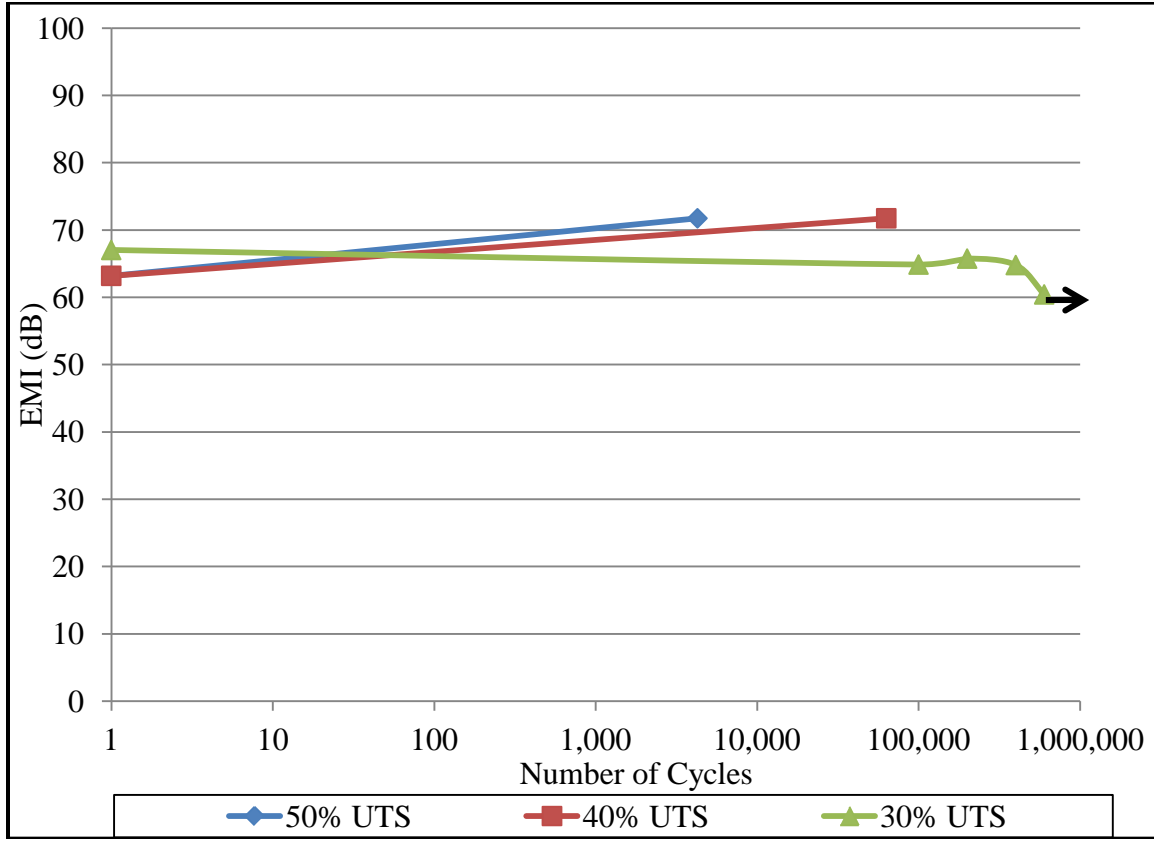
Figure 37. 2CNT/4G/2CNT EMI versus fatigue cycles at different stress levels

Shown in Figure 38, the normalized 2CNT/4G/2CNT EMI SE versus fatigue cycles for the different stress levels was not affected by the different stress levels. The EMI was normalized with respect to its initial value before fatigue. The change in EMI from the initial to the post failure measurement for all the different stress levels remained relatively unchanged and showed that the different stress levels don't affect EMI SE.
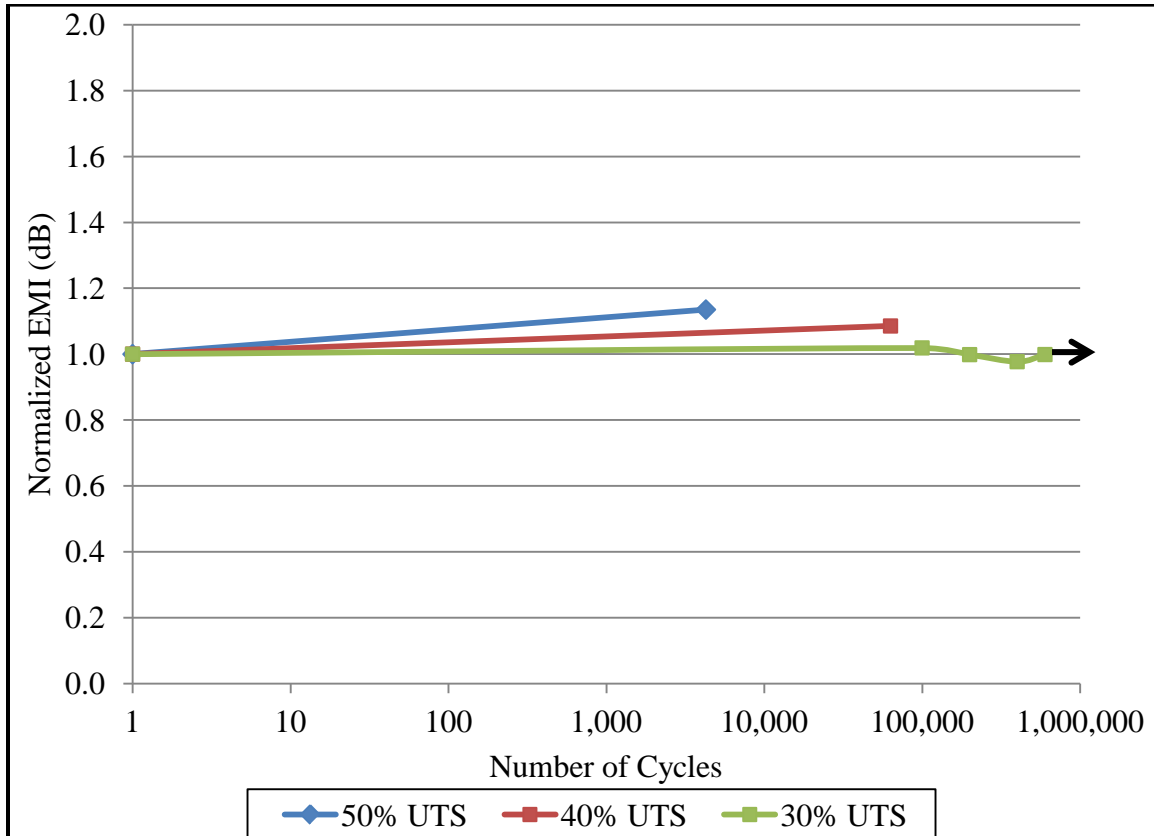
Figure 38. 2CNT/4G/2CNT normalized EMI versus fatigue cycles at different stress levels

Figure 39 shows a typical 2CNT/4G/2CNT at 30% UTS stress-strain curve from fatigue testing. The strain increased 712% from the initial cycle to the last cycle, which in this case was the 100,000th cycle.
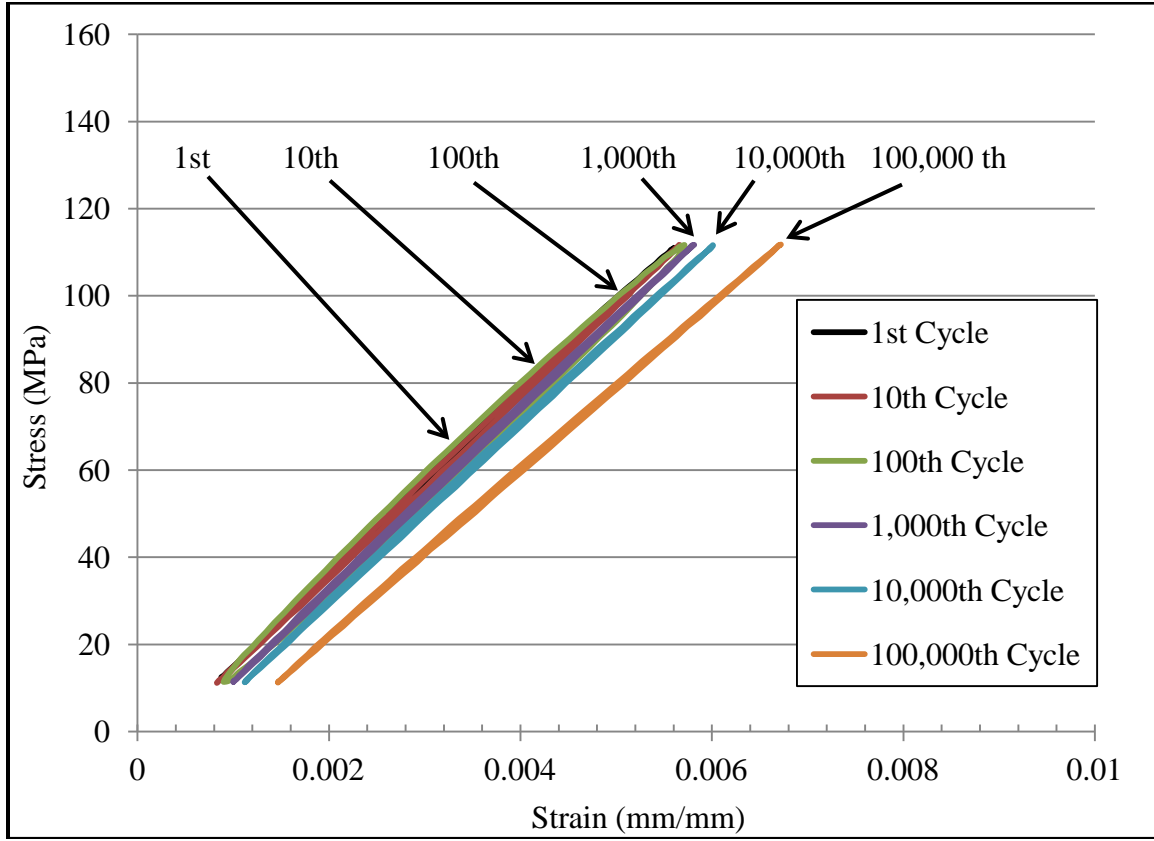
Figure 39. 2CNT/4G/2CNT (30% UTS) stress versus strain curve

4.2.5 EMI under Fatigue - 4G/4CNT

The 4G/4CNT nanocomposite's initial EMI average was 60.59 dB. The UTS was determined to be 399 MPa respectively from monotonic tension tests in a previous study [29]. The UTS percentage selected for the fatigue tests was 50%, 40%, and 25%. Table 8 shows the EMI and fatigue data for 4G/4CNT nanocomposite.

Table 8. 4G/4CNT EMI and fatigue results

Specimen	UTS (MPa)	% UTS	Cycles	Fail (Y/N)	EMI Avg
4G/4CNT	399	50	0	N	61.02
4G/4CNT	399	50	2,270	Y	63.84
4G/4CNT	399	40	0	N	65.07
4G/4CNT	399	40	35,222	Y	55.34
4G/4CNT	399	25	0	N	55.68
4G/4CNT	399	25	100,000	N	57.09
4G/4CNT	399	25	200,000	N	57.14
4G/4CNT	399	25	400,000	N	58.73
4G/4CNT	399	25	600,000	N	57.27

Figure 40 shows the 4G/4CNT EMI SE versus fatigue cycles for the different stress levels. The three 4G/4CNT test specimens EMI measurements from initial to final under fatigue testing showed minimal change between the three different stress levels.
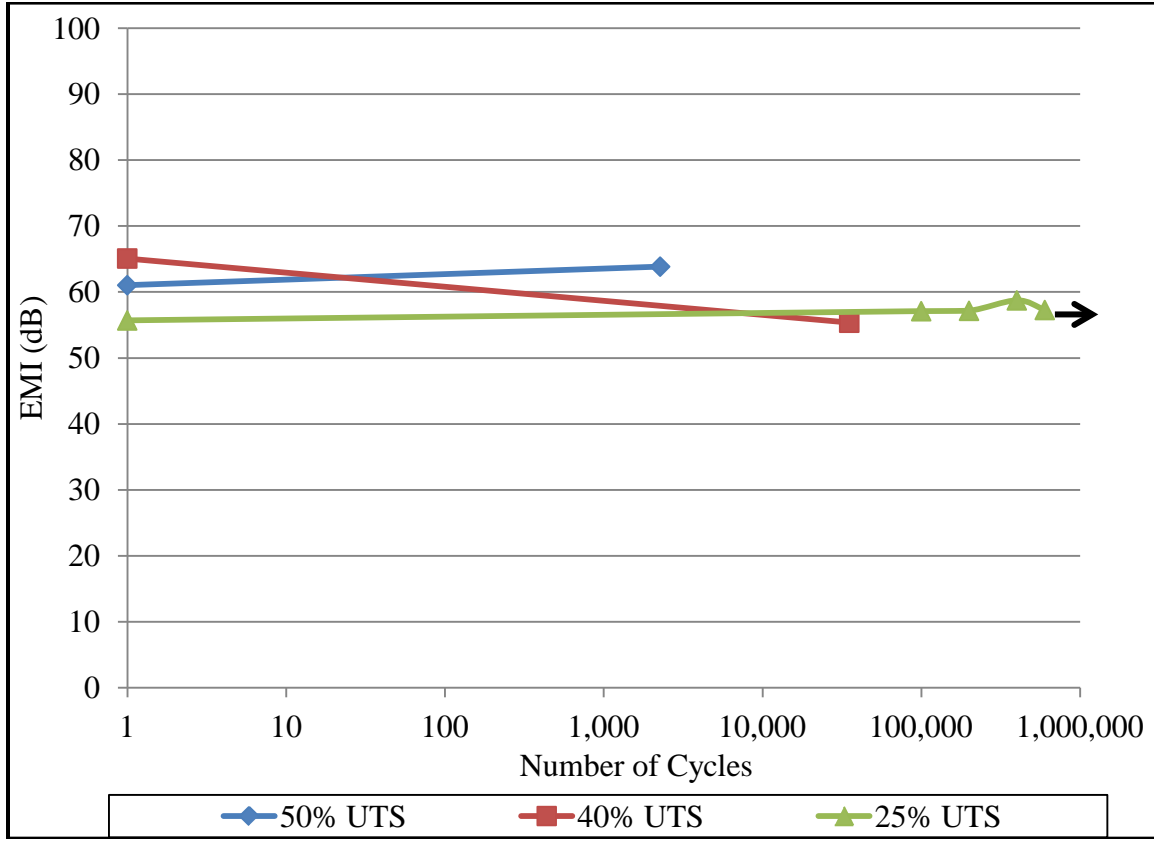
Figure 40. 4G/4CNT EMI versus fatigue cycles at different stress levels

Shown in Figure 41, the normalized 4G/4CNT EMI SE versus fatigue cycles for the different stress levels was not affected by the different stress levels. The EMI was normalized with respect to its initial value before fatigue. The change in EMI from the initial to the post failure measurement for all the different stress levels remained relatively unchanged and showed that the different stress levels don't affect EMI SE.
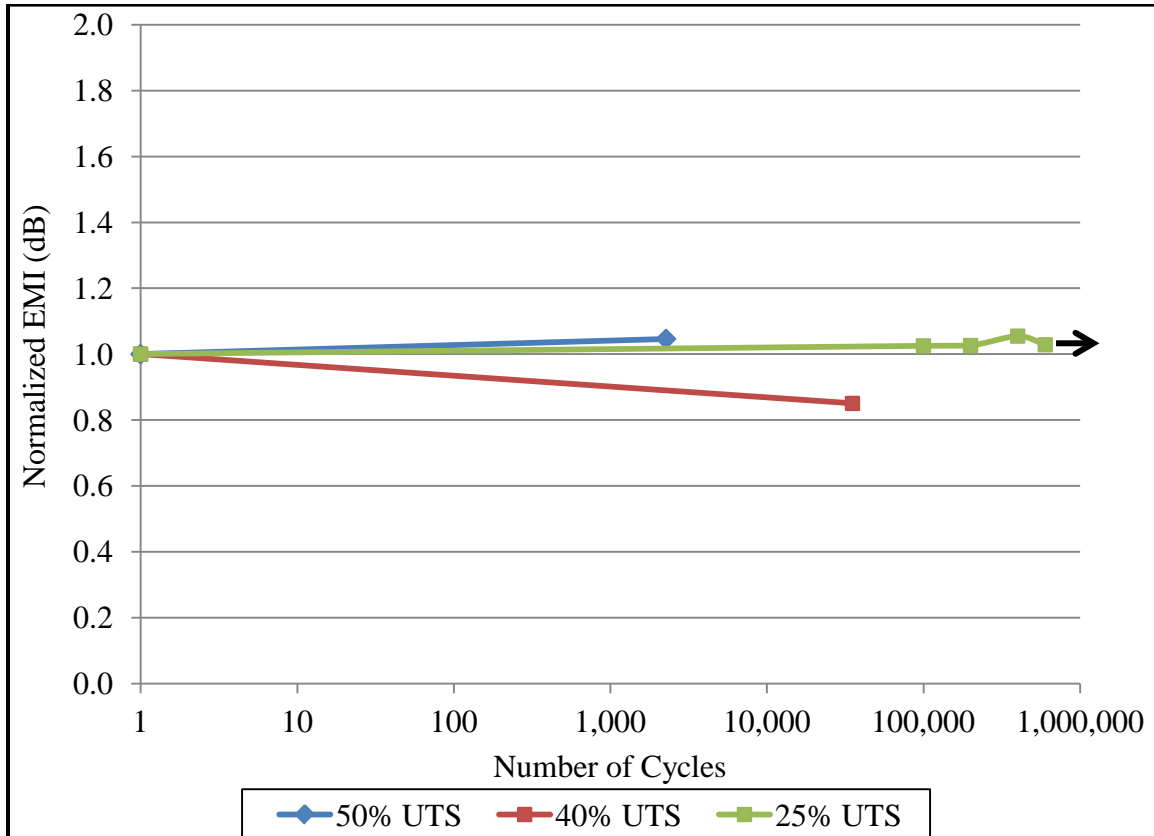
Figure 41. 4G/4CNT normalized EMI versus fatigue cycles at different stress levels

Figure 42 shows a typical 4G/4CNT at 25% UTS stress-strain curve from fatigue testing. The strain increased 675% from the initial cycle to the last cycle, which in this case was the 100,000th cycle.
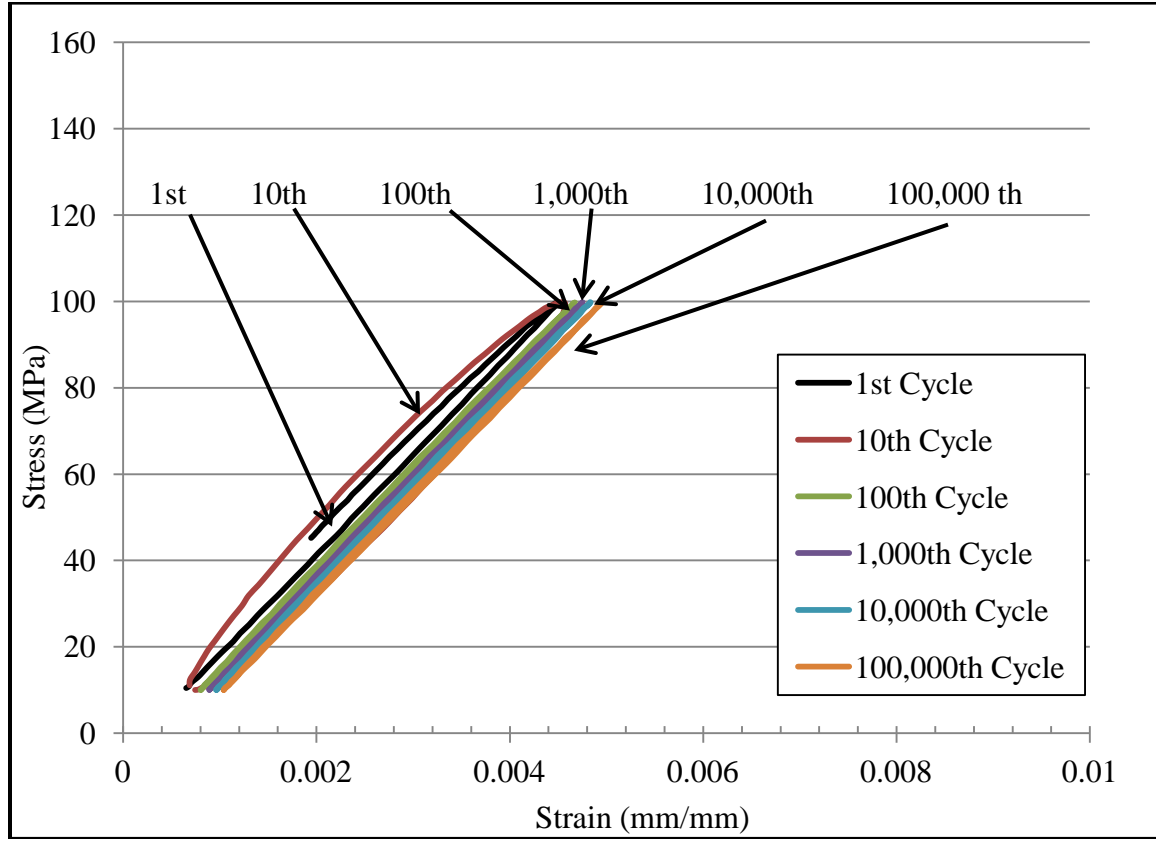
Figure 42. 4G/4CNT (25% UTS) stress versus strain curve

4.3 EMI Under Fatigue - Carbon Nanofibers Composites

The only CNF composite consisted of 8G/CNF. The stress ratio in all the fatigue tests was constant at 0.1. The 8G/CNF nanocomposite's initial EMI average was 20.57 dB. The UTS was determined to be 551 MPa respectively from monotonic tension tests in a previous study. The UTS percentage selected for the fatigue tests was 55%, 45%, 32%, 25%, and 18%. Table 9 shows the EMI and fatigue data for 8G/CNF nanocomposite.

Table 9. 8G/CNF EMI and fatigue results

Specimen	UTS (MPa)	% UTS	Cycles	Fail (Y/N)	EMI Avg
8G/CNF	551	55	0	N	17.82
8G/CNF	551	55	45,897	Y	18.17
8G/CNF	551	45	0	N	16.96
8G/CNF	551	45	10,000	N	17.83
8G/CNF	551	45	20,000	N	17.83
8G/CNF	551	45	30,000	N	17.72
8G/CNF	551	45	50,000	N	17.70
8G/CNF	551	45	66,680	Y	18.69
8G/CNF	551	32	0	N	22.89
8G/CNF	551	32	10,000	N	23.21
8G/CNF	551	32	20,000	N	23.31
8G/CNF	551	32	40,000	N	23.20
8G/CNF	551	32	90,000	N	23.23
8G/CNF	551	32	190,000	N	23.25
8G/CNF	551	32	490,000	N	23.48
8G/CNF	551	32	629,774	Y	23.32
8G/CNF	551	25	0	N	19.42
8G/CNF	551	25	7,362	Y	ND
8G/CNF	551	18	0	N	25.78
8G/CNF	551	18	10,000	N	23.21
8G/CNF	551	18	20,000	N	23.31
8G/CNF	551	18	30,000	N	23.20
8G/CNF	551	18	50,000	N	23.23
8G/CNF	551	18	100,000	N	15.94
8G/CNF	551	18	200,000	N	23.48
8G/CNF	551	18	300,000	N	23.32
8G/CNF	551	18	900,000	N	23.79

Figure 43 shows the 8G/CNF EMI SE versus fatigue cycles for the different stress levels. The four 8G/CNF test specimens EMI measurements from initial to final under fatigue testing showed minimal impact between the four different stress levels. 25% UTS

EMI data is not available since the specimen was not big enough to properly fit in the network analyzer after fatigue failure.
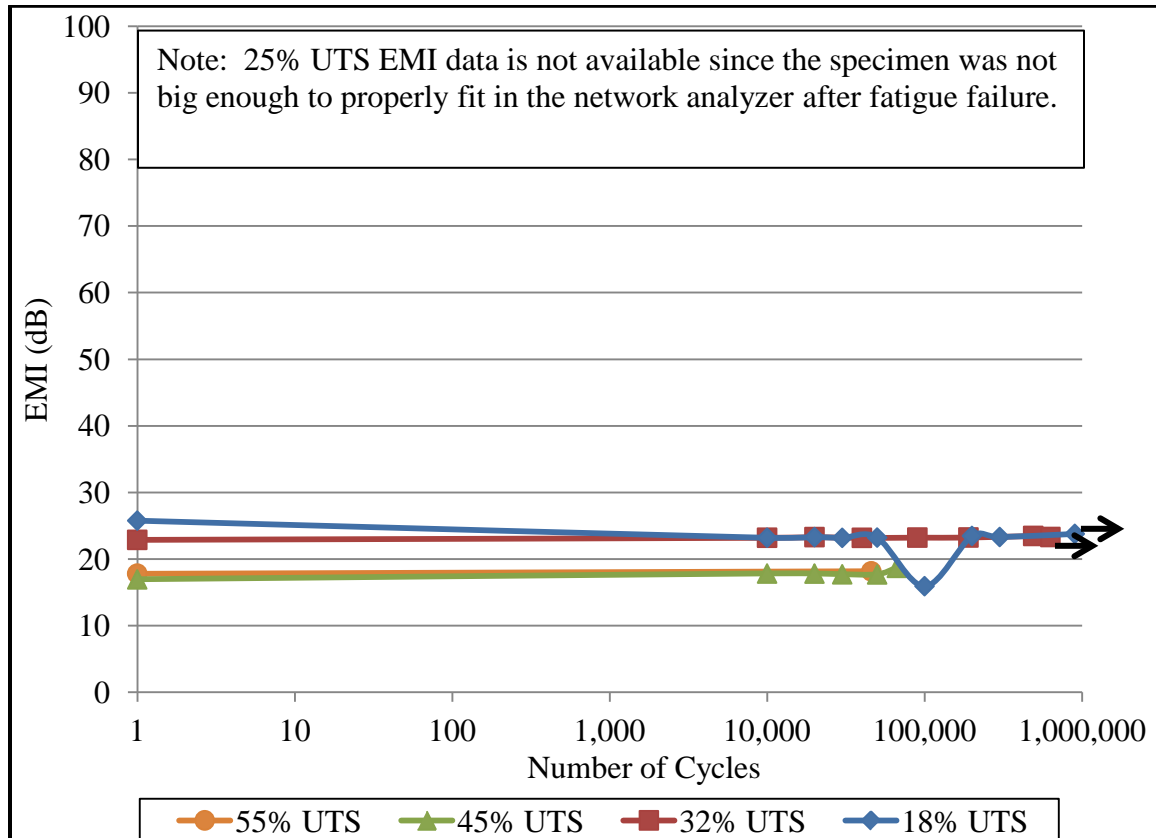

Figure 43. 8G/CNF EMI versus fatigue cycles at different stress levels

Shown in Figure 44, the normalized 8G/CNF EMI SE versus fatigue cycles for the different stress levels were not affected by the different stress levels. The EMI was normalized with respect to its initial value before fatigue. The change in EMI from the initial to the post failure measurement for all the different stress levels remained relatively unchanged and showed that the different stress levels don't affect EMI SE.
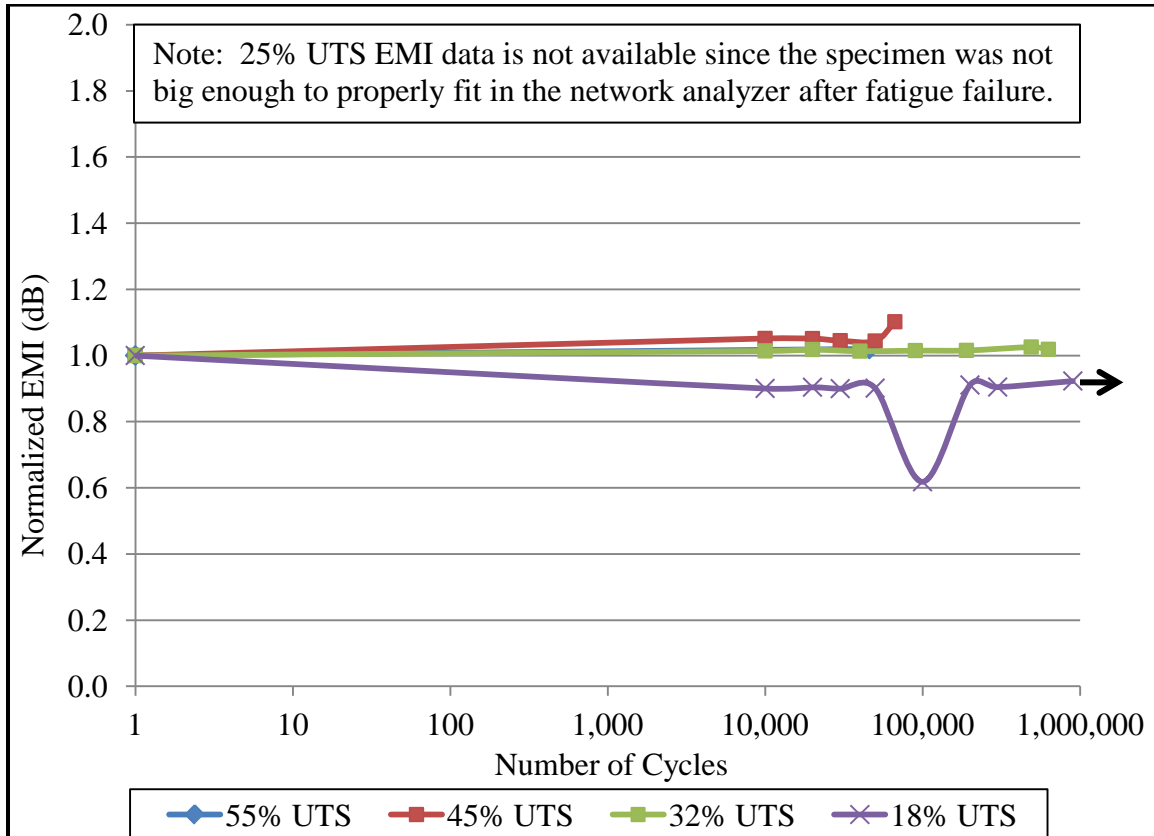
Figure 44. 8G/CNF normalized EMI versus fatigue cycles at different stress levels

Figure 45 shows a typical 8G/CNF at 55% UTS stress-strain curve from fatigue testing. The strain increased 569% from the initial cycle to the last cycle, which in this case was the 10,000th cycle before it failed at 45,897 cycles.
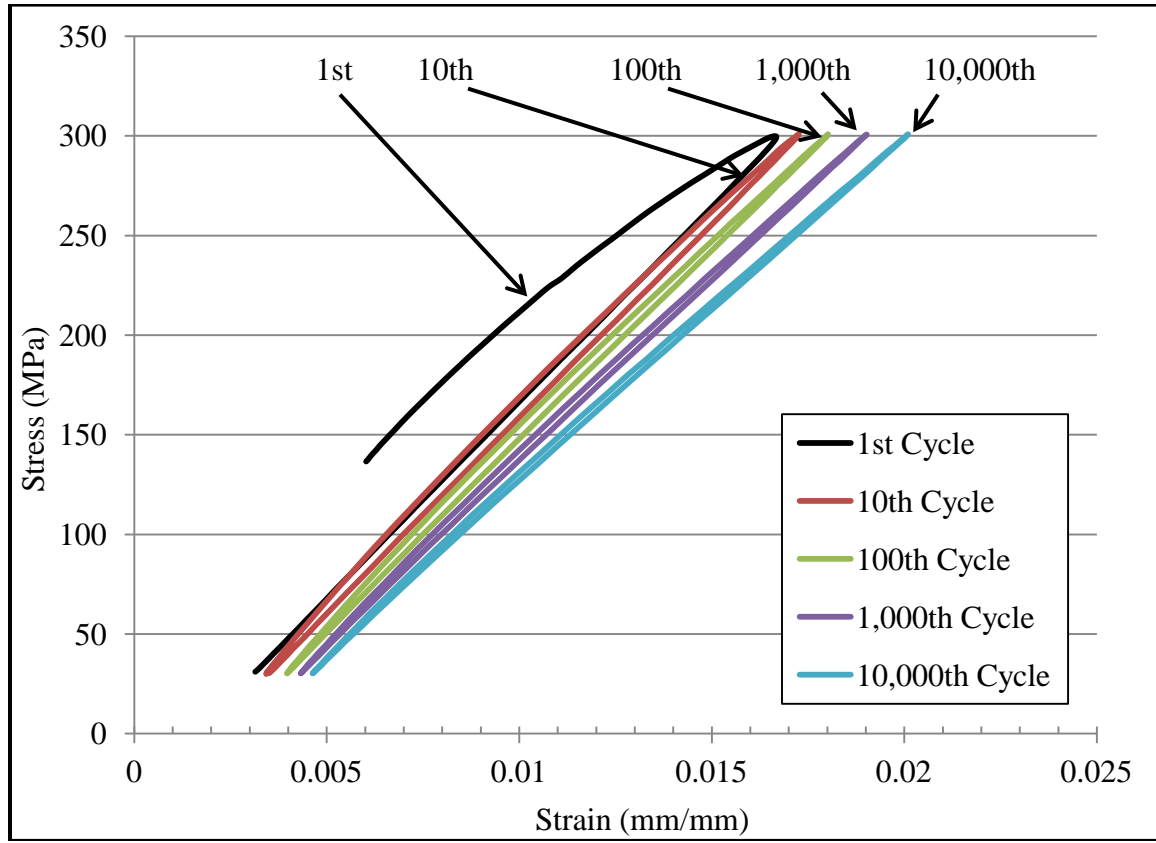
Figure 45. 8G/CNF (55% UTS) stress versus strain curve

4.4 Number of Cycles versus Stress Levels

All six different composite configurations showed linear trends when plotted on a semi-log scale. The decrease in maximum stress resulted in an increase of fatigue life. Figure 46 shows the results from the six different composite configurations where the maximum stress is plotted against the log scale of load cycles. 8G/CNT and 8G/CNF composites showed a greater resistance to fatigue compared to the 8G, (G/CNT)$_4$, 2CNT/4G/2CNT, and 4G/4CNT composites due to the fact that the glass fiber and matrix combination were distinctly different. The mechanical strength properties are slightly higher for the 8G/CNT and 8G/CNF glass fiber and epoxy combination compared to the

8G, (G/CNT)$_4$, 2CNT/4G/2CNT, and 4G/4CNT glass fiber and epoxy combination. The

8G/CNT and 8G/CNF consisted of 6781 S-2 glass fiber in CYCOM 5250-4 BMI matrix,

while the 8G, (G/CNT)$_4$, 2CNT/4G/2CNT, and 4G/4CNT consisted of S-glass

(Astroquartz II) fiber in CYCOM 5575-2 cyanate ester matrix.
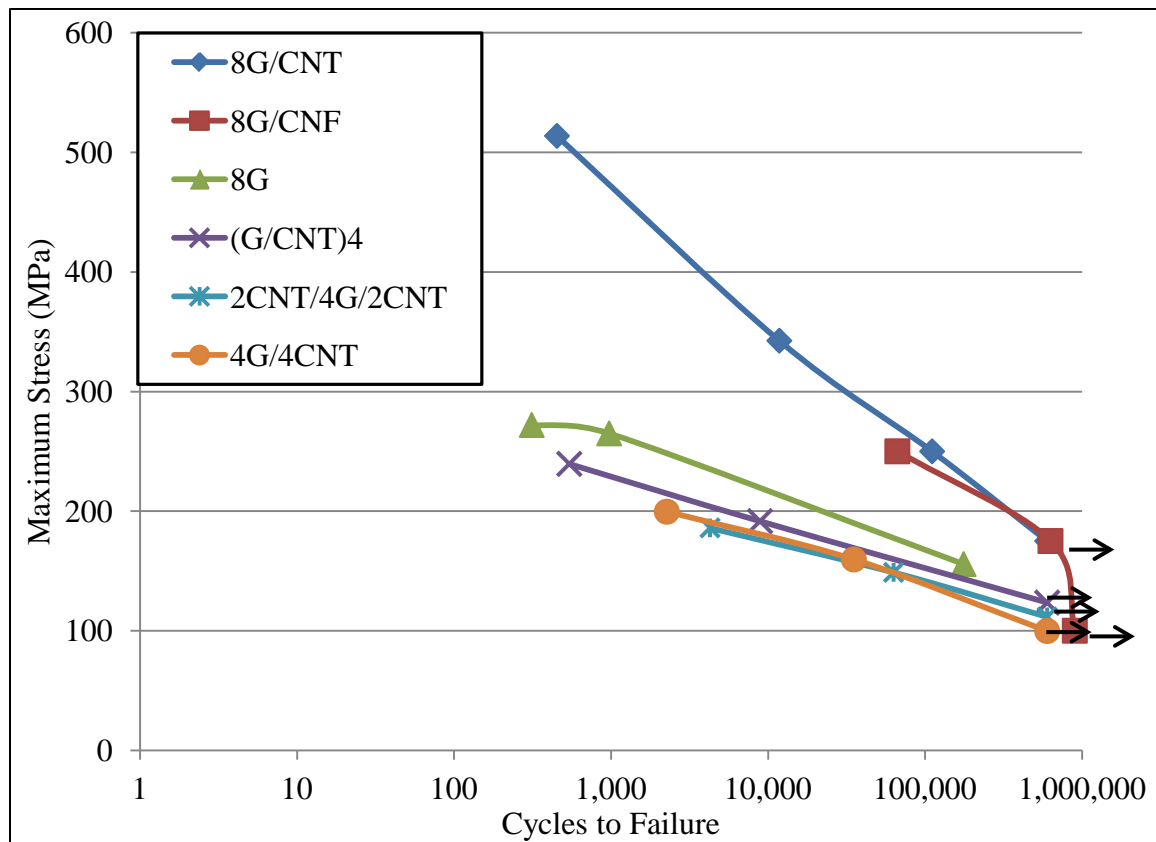
Figure 46. Maximum stress S-N curve

Figure 47 shows the six different composite configurations for % UTS plotted

against the log scale of load cycles. The linear trend was again similar for all six

configurations.
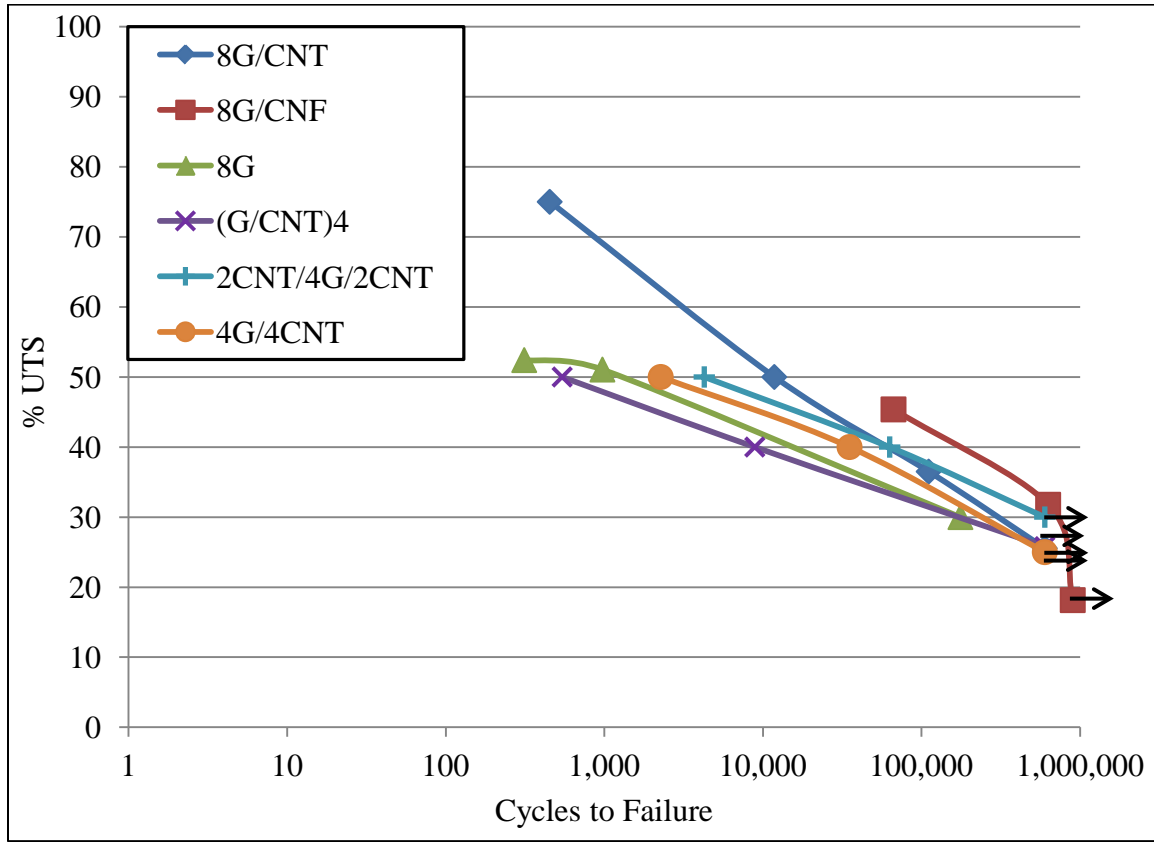
Figure 47. % UTS S-N curve

4.5 Failure Mechanisms Under Fatigue

Failure mechanisms on the post-fatigue specimens were inspected using an optical microscope (OM) and a Scanning Electron Microscope (SEM). The Zeiss OM with AxioVision 40 v4.8.1.0 software, located in AFIT building 640, room 268 was used for OM image collection. The FEI Quanta 600FEG SEM located in AFRL building 654, room 225 was used for SEM image collection. Figure 48 shows the fatigue tested specimens. Of the 18 specimens shown in Figure 48 13 exhibited failure.
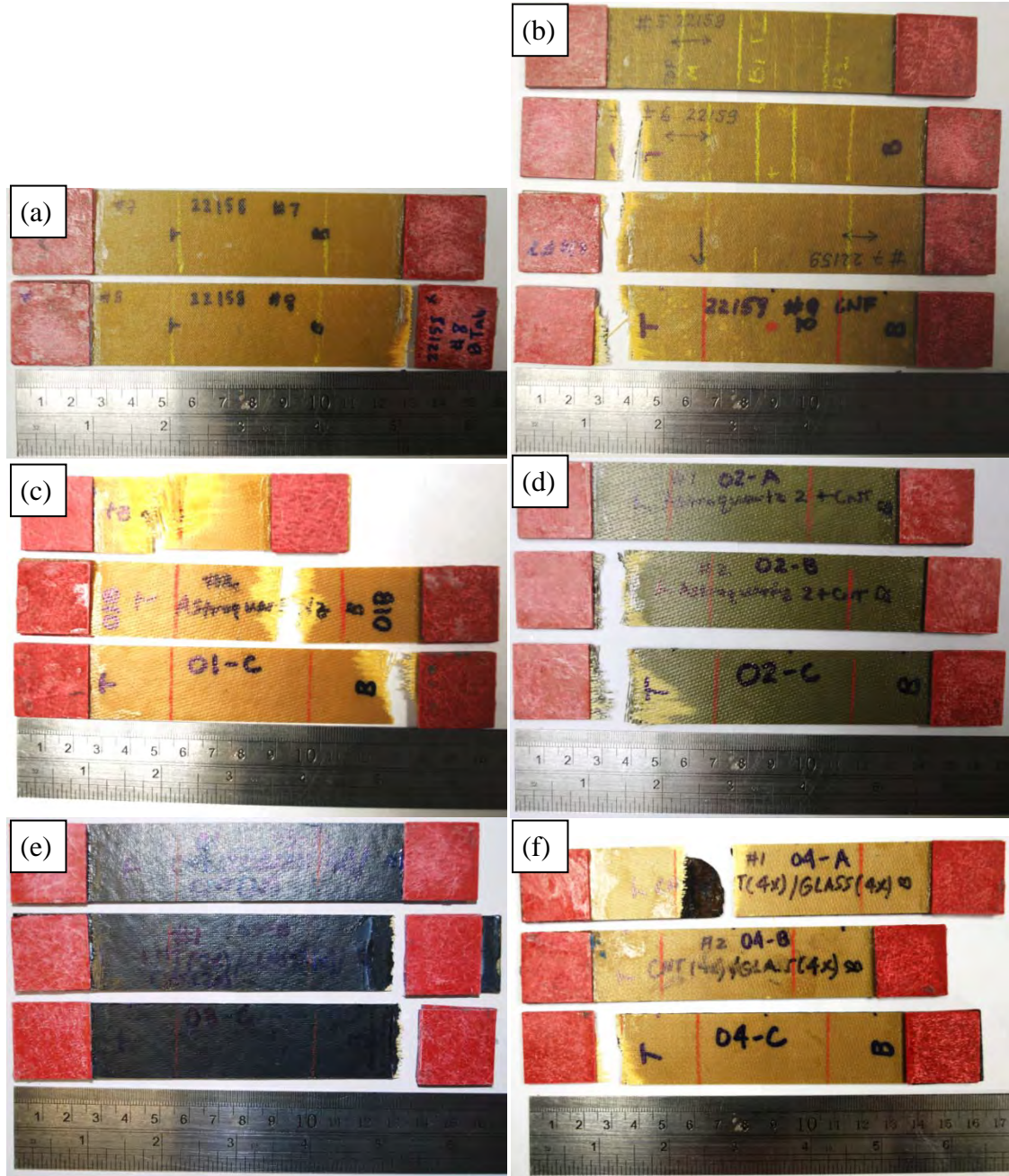
Figure 48. Test specimens: (a) 8G/CNT, (b) 8G/CNF, (c) 8G, (d) (G/CNT)₄, (e) 2CNT/4G/2CNT, (f) 4G/4CNT

The location of the fracture on the test specimens varied throughout the 13

specimens. Six of the 13 specimens fracture occurred near the top glass epoxy tabs. Four

of the 13 specimens fracture occurred near the bottom of the glass epoxy tabs. Three of

the 13 specimens fracture occurred near the middle of the test specimen. The type of

74

failures were common among the rectangular shaped specimens. The inspected test specimen failures consisted of transverse matrix cracking in the fill (90°) strands and delamination between the different plies. Delamination occurred between the warp (0°) and fill (90°) strands in the different plies. Under fatigue loading the specimens' transverse fiber direction (90°) would experience matrix cracks and this damage would lead to delamination of the different plies and eventually ultimate failure of the composite. Figure 49 shows the schematic of the warp and fill strands in a 3-harness satin weave and where in the laminate the transverse matrix cracking and delamination commonly occurred.
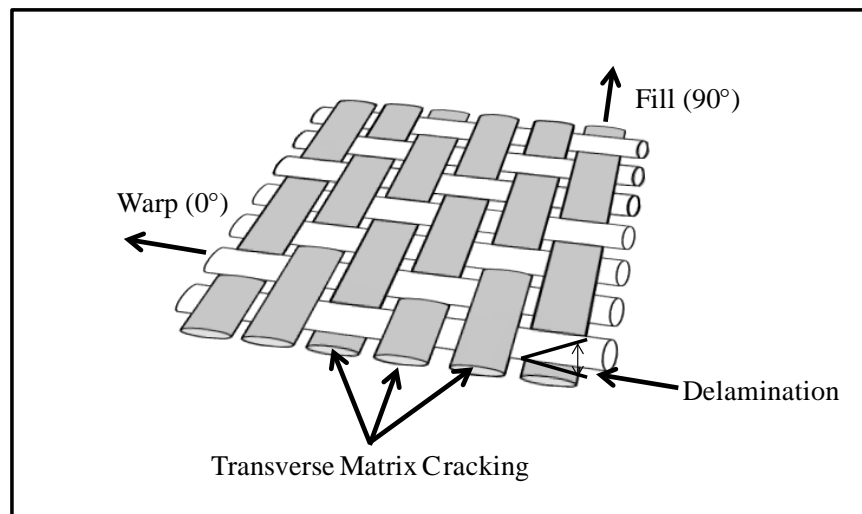
Figure 49. 3-harness satin weave and common failure mechanisms

Figure 50 shows 8G (51% UTS) near the fracture region where matrix cracks and delamination have occurred on the specimen. Figure 51 shows 8G/CNT (36% UTS) near the fracture region where matrix cracks and delamination have occurred on the specimen. Figure 52 shows (G/CNT)$_4$ (50% UTS) near the fracture region where matrix cracks and delamination have occurred on the specimen. Figure 53 shows 2CNT/4G/2CNT (40%

UTS) near the fracture region where matrix cracks and delamination have occurred on the specimen. Figure 54 shows 4G/4CNT (40% UTS) near the fracture region where matrix cracks and delamination have occurred on the specimen. Figure 55 shows 8G/CNF (32% UTS) near the fracture region where matrix crack and delamination have occurred on the specimen.
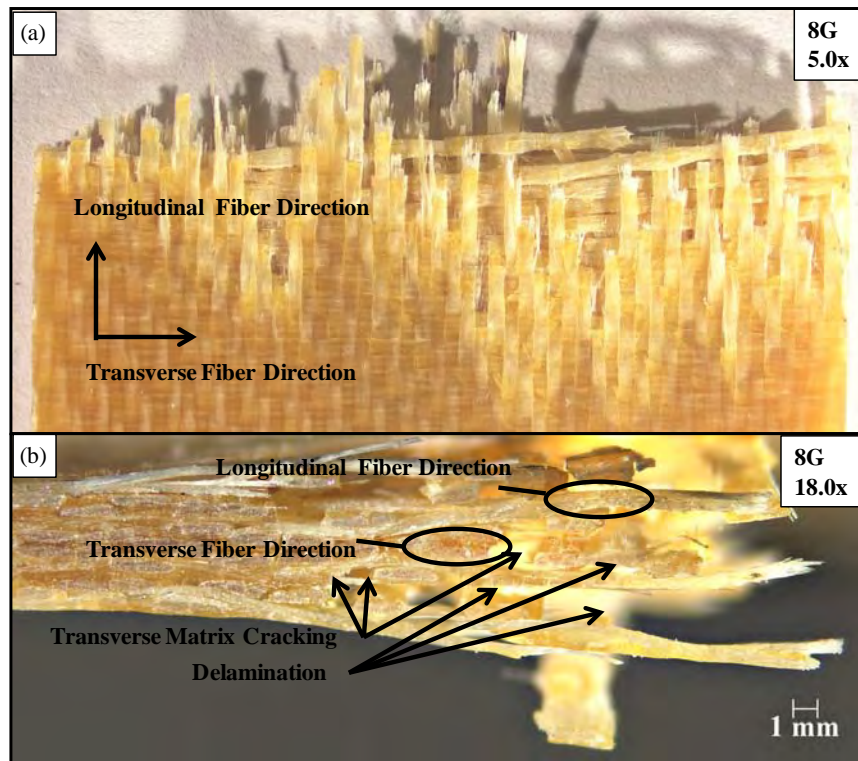
Figure 50. 8G (51% UTS): (a) top view of fracture at 5.0x, (b) side view of matrix cracks and delamination at 18.0x
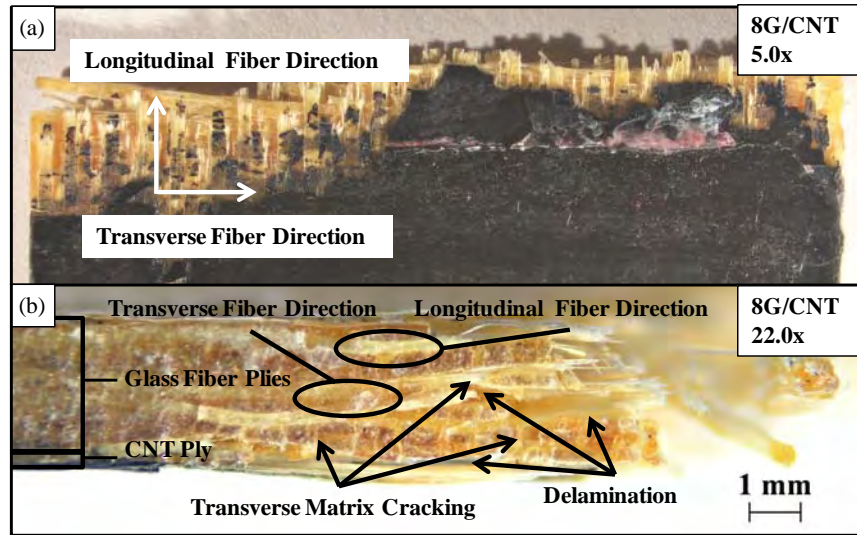
Figure 51. 8G/CNT (36% UTS): (a) top view of fracture at 5.0x, (b) side view of matrix cracks and delamination at 22.0x
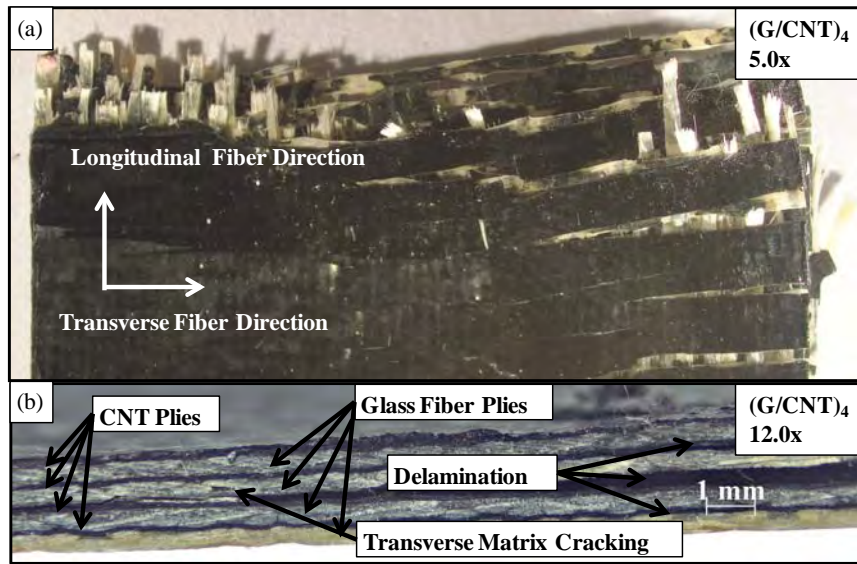
Figure 52. (G/CNT)$_4$ (50% UTS): (a) top view of fracture at 5.0x, (b) side view of matrix cracks and delamination at 12.0x
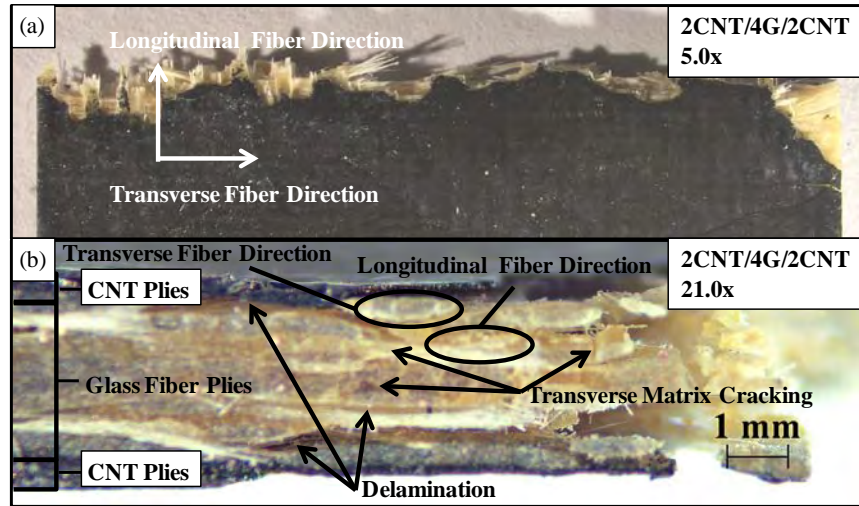
Figure 53. 2CNT/4G/2CNT (40% UTS): (a) top view of fracture at 5.0x, (b) side view of matrix cracks and delamination at 21.0x
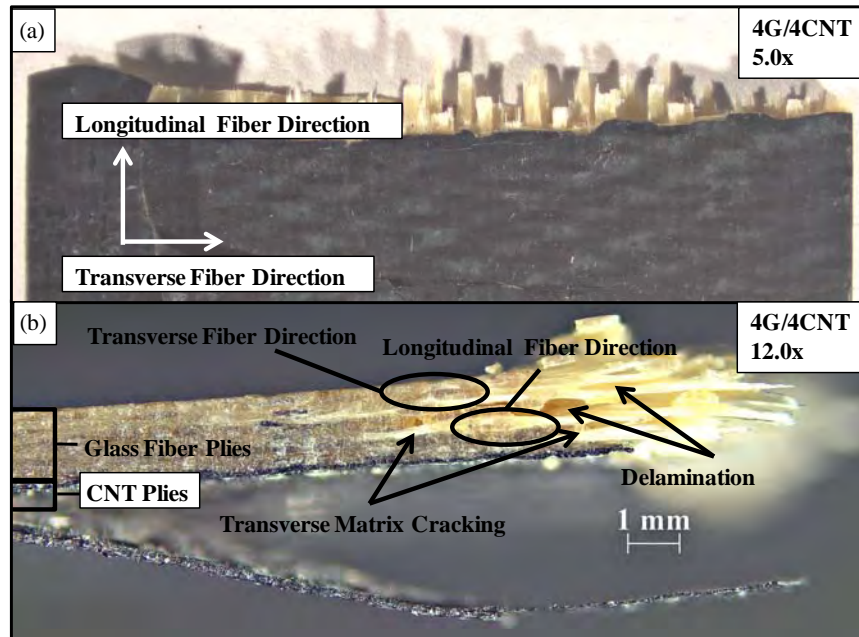
Figure 54. 4G/4CNT (40% UTS): (a) top view of fracture at 5.0x, (b) side view of matrix cracks and delamination at 12.0x
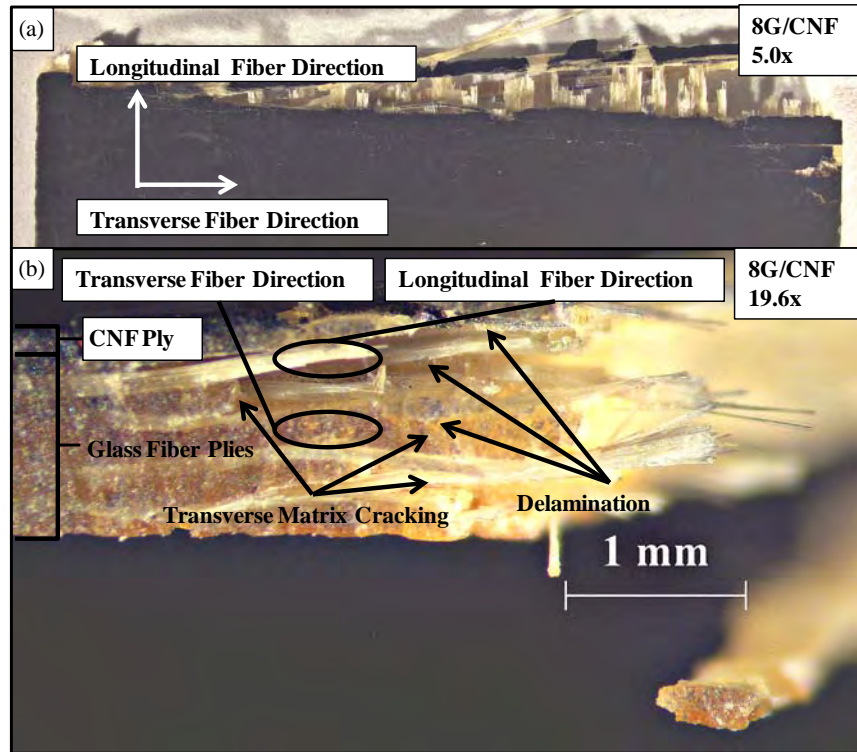
Figure 55. 8G/CNF (32% UTS): (a) top view of fracture at 5.0x, (b) side view of matrix cracks and delamination at 19.6x

OM images with greater magnification were collected to show further evidence of

transverse matrix cracking and delamination. Figure 56, 57, 58, 59, 60 and 61 provides

further the evidence of the above mentioned failure mechanisms for 8G, 8G/CNT,

(G/CNT)$_4$, 2CNT/4G/2CNT, 4G/4CNT, and 8G/CNF respectively.
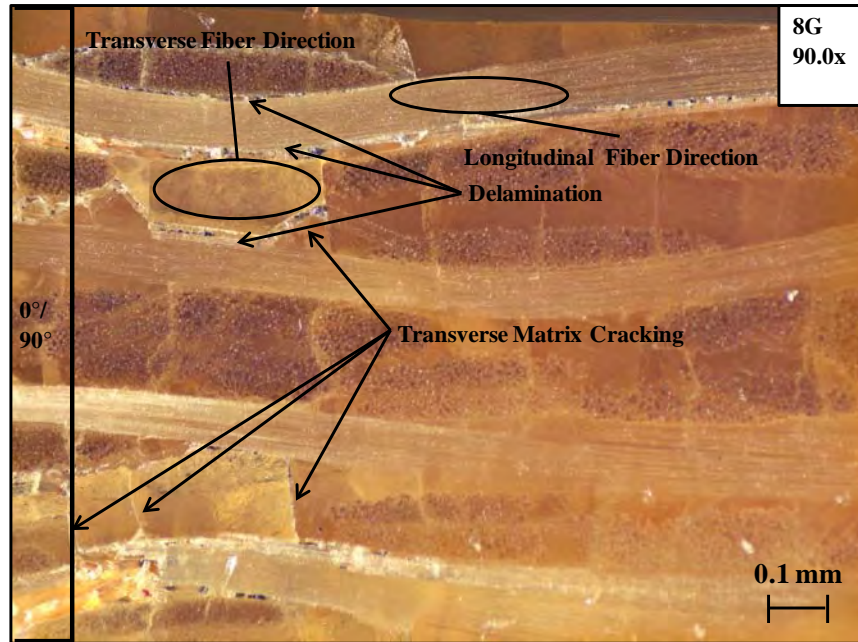
Figure 56. 8G (51% UTS) matrix cracks and delamination at 90.0x
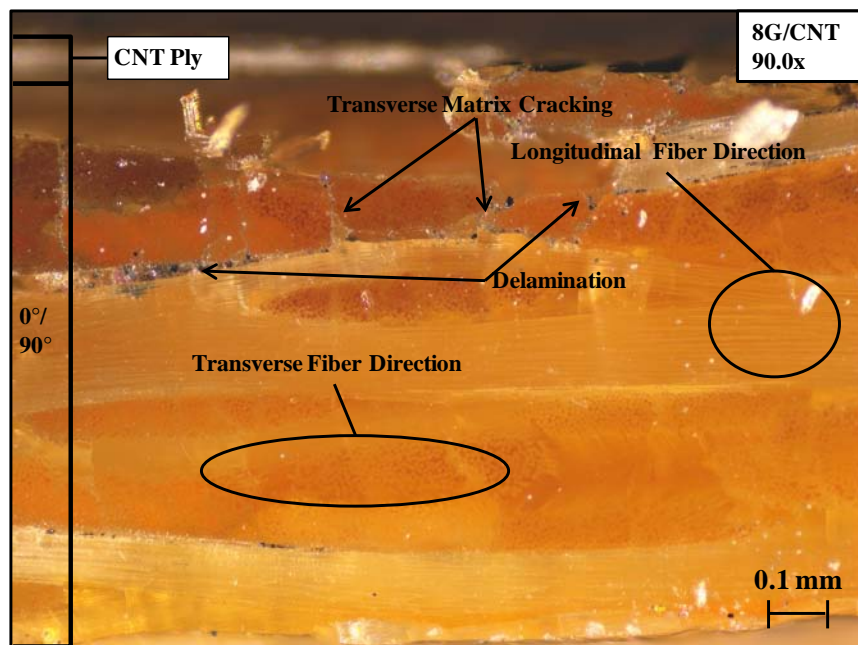
Figure 57. 8G/CNT (36% UTS) matrix cracks and delamination at 90.0x
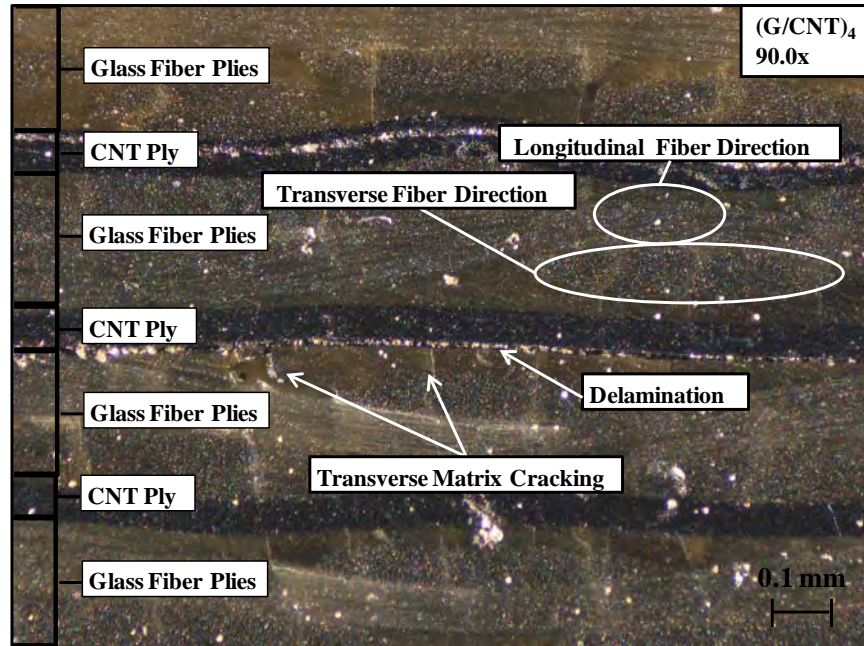
Figure 58. (G/CNT)$_4$ (50% UTS) matrix cracks and delamination at 90.0x
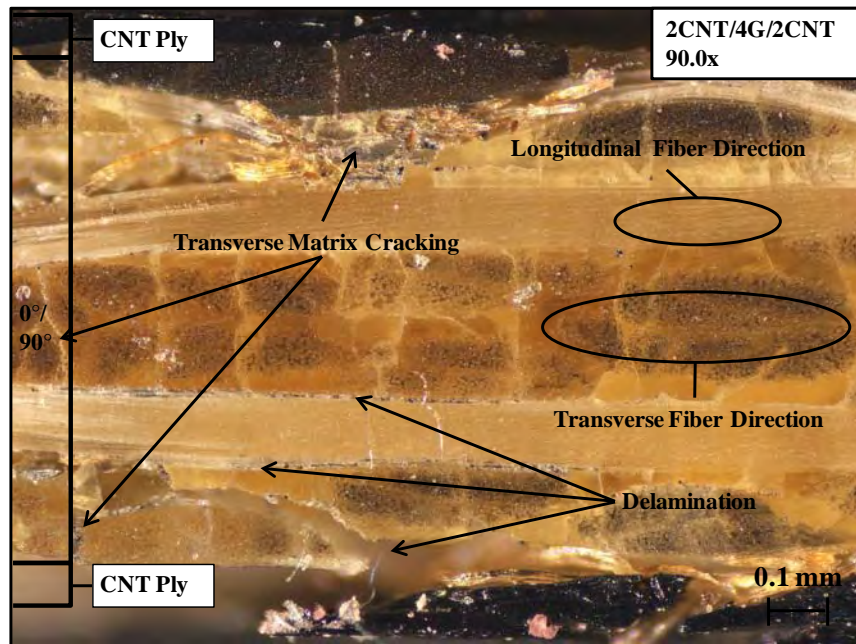
Figure 59. 2CNT/4G/2CNT (40% UTS) matrix cracks and delamination at 90.0x
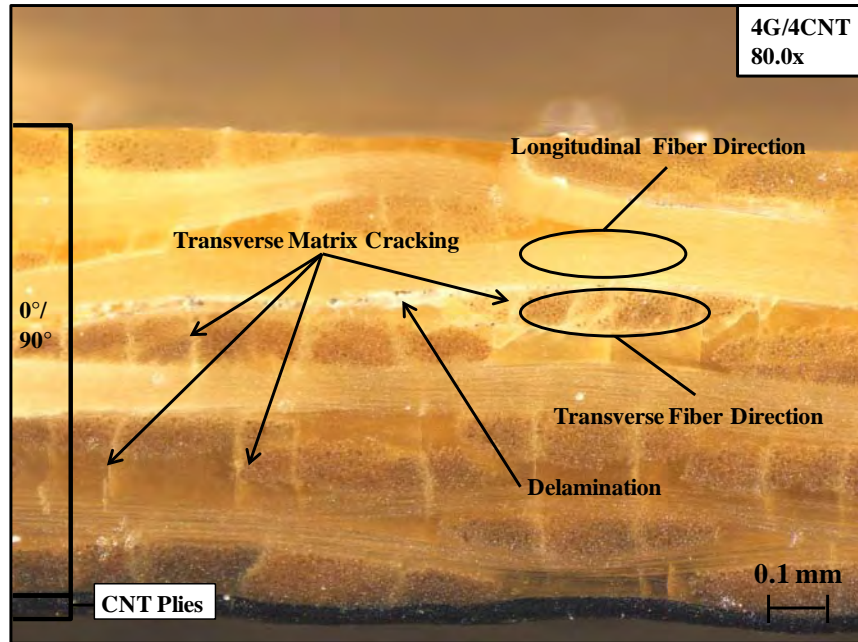
Figure 60. 4G/4CNT (40% UTS) matrix cracks and delamination at 80.0x
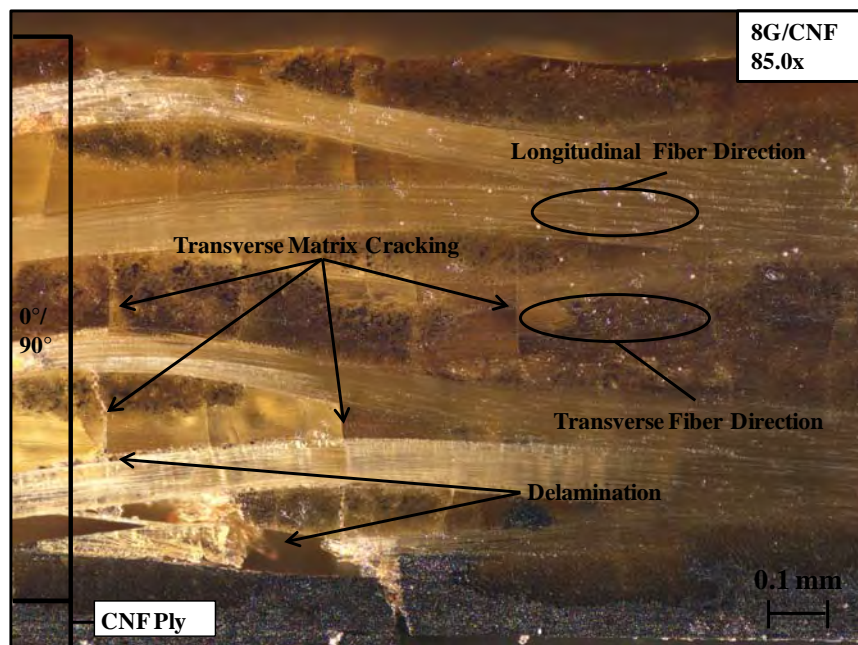
Figure 61. 8G/CNF (32% UTS) matrix cracks and delamination at 85.0x

SEM images were collected on the fractured test specimens to further support the failure mechanisms previously mentioned. Evidence from Figure 62 through Figure 74 show that near and also away from the fracture region the CNT and CNF plies remained

intact while the damage was consistent with the transverse matrix cracking and

delamination of the fiber glass plies along the warp (0°) and fill (90°) strands. The intact

CNT and CNF plies shown below in the SEM images provide support that the specimens'

can effectively shield against EMI after failure has occurred.
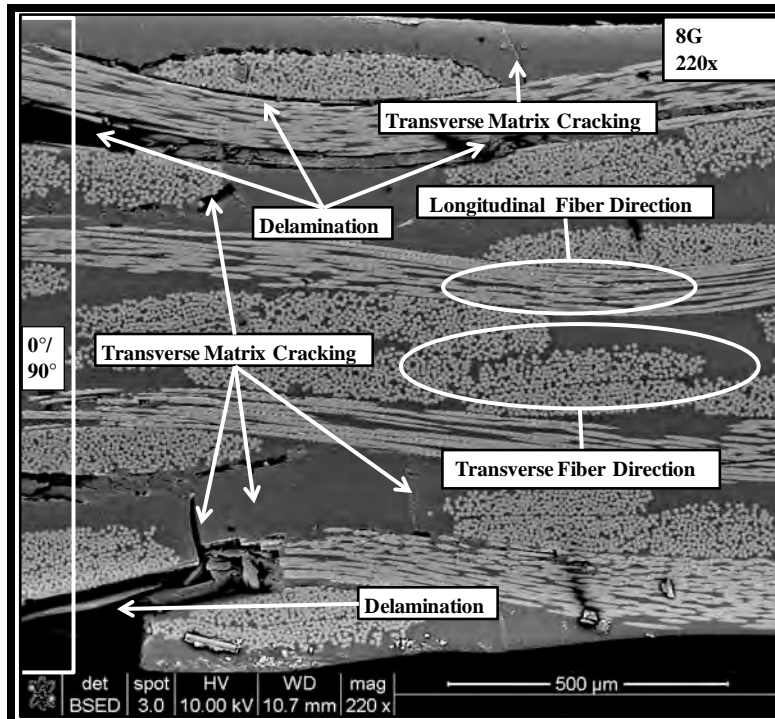
Figure 62. 8G (51% UTS) SEM image: matrix cracks and delamination at 220x
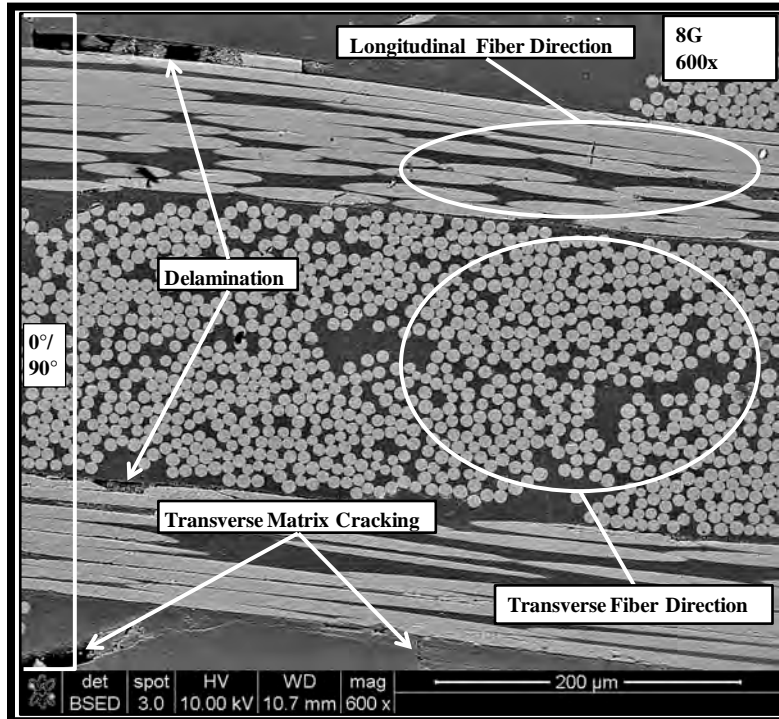
Figure 63. 8G (51% UTS) SEM image: matrix cracks and delamination at 600x
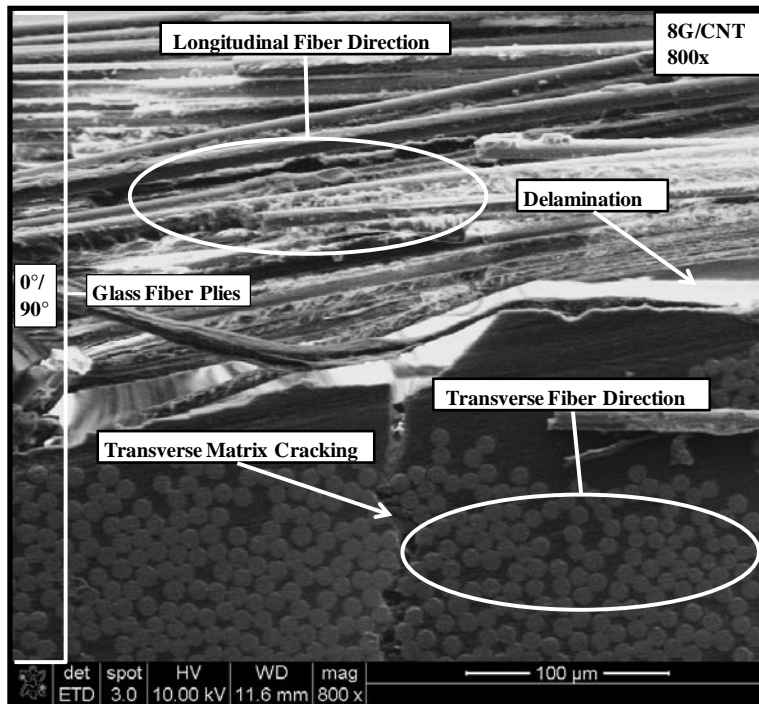
Figure 64. 8G/CNT (36% UTS) SEM image: matrix crack and delamination at 800x
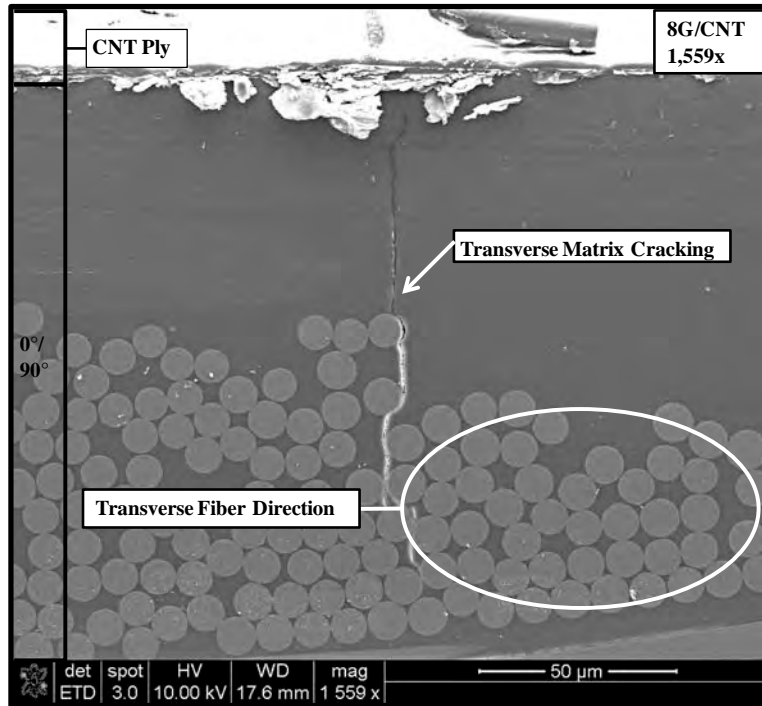
Figure 65. 8G/CNT (36% UTS) SEM image: matrix crack and intact CNT ply at 1,559x
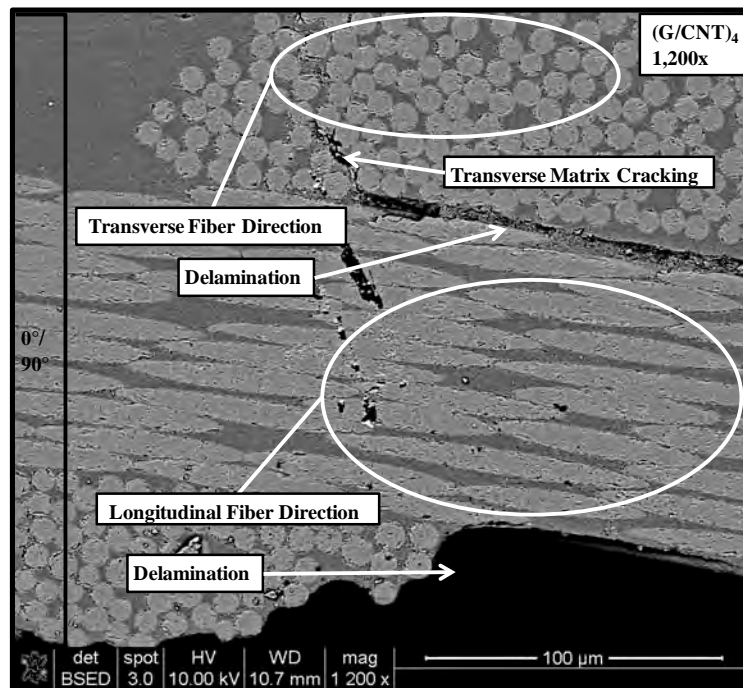
Figure 66. (G/CNT)₄ (50% UTS) SEM image: matrix cracks and delamination at 1,200x
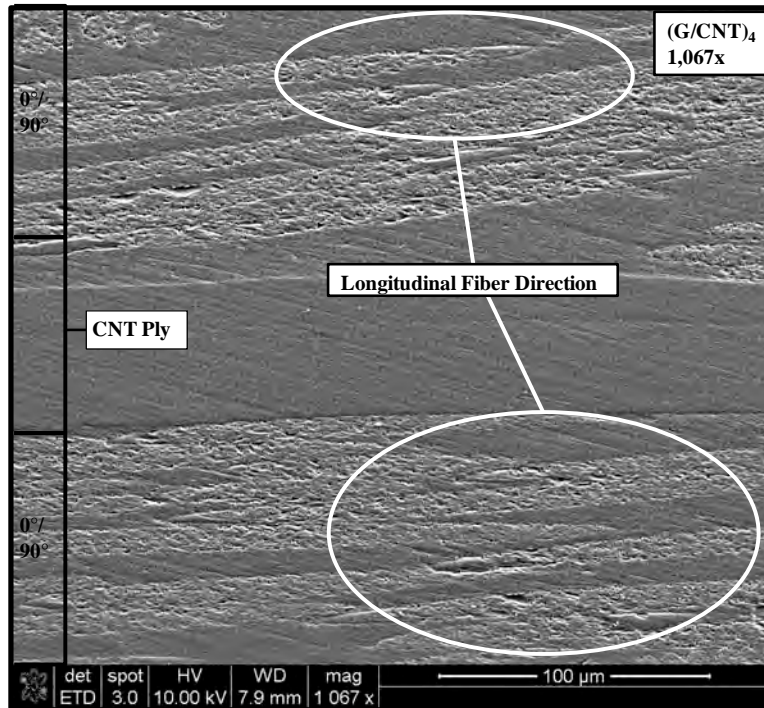
Figure 67. (G/CNT)$_4$ (50% UTS) SEM image: intact CNT ply at 1,067x
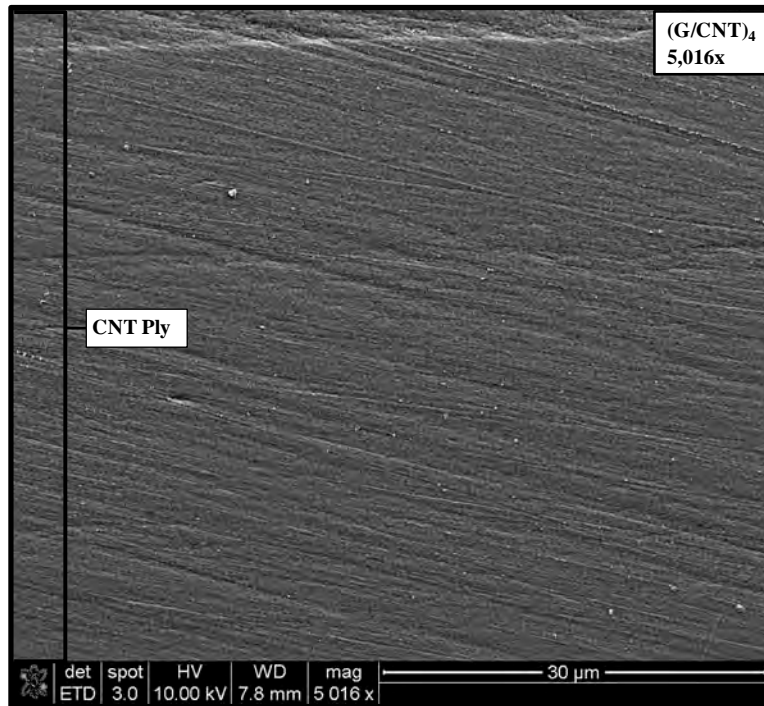
Figure 68. (G/CNT)4 (50% UTS) SEM image: intact CNT ply at 5,016x
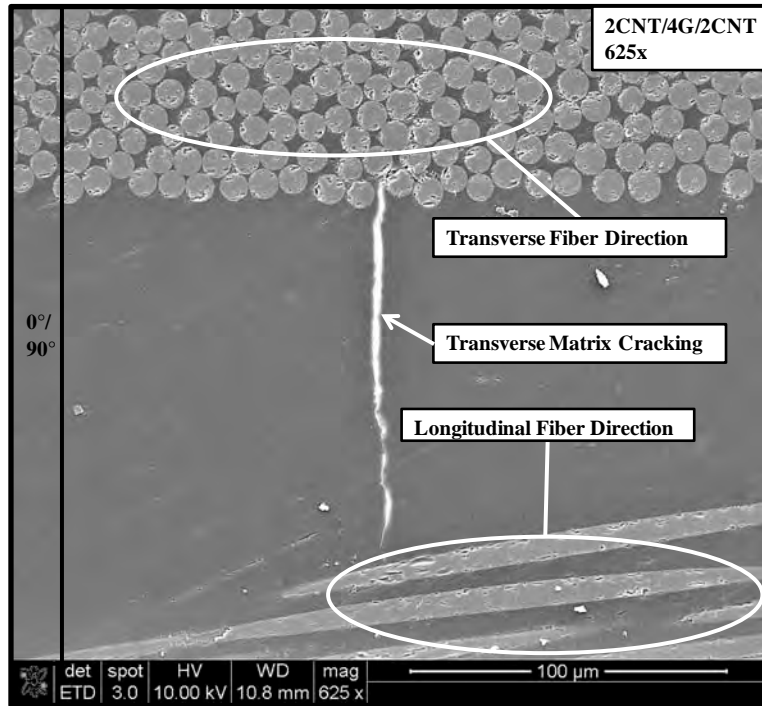
Figure 69. 2CNT/4G/2CNT (40% UTS) SEM image: matrix crack at 625x
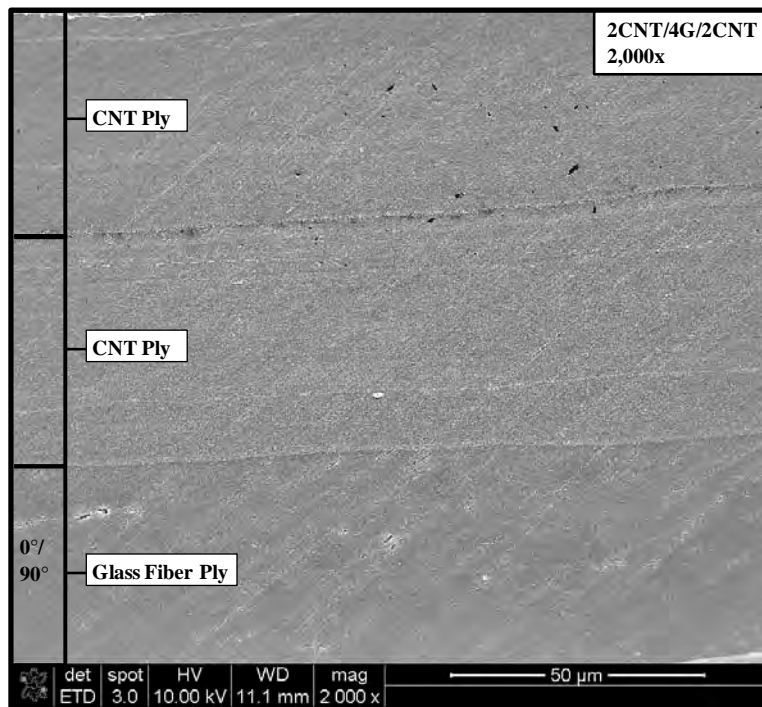
Figure 70. 2CNT/4G/2CNT (40% UTS) SEM image: intact CNT ply at 2,000x
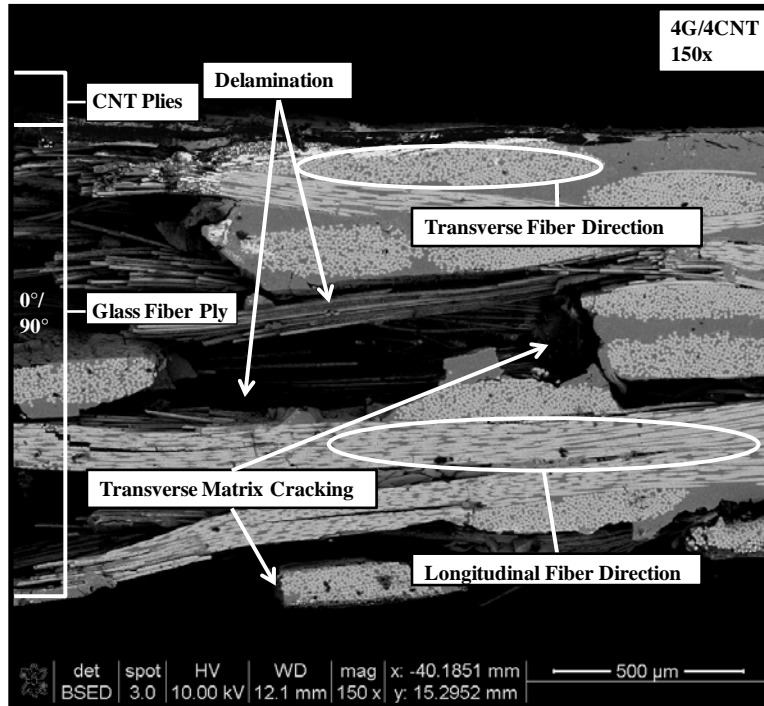
Figure 71. 4G/4CNT (40% UTS) SEM image: matrix cracks and delamination at 150x
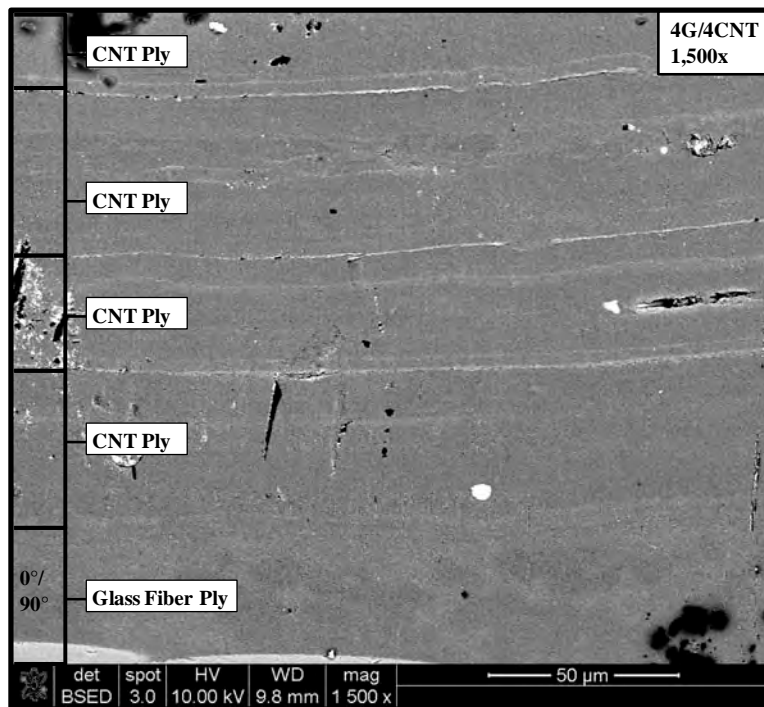
Figure 72. 4G/4CNT (40% UTS) SEM image: intact CNT ply at 1,500x
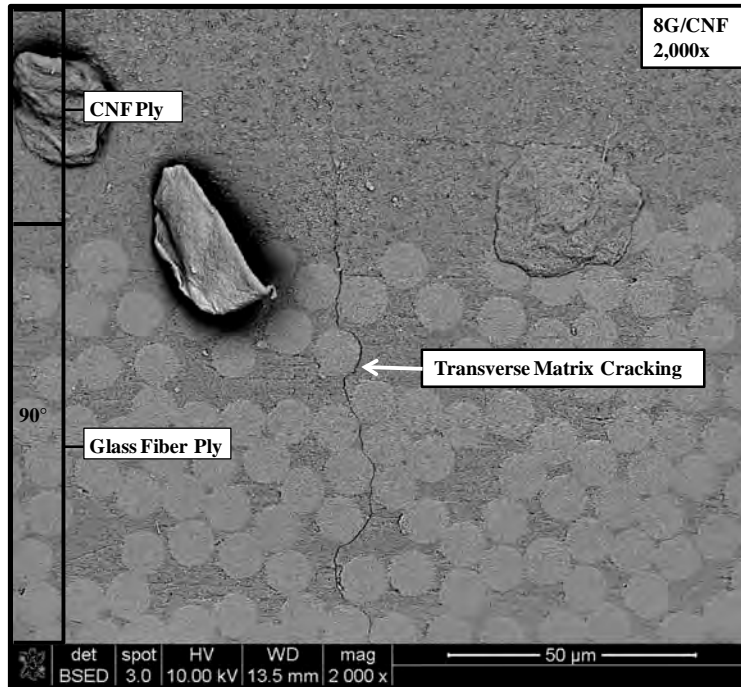
Figure 73. 8G/CNF (32% UTS) SEM image: matrix cracks and intact CNF ply at 2,000x
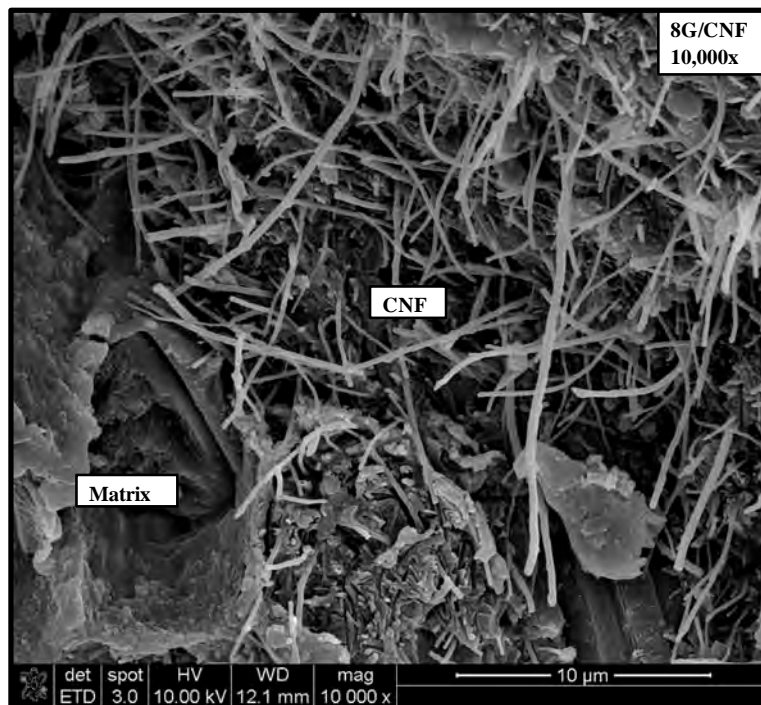
Figure 74. 8G/CNF (32% UTS) SEM image: CNF and matrix at 10,000x

Figure 76 shows a higher magnification of the intact CNF ply on the 8G/CNF (32% UTS) specimen near the fracture region, which is shown in a zoomed out view in Figure 75.
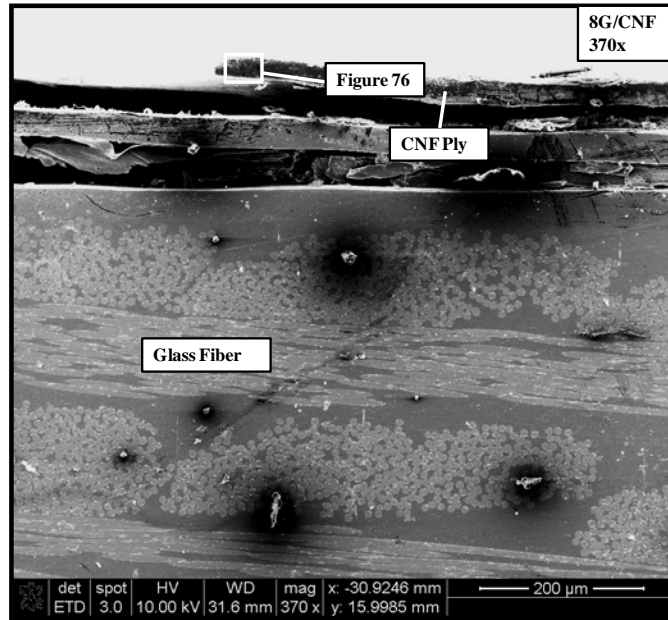
Figure 75. 8G/CNF (32% UTS) SEM image: CNF and glass fiber matrix at 370x
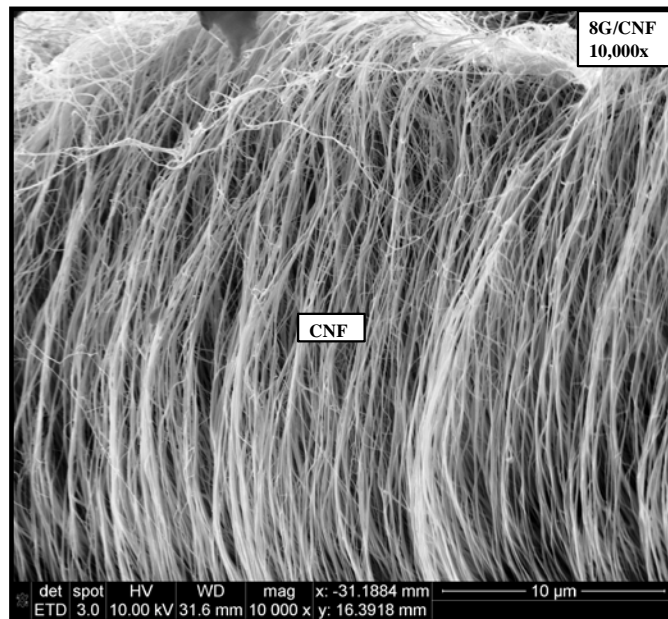
Figure 76. 8G/CNF (32% UTS) SEM image: CNF at 10,000x

V. Conclusions and Recommendations

This chapter provides a summary of the research and analysis of the results. Lastly, the conclusions of this research are outlined along with recommendations for future work.

5.1 Summary

The main objective of this research was to characterize the electromagnetic interference (EMI) shielding effectiveness (SE) of nanocomposites procured with a eight ply laminate of S-glass (Astroquartz II) fiber in a CYCOM 5575-2 cyanate ester matrix combined with different MWNT ply stacking sequences and a eight ply laminate of 6781 S-2 glass fiber in CYCOM 5250-4 BMI resin laminate with a externally deposited ply of CNTs or CNFs while subjected to fatigue. Current space vehicle materials that shield against EMI use metallic thin sheet or films. AFIT and AFRL are researching the potential use of EMI shielded nanocomposites in attempts to reduce the dry weight and ultimately cut manufacturing and launch costs on space vehicle systems. The results in this research characterized the effects of EMI SE under fatigue and helped determine the suitability of using CNT/CNF nanocomposites in space vehicle systems. Six different composites were procured and tested for their EMI SE before and after fatigue. The six different composites are shown in Figure 17 in section 3.2. The optical microscope images are available in Figure 50 through Figure 61 in section 4.5. The test equipment and procedures for this research are mentioned in Chapter III.

5.2 Conclusions

The following conclusions are derived from the analysis of the collected test data:

A. Effect of tension-tension cyclic loading on EMI SE

- Fatigue loading had minimal affect on EMI SE for all six different composite configurations. The EMI SE remained fairly constant throughout the fatigue testing up to failure or to the desired fatigue cycles (i.e. 600,000 cycles). Of all the six different composite configurations, the configuration with the highest initial EMI SE was 2CNT/4G/2CNT with 67.65 dB. The 2CNT/4G/2CNT's EMI SE exceeds the current EMI SE 60 dB threshold.

- The 2CNT/4G/2CNT, 4G/4CNT, and $(G/CNT)_4$ nanocomposites had 3.6 times more grams of CNTs compared to 8G/CNT. This suggests that CNT concentration contribute to the overall EMI SE performance of the nanocomposite.

B. Stacking sequence effect

- The 2CNT/4G/2CNT specimen showed the best EMI SE performance. This supports past studies that showed that exterior placement of conductive of CNT plies provides the best EMI SE performance over other configurations.

- The comparison of resistance to fatigue failure, when compared to stress, for $(G/CNT)_4$, 2CNT/4G/2CNT, and 4G/4CNT showed minimal differences between the different stacking sequences. This supports that idea that picking the exterior configuration, 2CNT/4G/2CNT, would not lead to a weaker configuration compared to the other two nanocomposite configurations.

C. Failure mechanisms

- An increase in stress caused a decrease in cycle life experienced in all test specimens. All of the test specimens fatigue tested under 30% UTS survived at least 600,000 fatigue cycles without failure.

- The 8G/CNT and 8G/CNF specimens showed a higher resistance to fatigue failure over the four other composites in this study, when compared to maximum stress. This suggests that a matrix's mechanical properties contribute to the overall strength of the composite.

- The failure mechanisms for all six composites were identical and not dependent upon configuration. Damage was consistent, i.e. transverse matrix cracks initiated first, followed by delamination and further matrix cracks, and eventually ultimate failure. Delamination occurred between the warp (0°) and fill (90°) strand, and sometimes between either CNT or CNF and glass fiber plies. The CNT plies remained intact until fracture of specimen. Damage was minimal to the CNT and CNF plies away from the fracture region. This minimal damage to the CNT and CNF plies was supported by EMI data after failure that showed the CNT and CNF EMI data was relatively unchanged compared to initial EMI data. This was further supported by OM and SEM images done on the CNT and CNF plies away from the fracture region that showed minimal damage.

5.3 Recommendations for Future Work

This research complements past studies in the use of nanocomposites with conductive properties for EMI SE. This is the first set of research to characterize the effects of EMI SE on S-glass (Astroquartz II) fiber in a CYCOM 5575-2 cyanate ester matrix combined with different MWNT ply stacking sequences and a eight ply laminate of 6781 S-2 glass fiber in CYCOM 5250-4 BMI resin laminate with a externally deposited ply of CNTs or CNFs while subjected to fatigue. By using the EMI SE results from monotonic tension tests and fatigue tests on the NS, CNT, and CNF nanocomposites, comparisons can be made between the different nanocomposites EMI SE performance before space environments exposure. The test results can be used for future work on modeling and parameterization. The modeling work can help predict the nanocomposite behavior and assist in conducting non-destructive evaluations that will eliminate costs from unnecessary destructive evaluations. Additional work on the effects of EMI SE under monotonic tension testing and fatigue testing post exposure to the space environment is necessary to build complete relationships and comparisons between the pre-exposure and post-exposure to the space environment on nanocomposites.

Appendix A. Material Properties - 6781 S-2 Glass Fiber

Physical

Density [30] ....2.46 g/cm^3 (0.0889 lb/in^3)

Mechanical

Maximum Tensile Strength [30]...............................4890 MPa (7.1 x 10^5 psi)

Young's Modulus [30] ....86.9 GPa (1.26 x 10^7 psi)

Electrical

Electrical Resistivity [30] ....9.05 x 10^{10} Ω-cm

Dielectric Constant (1 x 10^6 Hz) [30] 5.30

Thermal

Coefficient of Thermal Expansion (Linear) [30].......1.60 μm/m-°C (0.889 μin/in-°F)

Specific Heat Capacity [30] ....0.737 J/g-°C (0.176 BTU/lb-°F)

Thermal Conductivity [30] ....1.45 W/m-K (10.1 BTU-in/hr-ft²-°F)

Optical

Refractive Index [30] 1.521

Appendix B. Material Properties - CYCOM 5250-4 BMI Matrix

Mechanical[1]

Maximum Tensile Strength [31]................................103 MPa (14900 psi)

Young's Modulus [31] ....4600 MPa (6.7 x 10^5 psi)

Strain [31] ....4.8 % (48000 μin/in)

Thermal[1]

Coefficient of Thermal Expansion [31] ....44 x 10^6 in/in/°F

1. Standard cure + standard post-cure: 6 hrs at 350-375 °F + 4 hrs at 440 °F

Appendix C. Material Properties - S-Glass Fiber (Astroquartz II)

Physical

Density ....2.2 g/cm^3 (0.079 lb/in^3)

Mechanical

Virgin Single Filament...6.0 GPa (8.7 x 10^5 psi)

Impregnated Strand Tensile Test ....ASTM D-2343

(on 20 end roving)..3.6 GPa (5.3 x 10^5 psi)

Young's Modulus ....72 GPa (10 x 10^6 psi)

Poisson's Ratio 0.16

Electrical

Dielectric Constant (Dk)

1 MHz 3.70

10 GHz..3.74

Thermal

Linear Expansion Coefficient ....0.54 x 10^{-6}

Specific Heat @ 20°C (J.kg^{-1}.K^{-1})........................7.5 x 10^2

Heat conductivity @ 20°C (W.m^{-1}.K^{-1}) 1.38

Optical

Refractive Index @ 15°C.....................................1.4585

Note: n = Viscosity in Poise

Appendix D. Material Properties - FM 6555-1 Cyanate Ester Syntactic Core

Mechanical

Maximum Tensile Strength (dry at 77 °F) [32] ....17.92 MPa (2600 psi)

Young's Modulus (at 77 °F) [32] ....19.31 MPa (2800 psi)

Appendix E. Material Properties - Carbon Nanotubes

Physical

Density [33] ....1.3-1.4 g/cm^3 (0.047 lb/in^3)

Mechanical

Maximum Tensile Strength (SWNT) [33].............................100 GPa (8.7 x 10^5 psi)

Young's Modulus (SWNT) [33] ....1 TPa (145 x 10^6 psi)

Young's Modulus (MWNT) [33] ....1.28 TPa

Electrical

Conductance Quantization [33] ....(12.9 kΩ)$^{-1}$

Resistivity [33]..10^{-4} Ω-cm

Maximum Current Density [33]..10^{13} A/m^2

Thermal

Thermal Conductivity [33] ....~2000 W/m/K

Relaxation Time [33] ....~10^{-11}

Appendix F. Focused Beam Tunnel Test Procedures

Calibration

1. Connect cable from PNA Port #1 to amplifier INPUT

2. Connect cable from Amplifier OUTPUT to Tunnel INPUT (H-Pol or V-Pol depending on the orientation being tested)

3. Connect 30 dB attenuator to PNA port #2

4. Connect cable from Tunnel OUTPUT to 30 dB attenuator

5. Tightened all cables to proper torque with proper size torque wrench

6. Run RESPONSE calibration with no samples

7. Verify the set configuration

    a. Select SWEEP tab and place the cursor over "Select Number of Points"

        i.   Select 1601

    b. Select SWEEP tab and select "IF Bandwidth"

        i.   Set IF Bandwidth to 10 Hz by using the dialog box

    c. Select CHANNEL tab and select "Power" from the drop down menu

        i.   Set power level to -11 dbm from port 1

        ii. Check mark "Power On", "Port Power Coupled", and "Attenuator Control" under Auto

8. Select SWEEP tab and place the cursor over the TRIGGER tab and select "Single" from the drop down menu (this is the RESPONSE calibration trace)

9. Trigger "Gate" option with gate center equal to 0 ns and gate span equal 1 ns

10. Select the Memory/Math button and store RESPONSE trace

11. Select "Data>>Memory"

12. Select "Data/Memory"

13. A flat line at 0 dB should be displayed

14. Calibrations are valid if the conditions in the room remain constant

15. Recalibration is required if the following situations occurs

    a. Change in time is greater than 4 hours

    b. Change in room temperature is greater than 1°

    c. Change in room's relative humidity is greater than 5%

Specimen

1. Insert test specimen into holder. To prevent leakage tape and/or bolt as required

2. Perform the instructions for Mounting Specimen in Section 4

Testing Procedure

1. Remove attenuator form Port #2 of the PNA and connect RF cable directly to Port #2 (ensures proper function and prevents damage)

2. On the PNA start a Single Trace Scan

3. Start "Gate" option with gate center equal to 0 ns and gate span equal to 1 ns

4. A insertion loss of +30 dB will be present due in-line attenuator used during RESPONSE calibration

5. Subtract 30 dB from the trace measurement displayed to correct final data

6. Repeat the same procedures for additional specimens (steps 1-5 for Testing Procedures)

7. Recalibration is required if the following situations occurs

a. Change in time is greater than 4 hours

b. Change in room temperature is greater than $1°$

c. Change in room's relative humidity is greater than 5%

Notes:

1. Noise floor performance can be gained by decreasing the IF beam width

2. Gate parameters can be controlled to get response changes

3. PNA will perform time domain analysis

4. Significant periodic nulls in the trace measurement may be due to energy leakage around the edge of the sample

Appendix G. Detailed EMI Test Procedures

How to set frequency range

1. On main screen click Start Frequency.

2. Type 8.2GHz and hit Enter.

3. On main screen click Stop Frequency.

4. Type 12.4GHz and hit Enter.

5. Make sure that Start and Stop Frequency are 8.2 GHz and 12.4 GHz respectively.

How to create the proper trace (S_{12})

1. On main screen Click Trace/Chan.

2. Click New Trace.

3. Select the S_{12} trace option.

4. Select Create new traces in a new window.

5. Click Ok.

6. If you have multiple traces shown on the screen you can right click and delete the undesired trace. In addition, you can move the desired trace screen and expand using the mouse.

Calibration Steps

1. Locate the wooden calibration box in the lab marked X1164A WR-90 Calibration Kit.

2. Click Calibration.

3. Click Calibration Wizard.

4. Select UNGUIDED Calibration (Response, 1-port, 2-port) Use Mechanical Standards.

5. Under Cal Type Selection Select TRL.

6. Click View/Select Cal Kit.

7. Select TRL classes under choose class type.

8. Locate and select X1164A Calibration Kit for X1164A for 8.2-12.4 GHz - X-band.

9. Click Next.

10. Under TRL Reference Plane Select REFLECT Standard.

11. Under TRL Impedance Select LINE Standard.

12. Click Next.

13. Insert Short (solid plate) in between the two adapters and tighten screws with hex nuts and Phillips screw driver.

14. Click Short under Port 1 and Port 2.

15. Remove Short from adapters.

16. Insert 1/4 wavelength shim (plate with rectangle cutout) in between the two adapters and tighten screws with hex nuts and Phillips screw driver.

17. Click Line.

18. Select X-band 1/4 wavelength line.

19. Click Ok.

20. Remove 1/4 wavelength shim from adapters.

21. Put the two adapters together and tighten screws with hex nuts and Phillips screw driver.

22. Click Thru.

23. Click Next.

EMI testing process

1. Insert the specimen in between the two adapters and tighten screws with hex nuts and Phillips screw driver.

2. Right click anywhere on the graph output window and select Autoscale.

3. On main screen Click Channel.

4. Click Average.

5. Input 16.

6. Click Ok.

7. On main screen Click File.

8. Click Save As.

9. Select desired folder to save the file in.

10. Select file type .prn file.

11. Type desired file name.

12. Click Ok.

13. Repeat Steps 1-12 two or four times on the top and bottom sections of the specimen.

Appendix H. MATLAB Code for Importing Text Files into Excel Files

```matlab
function T = getdata(BaseFile, n)

    % Open the first file; must change the root file name each time with

    % the right file name!

    d(1) = fopen(['2011111501CT' '1.prn']);

    % Read the first two columns, skip the first 2 headerlines

    T1 = textscan(d(1), '%f %f','Delimiter',',','HeaderLines', 2);

    % Close the file, you don't need it any longer

    fclose(d(1));

for i = 2 : 3

    % Open consecutively each of the remaining files

    d(i) = fopen(['2011111501CT' num2str(i) '.prn']);

    % Skip the first column of the new file (an '*' to do this)    % and keep on building the

array

    T1 = [T1 textscan(d(i), '%*f %f','Delimiter',',','HeaderLines', 2)];

    % Close the file

    fclose(d(i));

        % Open the first file

        e(1) = fopen(['2011111501CM' '1.prn']);

        % Read the first two columns, skip the first 2 headerlines

        T2 = textscan(e(1), '%*f %f','Delimiter',',','HeaderLines', 2);

        % Close the file, you don't need it any longer
```

```matlab
    fclose(e(1));

  for i = 2 : 3

    % Open consecutively each of the remaining files

    e(i) = fopen(['2011111501CM' num2str(i) '.prn']);

    % Skip the first column of the new file (an '*' to do this)     % and keep on building

the array

    T2 = [T2 textscan(e(i), '%*f %f','Delimiter',',','HeaderLines', 2)];

    % Close the file

    fclose(e(i));

      f(1) = fopen(['2011111501CB' '1.prn']);

      % Read the first two columns, skip the first 2 headerlines

      T3 = textscan(f(1), '%*f %f','Delimiter',',','HeaderLines', 2);

      % Close the file, you don't need it any longer

      fclose(f(1));

    for i = 2 : 3

      % Open consecutively each of the remaining files

      f(i) = fopen(['2011111501CB' num2str(i) '.prn']);

      % Skip the first column of the new file (an '*' to do this)     % and keep on

building the array

      T3 = [T3 textscan(f(i), '%*f %f','Delimiter',',','HeaderLines', 2)];

      % Close the file

      fclose(f(i));
```

```
        end

    end

end

T=[T1 T2 T3]

end
```

The second .m file code is shown below to export the EMI data in Excel:

```
% Reset your memory and clear your screen

clear; clc

 % Provide base file name and number of files to be read

BaseFile = 'data_sheet';

n = 9;

 % Use the developed function to read data

T = getdata(BaseFile, n);

 % Transform your cell array into an ordinary matrix

A = T{1};

for i = 2 : n+1

    A = [A T{i}];

end

 % Show your data (had to convert 1st column to Giga scale)

% Matrix for Top Section

B1 = 1e-9*A(:,1);

C1 = A(:,2:4);
```

D1 = [B1 C1]

E1 = mean(C1,2);

 % Matrix for Middle Section

B2 = 1e-9*A(:,1);

C2 = A(:,5:7);

D2 = [B2 C2]

E2 = mean(C2,2);

 % Matrix for Bottom Section

B3 = 1e-9*A(:,1);

C3 = A(:,8:10);

D3 = [B3 C3]

E3 = mean(C2,2);

% Average for all the frequency ranges

B4 = 1e-9*A(:,1);

C4 = mean(A(:,2:10),2);

D4 = [B4 C4]

% Calculate the average for the Top Section from columns 2-4

Tempa = sum(D1(:,2:4));

Temp2a = -1*sum(Tempa);

[a1,b1]=size(C1);

AVG1 = Temp2a/(a1*b1)

% Calculate the average for the Middle Section from columns 2-4

```matlab
Tempb = sum(D2(:,2:4));

Temp2b = -1*sum(Tempb);

[a2,b2]=size(C2);

AVG2 = Temp2b/(a2*b2)

% Calculate the average for the Bottom Section from columns 2-4

Tempc = sum(D3(:,2:4));

Temp2c = -1*sum(Tempc);

[a3,b3]=size(C3);

AVG3 = Temp2c/(a3*b3)

% Total average for all 3 sections

TOTAVG = (AVG1 + AVG2 + AVG3)/3

% Arrange your information to be saved

% Make sure to change the # of Cycles, Test Date, and Specimen Name

Cycle = {'# of Cylces: 0'};

TestDate = {'Test Date: 15 Nov 2011'};

Specimen1 = {'01CT'};

Specimen2 = {'01CM'};

Specimen3 = {'01CB'};

Specimen4 = {'01C'};

% Don't change this information (standard for all the excel sheets)

Frequency = {'Frequency (GHz)'};

EMI = {'#1' '#2' '#3'};
```

EMIUnit = {'dB' 'dB' 'dB' 'Average (dB)'};

EMIUnitAvg = {'Average (dB)'};

D_Results1 = [D1];

D_Results2 = [D2];

D_Results3 = [D3];

D_Results4 = [D4];

Total_Avg = {'Total Avg'};

Avg_Results1 = [AVG1];

Avg_Results2 = [AVG2];

Avg_Results3 = [AVG3];

% Write your results matrix in one excel file (can add data later to the

% same excel file too)

% Top Section; make sure that you change the sheet name and cell location when

appropriate

xlswrite('Nanocomposite Data_Hunt.xlsx',Cycle,'01CT','A1');

xlswrite('Nanocomposite Data_Hunt.xlsx',TestDate,'01CT','C1');

xlswrite('Nanocomposite Data_Hunt.xlsx',Specimen1,'01CT','A2');

xlswrite('Nanocomposite Data_Hunt.xlsx',Frequency,'01CT','A3');

xlswrite('Nanocomposite Data_Hunt.xlsx',EMI,'01CT','B2');

xlswrite('Nanocomposite Data_Hunt.xlsx',EMIUnit,'01CT','B3');

xlswrite('Nanocomposite Data_Hunt.xlsx',D_Results1,'01CT','A4');

xlswrite('Nanocomposite Data_Hunt.xlsx',Total_Avg,'01CT','C205');

```
xlswrite('Nanocomposite Data_Hunt.xlsx',E1,'01CT','E4');

xlswrite('Nanocomposite Data_Hunt.xlsx',AVG1,'01CT','D205');

% Top Section for overall sheet; make sure that you change the sheet name

% and cell location when appropriate

xlswrite('Nanocomposite Data_Hunt.xlsx',Cycle,'01C Overall','A1');

xlswrite('Nanocomposite Data_Hunt.xlsx',TestDate,'01C Overall','C1');

xlswrite('Nanocomposite Data_Hunt.xlsx',Specimen1,'01C Overall','A2');

xlswrite('Nanocomposite Data_Hunt.xlsx',Frequency,'01C Overall','A3');

xlswrite('Nanocomposite Data_Hunt.xlsx',EMI,'01C Overall','B2');

xlswrite('Nanocomposite Data_Hunt.xlsx',EMIUnit,'01C Overall','B3');

xlswrite('Nanocomposite Data_Hunt.xlsx',D_Results1,'01C Overall','A4');

xlswrite('Nanocomposite Data_Hunt.xlsx',E1,'01C Overall','E4');

% Middle Section; make sure that you change the sheet name and cell location

% when appropriate

xlswrite('Nanocomposite Data_Hunt.xlsx',Cycle,'01CM','A1');

xlswrite('Nanocomposite Data_Hunt.xlsx',TestDate,'01CM','C1');

xlswrite('Nanocomposite Data_Hunt.xlsx',Specimen2,'01CM','A2');

xlswrite('Nanocomposite Data_Hunt.xlsx',Frequency,'01CM','A3');

xlswrite('Nanocomposite Data_Hunt.xlsx',EMI,'01CM','B2');

xlswrite('Nanocomposite Data_Hunt.xlsx',EMIUnit,'01CM','B3');

xlswrite('Nanocomposite Data_Hunt.xlsx',D_Results2,'01CM','A4');

xlswrite('Nanocomposite Data_Hunt.xlsx',Total_Avg,'01CM','C205');
```

112

```matlab
xlswrite('Nanocomposite Data_Hunt.xlsx',E2,'01CM','E4');

xlswrite('Nanocomposite Data_Hunt.xlsx',AVG2,'01CM','D205');

% Middle Section for overall; make sure that you change the sheet name and cell location

% when appropriate

xlswrite('Nanocomposite Data_Hunt.xlsx',Cycle,'01C Overall','G1');

xlswrite('Nanocomposite Data_Hunt.xlsx',TestDate,'01C Overall','I1');

xlswrite('Nanocomposite Data_Hunt.xlsx',Specimen2,'01C Overall','G2');

xlswrite('Nanocomposite Data_Hunt.xlsx',Frequency,'01C Overall','G3');

xlswrite('Nanocomposite Data_Hunt.xlsx',EMI,'01C Overall','H2');

xlswrite('Nanocomposite Data_Hunt.xlsx',EMIUnit,'01C Overall','H3');

xlswrite('Nanocomposite Data_Hunt.xlsx',D_Results2,'01C Overall','G4');

xlswrite('Nanocomposite Data_Hunt.xlsx',E2,'01C Overall','K4');

% Bottom Section; make sure that you change the sheet name and cell location

% when appropriate

xlswrite('Nanocomposite Data_Hunt.xlsx',Cycle,'01CB','A1');

xlswrite('Nanocomposite Data_Hunt.xlsx',TestDate,'01CB','C1');

xlswrite('Nanocomposite Data_Hunt.xlsx',Specimen3,'01CB','A2');

xlswrite('Nanocomposite Data_Hunt.xlsx',Frequency,'01CB','A3');

xlswrite('Nanocomposite Data_Hunt.xlsx',EMI,'01CB','B2');

xlswrite('Nanocomposite Data_Hunt.xlsx',EMIUnit,'01CB','B3');

xlswrite('Nanocomposite Data_Hunt.xlsx',D_Results3,'01CB','A4');

xlswrite('Nanocomposite Data_Hunt.xlsx',Total_Avg,'01CB','C205');
```

```matlab
xlswrite('Nanocomposite Data_Hunt.xlsx',E3,'01CB','E4');

xlswrite('Nanocomposite Data_Hunt.xlsx',AVG3,'01CB','D205');

% Bottom Section for overall; make sure that you change the sheet name and cell

location

% when appropriate

xlswrite('Nanocomposite Data_Hunt.xlsx',Cycle,'01C Overall','M1');

xlswrite('Nanocomposite Data_Hunt.xlsx',TestDate,'01C Overall','O1');

xlswrite('Nanocomposite Data_Hunt.xlsx',Specimen3,'01C Overall','M2');

xlswrite('Nanocomposite Data_Hunt.xlsx',Frequency,'01C Overall','M3');

xlswrite('Nanocomposite Data_Hunt.xlsx',EMI,'01C Overall','N2');

xlswrite('Nanocomposite Data_Hunt.xlsx',EMIUnit,'01C Overall','N3');

xlswrite('Nanocomposite Data_Hunt.xlsx',D_Results3,'01C Overall','M4');

xlswrite('Nanocomposite Data_Hunt.xlsx',E3,'01C Overall','Q4');

% Average for overall section; make sure that you change the sheet name and

% cell location when appropriate

xlswrite('Nanocomposite Data_Hunt.xlsx',Cycle,'01C Overall','S1');

xlswrite('Nanocomposite Data_Hunt.xlsx',TestDate,'01C Overall','T1');

xlswrite('Nanocomposite Data_Hunt.xlsx',Specimen4,'01C Overall','S2');

xlswrite('Nanocomposite Data_Hunt.xlsx',Frequency,'01C Overall','S3');

xlswrite('Nanocomposite Data_Hunt.xlsx',EMIUnitAvg,'01C Overall','T3');

xlswrite('Nanocomposite Data_Hunt.xlsx',D_Results4,'01C Overall','S4');
```

Appendix I. Detailed MTS Test Procedures

MTS Warm-up Procedures

1. Click Station Manager icon on desktop.

2. Open the desired configuration file.

3. Turn on the hydraulics by clicking the button with two lines (low) and then the button with three lines (high) on the right hand side next to HPU-J25.

4. Clear any system interlocks by clicking the Reset button.

5. On Function Generator.

   a. Select Channel: Ch 1.

   b. Select Control Mode: Displacement.

   c. Select Command Type: Cyclic.

   d. Adjust Target Setpoint: 0.000 mm (0.000 in).

   e. Adjust Amplitude: 6.35 mm (0.250 in).

   f. Adjust Frequency: 2.00 Hz.

   g. Select Wave Shape: Square.

   h. Select Compensator: None.

6. Select Run (arrow button) for 30 minutes.

7. Select Stop (square button) after 30 minutes.

MTS Auto-Tuning Steps (Force Control Mode)

1. Adjust lower grip by using Manual Command button under the Station Controls function on the right side of the window.

2. On Manual Controls.

      a. Select Channel: Ch 1.

      b. Select Control Mode: Displacement.

      c. Adjust the lower grip height the desired grip length by using the scroll
button.

3. Insert the test specimen into the upper grip and close the grip with the upper grip
knob on the MTS machine.

4. Ensure the test specimen is level by using a level tool available in the lab.

5. On Manual Controls.

      a. Select Control Mode: Force.

      b. Enter 0, hit enter, and close the bottom grip with the bottom grip knob on
the MTS machine.

6. Zero out the force and displacement under the Auto Offset controls.

7. Click the auto-tuning icon on the left hand side of the Function Generator screen.

8. Select the Tuning command at the top of the screen where it shows Operator.

9. Enter the correct password.

10. Under the Auto Tuning.

      a. Select Control Channel: Ch 1.

      b. Select Control Mode: Force.

      c. Select Mode to Tune: Force.

      d. Adjust Upper Limit: To desired maximum force.

      e. Adjust Lower Limit: To desired minimum force.

      f. Select Auto Tuning Type: Basic.

g.   Select Actuator Type: Normal.

11. Select Run (arrow button).

12. Press Accept to apply the reference tuning values.

13. Save the auto-tuning values.

MPT Procedures

1.   Select MultiPurpose TestWare under the Application menu.

2.   On the MPT screen.

    a.   Select Procedure Editor button.

    b.   Select the Segment Command under the Command Processes.

        i.   On Command Tab.

           1.   Select Segment Shape: Ramp.

           2.   Select Time.

           3.   Input 20.00.

           4.   Select units: (Sec).

           5.   Select Adaptive Compensators: None.

           6.   Select Channel: Ch 1.

           7.   Select Control Mode: Force.

           8.   Absolute End Level: To desired amplitude force and units.

      ii.   On Channels Tab.

           1.   Select Ch 1.

     iii.   On General Tab.

           1.   Change name to Ramp Up.

      2. Check the box Process Enabled.

      3. Input 1 for Execute Process.

      4. Select Counter Type: None.

  c. For Ramp Up under Start click <Procedure>.Start.

  d. For Ramp Up under Interrupt click Data Limit Detector 1.Done.

3. Select Timed Data Acquisition under Data Acquisition Process.

  a. On Acquisition Tab.

    i. Select Time Between Points and 0.049805 seconds.

    ii. Select Continuous Sampling.

  b. On Signals Tab.

    i. Select Time, Ch 1 Force, Ch 1 Force Command, Ch 1

       Displacement, and Ch 1 Displacement Command.

  c. On Destination Tab.

    i. Input Buffer Size: 1024.

    ii. Select Destination: User-specified data file.

    iii. Input User Data File: Ramp.csv.

    iv. Select Buffer Type: Linear.

    v. Check Write First Data Header Only box.

  d. On Output Units Tab.

    i. Check off Current Unit Assignment Set for SISETSM - SI (System

       International d'Unites) - small.

  e. On General Tab.

   i. Change name to Ramp Up Data.

   ii. Check the box Process Enabled.

   iii. Input 1 for Execute Process.

   iv. Select Counter Type: None.

 f. For Ramp Up Data under Start click <Procedure>.Start.

 g. For Ramp Up Data under Interrupt click Ramp Up.Done.

4. Select Cyclic Command under the Command Processes.

 a. On the Command Tab.

   i. Select Segment Shape: Sine.

   ii. Select Frequency for 1 Hz.

   iii. Check the Count box.

   iv. Input the number of fatigue cycles and select Cycles.

   v. Select Adaptive Compensators: APC.

   vi. Select Channel: Ch 1.

   vii. Select Control Mode: Force.

   viii. Input Absolute End Level 1: The desired maximum force and units.

   ix. Input Absolute End Level 2: The desired minimum force and units.

 b. On Channels Tab.

   i. Select Ch 1.

 c. On General Tab.

      i. Name Fatigue Part.

      ii. Check the box Process Enabled.

      iii. Input 1 for Execute Process.

      iv. Select Counter Type: None.

  d. For the Fatigue Part under Start click Ramp Up.Done.

  e. For the Fatigue Part under Interrupt click Data Limit Detector1.Done.

5. Select Peak/Valley Acquisition under Data Acquisition Process.

  a. On Acquisition Tab.

      i. Select Master Signal: Ch 1 Force.

      ii. Input Sensitivity: Desired sensitivity force.

      iii. Check Total Samples Box.

      iv. Input desired number of recorded samples.

  b. On Signals Tab.

      i. Select Time, Ch 1 Count, Ch 1 Force, Ch 1 Displacement, Ch 1

        Force Command, and Ch 1 Displacement Command.

  c. On Destination Tab.

      i. Input Buffer Size: 1024.

      ii. Select Destination: User-specified data file.

      iii. Input User Data File: PeakandValley.csv.

      iv. Select Buffer Type: Linear.

      v. Check Write First Data Header Only box.

  d. On Output Units Tab.

> i. Check off Current Unit Assignment Set for SISETSM - SI (System
>
>> International d'Unites) - small.
>
> e. On General Tab.
>
>> i. Change name to Peak/Valley Data.
>>
>> ii. Check the box Process Enabled.
>>
>> iii. Input 1 for Execute Process.
>>
>> iv. Select Counter Type: None.
>
> f. For the Peak/Valley Data under Start click Ramp Up.Done.
>
> g. For the Peak/Valley Data under Interrupt click Fatigue Part.Done.

6. Select Cyclic Data Acquisition under Data Acquisition Process.

> a. On Data Storage Tab.
>
>> i. Select Master Channel: Ch 1.
>>
>> ii. Select Data Storage Pattern: Logarithmic (1,2,5).
>>
>> iii. Input Maximum Cycle Stored: 10,000,000 cycle.
>>
>> iv. Input Store Data For: 1.0 cycles.
>
> b. On Acquisition Tab.
>
>> i. Select Acquisition Method: Timed.
>>
>> ii. Input Time Between Points: 0.0097656 Seconds.
>
> c. On Signals Tab.
>
>> i. Select Time, Ch 1 Count, Ch 1 Force, Ch 1 Displacement, Ch 1
>>
>> Force Command, and Ch 1 Displacement Command.
>
> d. On Destination Tab.

    i. Select Destination: User Data File.

    ii. Input User Data File: Fatigue Data.csv.

    iii. Check Write First Data Header Only box.

e. On Output Units Tab.

    i. Check off Current Unit Assignment Set for SISETSM - SI (System International d'Unites) - small.

f. On General Tab.

    i. Change name to Fatigue Data.

    ii. Check the box Process Enabled.

    iii. Input 1 for Execute Process.

    iv. Select Counter Type: None.

g. For Fatigue Data under Start click Ramp Up.Done.

h. For Fatigue Data under Interrupt click Fatigue Part.Done.

7. Select the Segment Command under the Command Processes.

    i. On Command Tab.

        1. Select Segment Shape: Ramp.

        2. Select Time.

        3. Input 20.00.

        4. Select units: (Sec).

        5. Select Adaptive Compensators: None.

        6. Select Channel: Ch 1.

        7. Select Control Mode: Force.

8. Absolute End Level: To zero force and units.

    ii. On Channels Tab.

        1. Select Ch 1.

    iii. On General Tab.

        1. Change name to Unload to Zero.

        2. Check the box Process Enabled.

        3. Input 1 for Execute Process.

        4. Select Counter Type: None.

b. For Unload to Zero under Start click Fatigue Part.Done.

c. For Unload to Zero under Interrupt click Data Limit Detector 1.Done.

8. Select Timed Data Acquisition under Data Acquisition Process.

a. On Acquisition Tab.

    i. Select Time Between Points and 0.049805 seconds.

    ii. Select Continuous Sampling.

b. On Signals Tab.

    i. Select Time, Ch 1 Force, Ch 1 Force Command, Ch 1

       Displacement, and Ch 1 Displacement Command.

c. On Destination Tab.

    i. Input Buffer Size: 1024.

    ii. Select Destination: User-specified data file.

    iii. Input User Data File: Unload.csv.

    iv. Select Buffer Type: Linear.

      v.   Check Write First Data Header Only box.

   d. On Output Units Tab.

      i.   Check off Current Unit Assignment Set for SISETSM - SI (System

         International d'Unites) - small.

   e. On General Tab.

      i.   Change name to Unload Data.

      ii. Check the box Process Enabled.

     iii. Input 1 for Execute Process.

     iv. Select Counter Type: None.

   f. For Unload Data under Start click Fatigue Part.Done.

   g. For Unload Data under Interrupt click Unload to Zero.Done.

9. Select Data Limit Detector under Event Processes.

   a. On Limits Tab.

      i.   Select Signal: Ch 1 Displacement.

      ii. Check Upper Limit box.

     iii. Input Upper Limit: Desired upper limit and units.

     iv. Check Lower Limit box.

      v.   Input Lower Limit: Desired lower limit and units.

   b. On Signals Tab.

      i.   Select: Ch 1 Displacement.

   c. On Settings Tab.

      i.   Check Limit Mode: Absolute.

  ii. Check Process completes when: Any selected signal exceeds its

   limit.

  iii. Check Log Message As box.

  iv. Select Check Log Message As: Warning.

  v. Select Action: None.

d. On Limit Table.

  i. Make sure that the desired upper and lower limits are indicated.

e. On General Tab.

  i. Change name to Data Limit Detector.

  ii. Check the box Process Enabled.

  iii. Input 1 for Execute Process.

  iv. Select Counter Type: None.

f. For Data Limit Detector 1 under Start click <Procedure>.Start.

g. For Data Limit Detector 1 under Interrupt click Unload to Zero.Done.

Appendix J. EMI Shielding Mathematical Relationships

Electromagnetic waves traveling through space that encounter a boundary will partially reflect, and partly transfer across the boundary and into the material (absorption). The SE of the material is the total sum of reflection and absorption, plus a correction factor to account for reflections from the back side of the boundary of the shield. This mathematical relationship to express shielding is the following:

$$SE(dB) = R(dB) + A(dB) + B(dB) \tag{10}$$

where

> SE is the SE (dB)
>
> R is the reflection factor (dB)
>
> A is the absorption term (dB)
>
> B is the correction factor (dB)

The reflection term is dominated by the relative disparity between the incoming wave and the surface resistance of the shield. Reflection terms and equations for electric, magnetic, and plane wave fields are given by the following expressions:

$$R_E(dB) = 353.6 + 10 \, log_{10} \frac{G}{f^3 \mu r_1^2} \tag{11}$$

$$R_H(dB) = 20 \, log_{10} \left[\frac{0.462}{r_1} \sqrt{\frac{\mu}{Gf}} + 0.136 r_1 \sqrt{\frac{fG}{\mu}} + 0.354 \right] \tag{12}$$

$$R_P(dB) = 108.2 + 10\,log_{10}\frac{G \cdot 10^6}{\mu f} \qquad (13)$$

$$R_{total} = R_E + R_H + R_P \qquad (14)$$

where

R_{total} is the reflection total (dB)

R_E is electric reflection wave fields (dB)

R_H is magnetic reflection wave fields (dB)

R_P is plane reflection wave fields (dB)

G is the relative conductivity referred to copper

f is the frequency (Hz)

μ is the relative permeability referred to free space

r_1 is the distance from the source to the shield (in)

The absorption term A is the same for all three waves and is the following expression:

$$A(dB) = 3.338x10^{-3} \cdot t\sqrt{\mu f G} \qquad (15)$$

where

A is the absorption or penetration loss (dB)

t is the thickness of the shield (mm)

f is the frequency (Hz)

G is the relative conductivity referred to copper

The variable B can be mathematically positive or negative (commonly negative), and becomes insignificant when A > 6 dB. It is only critical when metals are thin, and at low frequencies (i.e., below approximately 20 kHz).

$$B(dB) = 20 \, log_{10} \left| 1 - \left(\frac{(K-1)^2}{(K+1)^2} \right) \left(10^{-\frac{A}{10}} \right) \left(e^{-j \cdot 0.227A} \right) \right| \qquad (16)$$

where

A is absorption losses (dB)

$|K|$ is $\left| \frac{Z_S}{Z_H} \right| = 1.3 \sqrt{\frac{\mu}{fr^2 G}}$

Z_S is shield impedance

Z_H is impedance of the incident magnetic field

Bibliography

[1]   Tzu, S. (2011, Dec 28). *The Art of War by Sun Tzu* [Online] Available: http://suntzusaid.com/artofwar.pdf.

[2]   "NAVSTAR GPS Image," URL: http://www.spacetoday.org/Satellites/GPS.html.

[3]   NSS. "National Security Space Strategy Unclassified Summary," Jan 2011 URL: http://www.au.af.mil/au/awc/awcgate/space/nat_secur_space_strat_sum_jan2011.pdf.

[4]   NASA. "NASA'S Exploration Systems Architecture Study," Nov 2005 URL: http://www.nasa.gov/pdf/140649main_ESAS_full.pdf.

[5]   NASA. *NASA Fact Sheet FS-1996-08-09-LaRC* [Online] Available: http://www.nasa.gov/centers/langley/news/factsheets/Bldg-structures.html.

[6]   Herakovich, C. T., *Mechanics of Fibrous Composites,* New York: John Wiley & Sons, 1998, pp.450-451.

[7]   "Bucky Ball Image," URL: http://nanocusp.com/.

[8]   Arnero, "Carbon Nanotube Image," 2007. URL: http://commons.wikimedia.org/wiki/File:Carbon_nanotube_zigzag_povray.PNG.

[9]   S. Mall, "Carbon Nanotubes Based Nanocomposites and Nanoadhesives for EMI/ESD Applications in Space Structures," 1 Nov 2010.

[10]   S. E. Baker, K. Tse, M. Marcus, J. Streifer and R. J. Hamers . University of Wisconsin-Madison News Photos. 2005. URL: http://www.news.wisc.edu/newsphotos/nanobucky.html.

[11]   M. Mojarradi, P. B. Abel, T. R. Tyler and G. Levanas. "Electro-Mechanical Systems for Extreme Space Environments," NASA. Langley Research Center. 2011 [Online]. URL: http://ntrs.nasa.gov/archive/nasa/casi.ntrs.nasa.gov/20110008483_2011009048.pdf.

[12]   Baumjohann, W. and Treumann, R. A., *Basic Space Plasma Physics,* Imperial College Press, 1997.

[13]   Lai, S. T., *Fundamentals of Spacecraft Charging, Spacecraft Interactions with Space Plasmas,* New Jersey: Princeton University Press, 2012.

[14]   *2000 Special Issue on Space Plasmas* (2011, Dec 30). [Online] Available: http://public.lanl.gov/alp/ieee/tps/Space.html.

[15]   NASA/GSFC. Sun-Earth Connection Image. URL: http://www.physics.adelaide.edu.au/wiser/SER.html.

[16]   R. L. Patterson, A. Hammoud and M. Elbuluk. " Electronic Components for use in Extreme Temperature Aerospace Applications " NASA. Langley Research Center. 2008 [Online]. URL: http://ntrs.nasa.gov/archive/nasa/casi.ntrs.nasa.gov/20090004677_2009001235.pdf.

[17]   J. W. Howard Jr. and D. M. Hardage. "Spacecraft Environments Interactive: Space Radiation and its Effects on Electronic System," NASA. Marshall Space Flight Center. 1999 [Online]. URL: http://ntrs.nasa.gov/archive/nasa/casi.ntrs.nasa.gov/19990116210_1999175246.pdf.

[18]   National Geographic. (2011, Dec 30). *Orbital Objects* [Online] Available: http://science.nationalgeographic.com/science/space/solar-system/orbital/.

[19]   D. C. Ferguson and G. B. Hillard. "Low Earth Orbit Spacecraft Charging Design Guidelines," NASA. Marshall Space Flight Center, AL 35812. 2003 [Online]. URL: http://see.msfc.nasa.gov/LEO_Charging_Guidelines_v1.3.1.pdf.

[20]   Burrell, J. *"Disruptive Effects of Electromagnetic Interference on Communication and Electronic Systems,"* M.S. in Telecommunications, George Mason University.

[21]   S. Park, P. Theilmann, P. Asbeck and P. R. Bandaru. "Enhanced Electromagnetic Interference Shielding through the use of Functionalized Carbon Nanotube-Reactive Polymer Composites," 2009 [Online]. URL: http://nanomaterials.ucsd.edu/Publications_files/IEEE%20formatted_CNT_Polymer%20compsoites_Bandaru_Sep14_2009.pdf.

[22]   Mahan, G. D., *Condensed Matter in a Nutshell,* New Jersey: Princeton University Press, 2011.

[23]   "SWCNT Image," URL: http://inhabitat.com/tag/carbon-nanotubes/.

[24]   P. M. Ajayan andO. Z. Zhou. Applications of Carbon Nanotubes. pp. 30 Dec 2011.

[25]   Jorio, A. and Dresselhaus, M. S., *Carbon Nanotubes: Advanced Topics in the Synthesis, Structure, Properties and Applications,* New York: Springer Berlin Heidelberg, 2008.

[26]   D. Burton, P. Lake and A. Palmer. "Properties and Applications of Carbon Nanofibers (CNFs) Synthesized using Vapor-Grown Carbon Fiber (VGCF) Manufacturing Technology," Applied Sciences, Inc. Cedarville, OH. 2011 [Online]. URL: http://www.sigmaaldrich.com/materials-science/nanomaterials/carbon-nanofibers.html.

[27]   Rodriguez, J. *"Fatigue Evaluation of Nanocomposites as Lightweight Electronic Enclosures for Satellites' Applications,"* M.S. Thesis, AFIT/GMS/ENY/09-M03, Air Force Institute of Technology (AU), Wright-Patterson AFB, OH, Mar 2009.

[28]   Harder, B. T. *"Evaluation of Nanocomposites as Lightweight Electronic Enclosures for Satellites' Applications,"* M.S. Thesis, AFIT/GMS/ENY/08-J01, Air Force Institute of Technology (AU), Wright-Patterson AFB, OH, May 2008.

[29]   Chong, K. *"Evaluation of Nanocomposites for Shielding Electromagnetic Interference,"* M.S. Thesis, AFIT/GMS/ENY/11-S01, Air Force Institute of Technology (AU), Wright-Patterson AFB, OH, Sep 2011.

[30]   AGY Holding Corp. (2011, 31 Dec). *S-2 Glass Fiber* [Online] Available: http://www.matweb.com/search/datasheet_print.aspx?matguid=881df8cd9bde4344820202eb6d1e7a39.

[31]   CYCOM. (2011, Dec 31). *CYCOM 5250-4 RTM Resin System Data Sheet* [Online] Available: http://www.cytec.com/engineered-materials/products/Datasheets/CYCOM%20RTM%205250-4.pdf.

[32]   Cytec. (2012, Jan 20). [Online] Available: http://www.cytec.com/engineered-materials/products/FM6555-1SC.htm.

[33]   Adams II, T. A. (2011, 31 Dec). *Physical Properties of Carbon Nanotubes* [Online] Available: http://www.pa.msu.edu/cmp/csc/ntproperties/.

Vita

Captain Peter A. Hunt graduated from Charlotte High School in Charlotte, Michigan (MI) in June 1997. In August 1997, he entered undergraduate studies at Michigan State University in East Lansing, MI where he graduated with a Bachelor of Science degree in Chemical Engineering in May 2002. In April 2003, he entered Officer Training School at Maxwell AFB, Alabama where he received his commission in June 2003.

His first assignment started in July 2003 in the Battle Management Command, Control, and Communication Capabilities Systems Program Office, Electronic Systems Center at Hanscom AFB, Massachusetts (MA) where he was the Chief for Fielding and Training for the Time Critical Targeting Functionality Program. In June 2005, he assumed project lead for Theater Battle Management Core Systems, Unit Level Intelligence at Hanscom AFB, MA. In June 2006, he was assigned to the 86th Fighter Weapons Squadron at Eglin AFB, Florida (FL) where he was the Precision-Guided Weapons Target Telemetry Systems Engineer. During the same time he entered a master's program online through Colorado State University at Fort Collins, Colorado and graduated with a Master's of Business Administration in May 2008. In June 2009 he assumed the role of Chief Engineer and Technical Support while still in the 86th Fighter Weapons Squadron at Eglin AFB, FL. In May 2010 he entered the Graduate School of Engineering and Management, AFIT and earned a membership to Tau Beta Pi in June 2011. Upon graduation, he will be assigned to the Air Force Corrosion Prevention and Control Office at Robins AFB, GA.

REPORT DOCUMENTATION PAGE

1. REPORT DATE (DD-MM-YYYY)	2. REPORT TYPE	3. DATES COVERED (From – To)
03-22-2012	Master's Thesis	June 2011 – March 2012

4. TITLE AND SUBTITLE	5a. CONTRACT NUMBER
Electromagnetic Interference Behavior of Multiwall Carbon Nanotubes and Carbon Nanofibers Composites Under Fatigue	5b. GRANT NUMBER
	5c. PROGRAM ELEMENT NUMBER

6. AUTHOR(S)	5d. PROJECT NUMBER
Hunt, Peter A., Captain, USAF	5e. TASK NUMBER
	5f. WORK UNIT NUMBER

7. PERFORMING ORGANIZATION NAMES(S) AND ADDRESS(S)	8. PERFORMING ORGANIZATION REPORT NUMBER
Air Force Institute of Technology Graduate School of Engineering and Management (AFIT/EN) 2950 Hobson Way, Building 640 WPAFB OH 45433-8865	AFIT/GMS/ENY/12-M01

9. SPONSORING/MONITORING AGENCY NAME(S) AND ADDRESS(ES)	10. SPONSOR/MONITOR'S ACRONYM(S)
Undisclosed sponsor	11. SPONSOR/MONITOR'S REPORT NUMBER(S)

12. DISTRIBUTION/AVAILABILITY STATEMENT

APPROVED FOR PUBLIC RELEASE; DISTRIBUTION UNLIMITED.

13. SUPPLEMENTARY NOTES
This material is declared a work of the U.S. Government and is not subject to copyright protection in the United States.

14. ABSTRACT

The United States (U.S.) military is researching the use of nanocomposite materials for structural applications on space vehicle systems. To reduce the weight and mitigate electromagnetic interference (EMI), brought on by the harsh space environment, composites coated with expensive conductive materials are used in today's space vehicles. Research on composites with carbon nanotubes (CNT) and carbon nanofibers (CNF) have shown better EMI shielding and offer the potential to replace the current composites coated with expensive conductive materials as a high specific strength material. This study evaluated the effects of EMI behavior on one control composite (i.e. without nanocomposite) and five different configured nanocomposites under fatigue. The control specimen, 8G, consisted of eight plies S-glass (Astroquartz II) fiber in CYCOM 5575-2 cyanate ester matrix. The first nanocomposite, 8G/CNT, consisted of eight plies of 6781 S-2 glass fiber in CYCOM 5250 4 Bismaleimide (BMI) matrix with a externally deposited layer of CNTs. The second nanocomposite, 8G/CNF, consisted of eight plies of 6781 S-2 glass fiber in CYCOM 5250 4 BMI matrix with a externally deposited layer of CNFs. The last three nanocomposites, (G/CNT)4, 2CNT/4G/2CNT, and 4G/4CNT, consisted of different stacking sequences of multi-wall CNTs (MWNT) with S-glass (Astroquartz II) fiber in CYCOM 5575-2 cyanate ester matrix.

15. SUBJECT TERMS

nanocomposites, space environment protection, fatigue testing, carbon nanotubes, multi-walled carbon nanotubes, carbon nanofibers, electromagnetic interference shielding effectiveness

16. SECURITY CLASSIFICATION OF:			17. LIMITATION OF ABSTRACT	18. NUMBER OF PAGES	19a. NAME OF RESPONSIBLE PERSON
a. REPORT	b. ABSTRACT	c. THIS PAGE	UU	151	Shankar Mall, Ph.D.
U	U	U			19b. TELEPHONE NUMBER (Include area code) (937) 255-6565, ext 4587 (shankar.mall@afit.edu)